3-1975

Correlation of Theory and Experiment for the Dynamics of a Pressurized Water Reactor

J. G. Thakkar
University of Tennessee - Knoxville

To the Graduate Council:

I am submitting herewith a thesis written by J. G. Thakkar entitled "Correlation of Theory and Experiment for the Dynamics of a Pressurized Water Reactor." I have examined the final electronic copy of this thesis for form and content and recommend that it be accepted in partial fulfillment of the requirements for the degree of Master of Science, with a major in Nuclear Engineering.

T. W. Kerlin, Major Professor

We have read this thesis and recommend its acceptance:

Julian E. Roth, P. F. Pasqua, J. C. Robinson

Accepted for the Council:
Carolyn R. Hodges

Vice Provost and Dean of the Graduate School

(Original signatures are on file with official student records.)

January 17, 1975

To the Graduate Council:

I am submitting herewith a thesis written by J. G. Thakkar entitled "Correlation of Theory and Experiment for the Dynamics of a Pressurized Water Reactor." I recommend that it be accepted in partial fulfillment of the requirements for the degree of Master of Science, with a major in Nuclear Engineering.

T. W. Kerlin, Major Professor

We have read this thesis and recommend its acceptance:

Accepted for the Council:

Vice Chancellor
Graduate Studies and Research

CORRELATION OF THEORY AND EXPERIMENT FOR THE DYNAMICS OF A PRESSURIZED WATER REACTOR

A Thesis

Presented for the

Master of Science

Degree

The University of Tennessee

J. G. Thakkar

March 1975

ACKNOWLEDGEMENTS

The author wishes to thank Dr. T. W. Kerlin for his continuous guidance and suggestions during the entire course of this project; particularly his expert instructions during the theoretical phases of this study and for his assistance in interpreting experimental results. The author would also like to thank Ms. E. M. Katz and the group led by Dr. Kerlin who performed the dynamic tests on H. B. Robinson and made results available.

The author wishes to acknowledge Mr. M. R. Ali for his help during the modeling work. Mrs. Juanita Rye typed the manuscript and Mr. Alan Chen helped to set up the plot subroutines. These are also gratefully acknowledged.

ABSTRACT

Dynamic tests were performed on the Carolina Power and Light Company's H. B. Robinson Unit 2 to determine the frequency response of the PWR steam supply system. Step inputs and multi-frequency binary signals of various sequence lengths and bit durations were used. The signals were introduced manually by the operator both for reactivity perturbation and steam flow perturbation tests. The experimental results were analyzed on an IBM 360/65 computer. The test results were compared with theoretical results predicted by a mathematical model of the system.

A mathematical model for the H. B. Robinson system was formulated. In most cases, the experimental results were in good agreement with the results. An unexplained time delay of about nine to fourteen seconds was observed between the opening of the main steam valve and reactor coolant cold leg temperature. The time delay is much longer than the transport time.

TABLE OF CONTENTS

CHAPTER PAGE

LIST OF TABLES

LIST OF FIGURES

FIGURE PAGE

FIGURE PAGE

CHAPTER I

INTRODUCTION

A good understanding of the dynamic behavior of a nuclear system is of primary interest for its safe operation. The design of nuclear plants is based on mathematical models. It is very important to determine the adequacy of these models. One way of determining the adequacy of the models is to compare the frequency response predicted by the model with the experimentally determined frequency response. Besides verifying the model, the experimental data will provide information which will help:[1,2]

(1) To improve the coefficients used in the model, optimize its sophistication, and reduce the uncertainties in the predicted performance

(2) To evaluate system stability margins and detect their trends as the operating conditions change

(3) To optimize controller parameters.

The most straightforward approach for dynamic testing in nuclear reactors is the oscillator method which employs a sinusoidal reactivity input. But economic and operational considerations prohibit the use of oscillator tests in commercial power reactors. The periodic, discrete-level binary signals are more suitable for frequency response testing in commercial power reactors. These signals offer advantages over the oscillator tests because of reduced experiment duration and equipment costs. Moreover, the tests can be performed

during normal operation with the existing plant hardware. Another advantage of these signals is that a number of frequencies can be covered in a single test.

Several frequency response tests have been performed on pressurized water reactors using both oscillator and binary input signals.[1] Dynamic tests on H. B. Robinson Unit 2 were performed by E. M. Katz and the group led by Dr. T. W. Kerlin. The purpose of the work reported herein was to analyze and interpret the test results and compare them with theoretical results predicted by the system models. The detailed reactor model was originally developed by E. M. Katz for the Oconee system;[11] and major contributions in modeling the U-tube and shell type steam generator came from M. R. Ali.[7]

CHAPTER II

SYSTEM DESCRIPTION AND MATHEMATICAL FORMULATION

I. PHYSICAL DESCRIPTION

The H. B. Robinson Unit 2 is a 739 MWe (2200 MWt) pressurized water reactor type nuclear power plant. The nuclear steam supply system (NSSS) consists of three reactor coolant loops. The loops are connected in parallel to the reactor vessel. Each loop contains a U-tube and shell type steam generator and a circulating pump. The system also includes a pressurizer. The flow diagram of one of the reactor coolant loops is shown in Figure II-1.*

A. Reactor

The H. B. Robinson plant contains a Westinghouse pressurized water reactor. The reactor core and vessel internals are shown in Figure II-2.

Reactor coolant enters the reactor vessel just above the core and flows downwards, through the annular space between the vessel wall and the core barrel, into the lower plenum. The coolant enters the core at the bottom and flows upwards through the core. All the coolant coming from the different radial sections of the core is mixed in the upper plenum. The mixed coolant then flows to the steam generators through three different hot leg pipes.

Table I lists some of the important design parameters of the reactor, particularly those which affect the dynamic response of the system. The ranges shown in the kinetic coefficients, in Table I, do

---

*All figures will be found in Appendix E.

TABLE I

REACTOR DESIGN DATA

	STRUCTURAL CHARACTERISTICS[4]*	
1.	Fuel Weight (UO_2), lbs.	176,200
2.	Cladding Weight (Zircaloy), lbs.	36,300
3.	Core Diameter, inches	119.7
4.	Core Height, inches	144
5.	H_2O/U Volume Ratio (cold)	4.18
6.	Number of Fuel Assemblies	157
7.	UO_2 Rods per Assembly	204
	KINETIC CHARACTERISTICS[4]*	
8.	Doppler Coefficient $(\Delta K/K)/°F$	-1.0×10^{-5} to -1.6×10^{-5}
9.	Moderator Temperature, Coefficient $(\Delta K/K)/°F$	$+3.0 \times 10^{-5}$ to -3.5×10^{-4}
10.	Moderator Pressure coefficient, $(\Delta K/K)/psi$	-3.0×10^{-7} to 3.5×10^{-7}
11.	Prompt Neutron Lifetime, sec	1.4×10^{-5} to 1.8×10^{-5}
12.	Delayed Neutron Fraction, %	0.52 to 0.72

TABLE I (continued)

13. Delayed Neutron Constants[5]**

Mean Life sec	Decay Constant λ_i, sec^{-1}	Fraction of Total Neutrons
80.4	0.0124	0.00021
32.8	0.0305	0.00140
8.98	0.111	0.00125
3.32	0.301	0.00253
0.88	1.14	0.00074
0.332	3.01	0.00027

THERMAL AND HYDRAULIC CHARACTERISTICS[4]***

14.	Total Primary Heat Output, MWt	2200 (7508 x 10^6 Btu/hr)
15.	Nominal System Pressure, psi	2250
16.	Total Coolant Flow Rate, lbs/hr	101.5 x 10^6
17.	Average Coolant Velocity Along Fuel Rods, ft/sec	14.3
18.	Total Mass of Primary Coolant, lbs	406,050
19.	Average Coolant Mass Velocity, lb/hr-ft^2	2.32 x 10^6
20.	Nominal Coolant Inlet Temperature, °F	546.2
21.	Nominal Coolant Outlet Temperature, °F	602.1
22.	Active Heat Transfer Surface Area, ft^2	42,460
23.	Average Heat Flux, Btu/hr-ft^2	171,600
24.	Maximum Thermal Output kw/ft	17.9

TABLE I (continued)

25. Maximum Average Clad Temperature, °F	715
26. Maximum Fuel Central Temperature at 100% Power, °F	4030

*Reference 4; Table 3.2.1-1.

**Reference 5, p.21.

***Reference 4, Table 3.2.2-1.

not represent uncertainties in the measurement or unavailability of the actual coefficients but they vary depending upon the boron concentration in the reactor coolant, power level, operating temperatures, and burnup.

Since the reactivity perturbations for the experimental tests reported here were introduced by moving a bank of control rods, a brief description of the control systems will be given. A more detailed description of the reactor and the control system is given in Reference 4.

The reactor is controlled by 53 rod cluster control (RCC) assemblies of which 45 are full length and 8 are part length rods. The full length rods are divided into three groups: a shutdown group comprising two banks of 8 rods each, a control group consisting of four banks containing 8, 8, 8, and 5 control rods, and an x-y Xenon Control group consisting of two banks of 4 rod clusters each. Each main bank has two subgroups. Silver-indium-cadmium alloy is used as the absorber material in the control rods.

The schematic of the RCC magnetic jack drive mechanism assembly is shown in Figure II-3. It consists of the operating coil stack, the drive shaft assembly, the pressure housing, and the position indicator coil stack. Three magnetic coils are turned off and on in a fixed sequence. The sequencing of the magnets produces step motion over the 144 inches of normal control rod travel. Each sequence moves the rod by 5/8 inch and each sequence can be repeated up to 72 steps per minute.

B. Steam Generator

Each reactor coolant loop contains a vertical shell and U-tube type steam generator. The steam generator consists of two integral

sections: an evaporator, and a steam drum section. The evaporator section consists of a U-tube heat exchanger where heat from the primary side coolant is transferred through the tube walls to convert secondary side feedwater to steam. The steam drum section is located above the U-tube bundle, and it contains moisture separating equipment. The arrangement of different parts in the steam generator is shown in Figure II-4, and the flow patterns of the primary and secondary side fluids are explained below.

In the primary loop, reactor coolant enters the U-tube bundle at the bottom of the steam generator through an inlet plenum and flows through the U-tubes to an outlet plenum and leaves the steam generator. The U-tubes extend through the subcooled region and into the boiling region then they curve back and again pass through the non-boiling region.

In the secondary side, feedwater from the feedwater heaters enters the steam generator just above the U-tube bundle through a feedwater ring and mixes with the recirculating water. The mixed water then flows downwards through a downcomer and enters the evaporator section at the bottom.

The steam-water mixture from the tube bundle passes through the steam swirl vane assembly which imparts centrifugal motion to the steam-water mixture and removes most of the water from the steam. The water recirculates back into the downcomer for another pass through the tube bundle and steam rises through the additional separators to increase the steam quality to 99.75 percent.[4] The dried saturated steam then flows to the turbine.

The important steam generator parameters are tabulated in Table II. More detailed information on the steam generator may be found in References 3, 4, and 7.

C. Pressurizer

One of the three coolant loops is connected to the pressurizer. The main function of the pressurizer is to provide a surge chamber and a water reserve to accomodate changes in the reactor coolant volume due to temperature changes in the primary side. It also maintains the required coolant pressure during steady state operations and limits the pressure changes during transients. This is accomplished by maintaining water and steam in the pressurizer at the saturation temperature corresponding to the system pressure. During load transients, the following sequence of events takes place (for a load decrease):

1. Plant load decreases.
2. Primary side temperature increases.
3. Reactor coolant volume increases and some of the coolant flows into the pressurizer.
4. Pressurizer pressure increases.
5. The spray system (which is fed from the cold leg of the coolant loop) condenses some of the steam in the pressurizer to reduce the pressure to normal.

During an increase in the plant load, primary side temperature decreases and water outsurges from the pressurizer. The pressure is maintained, to prevent boiling in the reactor, by flashing water to steam and by generating steam using the electric heaters.

TABLE II

STEAM GENERATOR DATA*
(For Each Unit)

	STEAM GENERATOR	
1.	Design Pressure, Reactor Coolant/steam, psig	2485/1085
2.	Design Temperature, Reactor Coolant/steam, °F	650/556
3.	Overall Height, ft-in	63-1.6
4.	Shell OD, Upper/lower, in.	166/127.5
5.	Shell Thickness, Upper/lower, in	3.5/2.63
6.	Number of U-tubes	3260
7.	U-tube Diameter, in	0.875
8.	Tube Wall Thickness, (average), in	0.050
9.	Mass of U-tube metal, lbs	91,800
10.	Total Heat Transfer Area, ft^2	44,430
	STEAM CONDITIONS AT FULL LOAD	
11.	Steam Flow, lb/hr	3.169×10^6
12.	Steam Temperature, °F	516
13.	Steam Pressure, psig	770

TABLE II (continued)

	PRIMARY SIDE COOLANT	
14.	Reactor Coolant Flow, lbs/hr	33.93×10^6
15.	Reactor Coolant Water Volume, ft^3	928
	SECONDARY SIDE FLUID	
16.	Feedwater Temperature, °F	425
17.	Recirculation Ratio**	9
18.	Secondary Side Water Volume, (Full Power), ft^3	1526
19.	Secondary Side Steam Volume, (Full Power), ft^3	3203

*Reference 4, Table 4.1-4.

**Reference 7.

The pressurizer consists of the pressurizer vessel, electric heaters, the spray system, relief and safety valves, and pressure sensing and control devices. The general arrangement of the pressurizer is shown in Figure II-5 and design and operating parameters are tabulated in Table III. More detailed information about the pressurizer may be found in References 4, 8, and 9.

II. MATHEMATICAL FORMULATION OF THE SYSTEM

Theoretical results for the H. B. Robinson power plant were obtained using simplified models of NSSS components. A more detailed model of the steam generator is under development[7] and it should be able to predict some of the system parameters, particularly, cold leg temperature, steam outlet pressure, steam flow rate, and feedwater flow rate more accurately, than the simplified model used in this analysis, once it is fully developed.

The pressurized water reactor dynamic behavior is described by a twelve state variable, lumped-parameter model. Of the twelve, seven variables are used to describe reactor kinetics. They include reactor power and six groups of delayed-neutron precursors. The point kinetics equations were used.[10]

The reactor power equation also includes reactivity feedbacks due to change in the fuel temperature, coolant temperature, and coolant pressure.

A simplified model, consisting of five state variables, is used to describe heat transfer processes in the reactor rather than a more detailed model (47 state variables) available at The University of Tennessee.[11] The detailed model has fifteen fuel lumps: five

TABLE III

PRESSURIZER DESIGN DATA*

1.	Design/Operating Pressure, psig	2485/2235
2.	Design/Operating Temperature, °F	680/653
3.	Surge Line Maximum Flow Rate, gpm	19,390
4.	Water Volume, Full Power, ft^3	780
5.	Steam Volume, Full Power, ft^3	520
6.	Electric Heater Capacity: kw (total)	1300
7.	Heat up Rate of Pressurizer, Hot Standby Condition, °F/hr	55
8.	Continuous Spray Rate, gpm	1.0
9.	Design Spray Rate, for Valves Full Open, gpm	840

*Reference 4, Table 4.1-3.

in the axial direction and three in the radial direction and thirty coolant lumps; two for each fuel lump. This model is very useful if one is interested in the detailed fuel and coolant temperature distribution in the core region.

The simplified version of the core heat transfer model is used here because it reduces computer costs and it gives results that compare favorably with results from a more detailed model. Calculations both in the time domain and in the frequency domain are much faster for the 12 x 12 matrix than for the 54 x 54 matrix. Also, the simplified model predicts reactor power and the reactor coolant core outlet temperature fairly accurately and is comparable with the detailed model. A comparison of the results obtained from both models, for a step input in reactivity, shown in Figure II-6. Both models assume constant inlet coolant temperature (no steam generator representation in this comparison of core models).

The five variables, in the simplified heat transfer model, include average fuel temperature and four nodes for coolant temperature; two in the core region, one in the upper plenum, and one in the lower plenum. The heat transfer from the fuel to the coolant is determined by the temperature difference between the average fuel and the average coolant temperatures in the core. The heat transferred from the fuel is evenly divided between the two coolant lumps. The schematic drawing of the heat transfer from fuel to the coolant is shown in Figure II-7.

Two equations that describe the lower plenum and the upper plenum temperature use the well stirred tank approach to determine the core inlet and the reactor coolant outlet temperatures. The differential equations used in the reactor model are shown in Appendix A.

The simplified steam generator model, used in the analysis, has five differential equations to determine the steam generator dynamics. The basic approach is described here and the detailed model description is given in Appendix B. Two differential equations describe primary side coolant temperatures in the inlet and the outlet plenums of the steam generator. The other three differential equations include: primary side coolant temperature, U-tube metal temperature, and steam pressure.

The equation for the primary side coolant temperature which describes heat transfer from the primary side coolant to the U-tube metal is derived from the energy balance in the primary side. The tube metal temperature is derived from the energy balance on the tube metal.

The steam pressure equation is derived from three differential and two algebraic equations. Three differential equations include: mass balance of water in the secondary side, mass balance of steam, and energy balance in the secondary side. The two algebraic equations are: gas law (equation of state) and volume balance of water and steam in the secondary side. The derivation of the steam pressure equation and other equations used in the steam generator model are shown in Appendix B.

The dynamic model of the pressurizer is similar to the model used for the shell and U-tube type steam generator. The pressurizer pressure equation was derived from the mass, energy, and volume balances of water and steam in the pressurizer. The derivation of the pressure equation is very similar to that of steam pressure equation in the steam generator model. The details are shown in Appendix C.

Transients in the pressurizer occur due to temperature changes in the primary side coolant. The primary side coolant temperatures are coupled to the pressure equation. One of the limitations of the pressurizer model used in the analysis is it does not include an automatic control system. The automatic control system maintains the pressure within the prescribed limits.

CHAPTER III

EXPERIMENTAL PROCEDURES AND DATA ANALYSIS

The general procedure for any frequency response test on a large system like the NSSS can be divided into four parts: (1) the patterns and types of the input signals are determined beforehand (This depends upon the frequency range of interest and the type of the information to be obtained from the tests.), (2) the selected input signals must be imposed upon the system, (3) the input signals and the resulting output signals are measured and recorded, and (4) the recorded signals are analyzed.

There are a number of ways in which one can perform each of the above steps. In this section, the methods used to obtain the frequency response results for the H. B. Robinson PWR will be presented.

I. TEST PATTERNS

Before determining the test patterns, one should take several things into consideration.[1,12]

1. The test should make maximum use of the plant hardware and instrumentation to minimize the cost and trouble to the utility company.
2. Large amplitudes for the input signals help to increase signal-to noise ratio, but the amplitude should be limited so that normal system operation is not distrubed.

3. Increasing the duration of the test also helps to diminish the effect of noise on the signals, but the duration of the test should be limited so that possible departure from the normal control policies is as brief as possible.
4. The noise contamination in the signals also influences the selection of the test signals. This occurs because the permissible signal amplitude and test duration determine the total signal energy available. Once these are fixed, the only way to increase the signal to noise ratio at any frequency is by adjusting the allocation of signal energy among the available frequencies. If the noise contamination is small, the available energy can be allocated to a number of frequencies. If the noise is large, the majority of the signal energy must be concentrated in a few harmonics.

Taking all these aspects into consideration, two types of signals were used to obtain the results. These were step input and multi-frequency binary sequence (MFBS) input.

A. Step Tests[1]

The step tests are useful in obtaining estimates of the frequency response if the output settles to a constant value after the step input. The useful energy in a test is limited, and it is usually not possible to obtain very large signal-to-noise ratios. However, the tests are easy to perform and are useful for augmenting more accurate tests such as those using periodic input signals.

The step tests were used both in the case of reactivity perturbation and the steam flow rate perturbation tests.

B. MFBS[1,13] (Multi-Frequency Binary Sequence)

The main advantage of the MFBS over other periodic test signals is that its spectrum can be tailored by the user to suit the test objectives. The MFBS signal can be concentrated in frequencies of interest with the result that the energy waste is minimized. This allows the maximum signal-to-noise ratio for a given test duration.

The MFBS signal is generated by a random search optimization of the polarities of the bits in the binary pulse chain (each pulse in the chain is called a bit). The criterion function to be minimized is the sum of the squared difference of the desired signal power and the actual signal power at the selected frequencies.

$$J = \sum_{i=1}^{N} (P_i - 2|C_i|^2)$$

where P_i is the desired power at the ith frequency and C_i is the complex Fourier coefficient of the binary signal at the ith frequency.

A computer code is available for generating the MFBS signals.[13] Experience shows that the procedure gives sequences which concentrate 70 to 80 percent of the total signal power in the selected harmonics.

For the MFBS signal, like any other periodic signal, the lowest frequency containing the information is, of course, the fundamental frequency,

$$w_0 = \frac{2\pi}{T}$$

where w_0 is the fundamental frequency in radians/second, and T is the period in seconds. The selected signals* with their important characteristics are given below.

---

*Most of the signal selection work was done by E. M. Katz.

1. 256 bit MFBS

   Bit duration (Δt) = 3 sec

   Period (T) = 768 sec

   Fundamental frequency = 8.181×10^{-3} rad/sec

   Number of frequencies = 12

   Selected harmonics: 1, 3, 5, 7, 9, 13, 17, 21, 25, 29, 33 and 37

   Highest frequency = 0.3027 rad/sec

   Sampling rate = 4 samples/sec

   Number of periods = 6

2. 128 bit MFBS

   Bit duration = 1 sec

   Period = 128 sec

   Fundamental frequency = 0.0491 rad/sec

   Number of frequencies = 12

   Selected harmonics: 1, 3, 5, 7, 9, 13, 17, 21, 25, 29, 33, and 37

   Highest frequency = 1.816 rad/sec

   Sampling rate = 10 samples/sec

   Number of periods = 17

3. 64 bit MFBS

   Bit duration = 20 sec

   Period = 1280 sec

   Fundamental frequency = 4.91×10^{-3} rad/sec

   Number of frequencies = 12

   Selected harmonics: 1, 3, 5, 7, 9, 11, 13, 15, 17, 19, 21, and 27

Highest frequency = 0.1325 rad/sec

Number of periods = 3

Two hundred fifty-six bit and one hundred twenty-eight bit MFBS signals were used for the reactivity perturbation tests and a 64 bit MFBS was used for the steam flow perturbation tests.

Since the purpose of this report is to describe the interpretation of the tests rather then the test procedures, the experimental procedures will be only briefly outlined here. The MFBS signals were introduced manually by the operator for the reactivity perturbation tests and for the steam valve perturbation tests. In each case, the desired pattern was pre-recorded on a strip chart recorder. A paper strip was taped to the window of the recorder as shown in Figure III-1. The operator watched the signal on the chart and moved the input in the specified direction when the move indication passed beneath the paper strip. This method allowed the operator to anticipate upcoming actions.

The operator used the rod control stick on the control panel in the reactivity tests. He had no trouble in obtaining either one step or two steps as requested by varying the length of time he held the control stick in the insert or withdraw position. The steam valve perturbation test used the steam flow servo. The control panel included a panel that had a steam flow demand set point adjuster. The operator could depress a button to increase or decrease the steam flow demand. After this was set, he could cause the steam flow change by depressing another button that caused the controller to seek the new point. The procedure was to adjust the set point between changes in steam flow and to depress the "GO" button when the change was desired.

The signals for the system responses were obtained at the junction box where signals entered the plant computer. These were low pass filtered, amplified, and fed to an ANSCAN digital data acquisition system. The ANSCAN digitized and recorded the signals and wrote a digital tape recording.

II. DATA ANALYSIS METHODS

The purpose of the dynamic tests was to determine the frequency response of a large PWR type NSSS. The digitized data from the ANSCAN tapes were analyzed to obtain frequency response, coherence function, and standard deviation, on the IBM-360/65 computer at The University of Tennessee.

The frequency response G(jw), at frequency, w, is given by the ratio of the Fourier transform of the output signal to the Fourier transform of the input signal

$$G(jw) = \frac{\int_0^T O(t)\, e^{-jwt}\, dt}{\int_0^T I(t)\, e^{-jwt}\, dt} . \qquad (1)$$

Here we have assumed a periodic input signal with period, T.
From Equation (1), we obtain:

$$G(jw) = \frac{\int_0^T O(t)\, \cos wt\, dt - j \int_0^T O(t)\, \sin wt\, dt}{\int_0^T I(t)\, \cos wt\, dt - j \int_0^T I(t)\, \sin wt\, dt} \qquad (2)$$

once, G(jw) is calculated using Equation (2), gain and phase may be obtained using the following relationships.

$$GAIN = |G(jw)| = \sqrt{[Re\ \{G(jw)\}]^2 + [Im\ \{G(jw)\}]^2} \qquad (3)$$

and

$$\text{PHASE} = \tan^{-1} [\text{Im } \{G(jw)\}/\text{Re } \{G(jw)\}] \qquad (4)$$

In the case of experimental results, the gain and phase were obtained by averaging real and imaginary values of the frequency response over different blocks of data. Each block contained one period of MFBS signal.

Two computer codes, using different methods, were used to calculate the frequency response results from the experimental data.

A. FOURCO[14]

FOURCO capitalizes on the similarity between the Fourier transform integral and the convolution integral for calculating Fourier transforms of the input and the output signals. This is done by a digital simulation of a sine-cosine filter. The method is very efficient and takes about one-third the time required for the direct integrations required in classical Fourier analysis. The analysis of 6 cycles of data of 256 bit MFBS with 3 sec bit duration (38,864 input and output data samples) required only 3 minutes and 48 seconds for calculating the frequency response for 12 different frequencies on the IBM-360/65.

B. HFFT[15]

HFFT uses a simple recursion relationship which gives a result that is easily transformed into the desired Fourier integrals. HFFT takes about the same computing time as FOURCO, but much less core storage. The analysis of three periods of the 256 MFBS with a 3 sec

bit duration (18,432 input and output data samples) required only 2.5 minutes and 72K core for the calculation of frequency response results for 12 different frequencies.

Since the Fourier transform of a signal that does not return to its initial value are not defined, methods used in HFFT or FOURCO need slight modifications to handle step response tests. A small computer code was written using the method suggested in Reference 1 to calculate the frequency response results from the step tests. The results were compared using another code, based on Samulon's method,[16] written at the Oak Ridge National Laboratory, and were found to agree.

The coherence function values discussed in Chapter IV are a measure of degree to which an output of the system is related to a selected input. Mathematically, the coherence function between the input I(t) and the output O(t) is a real valued function defined by[1]

$$\gamma^2_{IO} = \frac{|\phi_{IO}|^2}{\phi_{II}\,\phi_{OO}} \tag{5}$$

where

γ^2_{IO} = coherence function

ϕ_{II} = power-spectrum of the input signal

ϕ_{OO} = power-spectrum of the output signal

ϕ_{IO} = cross power spectrum of the input to the output signal

The coherence function is always between zero and one. For the ideal case of constant parameter linear system with only one input and one output and with no uncorrelated system noise, it is always unity. If I(t) and O(t) are completely unrelated, the coherence

function will be zero. If it is greater than zero, but less than unity, one or more of the following situations exists.[1,17]

1. Extraneous noise is present in the measurements.
2. The system relating I(t) and O(t) is a nonlinear system.
3. O(t) is an output due to an input I(t) as well as other parameters.

CHAPTER IV

EXPERIMENTAL RESULTS

In this chapter, experimental results obtained in the tests will be presented and discussed. The results will be divided into two parts for discussion and presentation purposes: reactivity perturbation and steam flow perturbation tests.

I. REACTIVITY PERTURBATION TESTS

The reactivity perturbation tests were carried out by moving a bank of control rods. Two different signals were used to obtain frequency response results: 256 bit, 2-step (the control rod bank containing five rods was moved two steps each time) MFBS with 3 second bit duration, and 128 bit, 1-step (the control rod bank was moved only one step each time) MFBS with 1 second bit duration.

During both tests, the following system variables were measured and recorded.

1. Reactor power (neutron level)
2. Reactor coolant (RC) core outlet temperature
3. RC hot leg temperature
4. RC cold leg temperature
5. Steam pressure
6. Pressurizer pressure
7. Steam generator level
8. Steam flow rate

9. Steam generator feedwater flow rate
10. Control rod position

Results obtained for the above system variables along with the input signal are presented, in the time domain, for one period of data, in Figures IV-1 through IV-6. It was noted that the rod position measured by the linear variable differential transformer (LVDT) had a bump in it every time the rods were inserted. Furthermore, the bump was observed to occur after the neutron flux signal had started its response to a rod position change. The bump is believed to be due to the interaction between the magnetic field from the CRDM and the LVDT. Since the rods actually move when the magnetic flux is generated at the CRDM; the signal from the LVDT is misleading because it gives the impression that the rods only start to move after the bump.[18] The apparent rod position signal was corrected as follows:

(1) The rod position (measured by the LVDT) and the neutron flux signals were plotted and the MFBS signal (as specified prior to the test) was superimposed on both rod position and flux signals. This is shown in Figure IV-7 for the 2-step test and in Figure IV-8 for the 1-step test.

(2) The next step in the data correction consisted of holding the MFBS signal in a fixed position on the time axis and shifting the neutron level signals back and forth, until the starting point of each transition indicated by the flux change agreed with the corrected MFBS transition as closely as possible.

3. After this shift of the time axis, there were still small differences between the apparent transition times observed in the neutron level and the MFBS signals. To remove this discrepancy, slight modifications in the number of points in each pulse of the MFBS signal were made so that the MFBS signal transitions would occur as closely as possible, at the same times as the start of the flux changes associated with the rod movement. In short, the MFBS signal was adjusted using the neutron level signal as a guide. The modified MFBS with the flux and rod position signals are shown in Figures IV-9A (2-step test) and Figure IV-9B (1-step test).

The apparent (measured) rod position and the actual rod position signal were analyzed to obtain a rod position frequency response correction factor (δ measured position/δ actual position). The correction factors for the 2-step are shown in Table IV-1 and for the 1-step are shown in Table IV-2.

System frequency responses were obtained using the measured rod position signal as the input and were corrected using the correction factor, at each frequency. For example, the reactor power to reactivity frequency response (Figure IV-19) was obtained as follows:

(1) δ neutron level/δ rod position (measured) was computed using FOURCO and HFFT computer codes.

(2) The corrected gains were obtained by multiplying the gains obtained in (1) by the correction factor, from Table IV-1

TABLE IV-1

CORRECTION FACTORS FOR 2-STEP TEST

Harmonic Number	Gain	Phase
1	1.0552	10.31
3	1.2394	- 3.54
5	1.1797	- 3.37
7	1.2513	- 6.49
9	1.1810	-11.36
13	1.1474	-17.66
17	1.1883	-17.81
21	1.2000	-23.10
25	1.1488	-30.14
29	1.1796	-32.62
33	1.1481	-36.01
37	1.2066	-42.04

TABLE IV-2

CORRECTION FACTORS FOR 1-STEP TEST

Harmonic Number	Gain	Phase
1	0.805	17.41
3	1.097	- 14.88
5	0.842	- 31.26
7	0.994	- 50.94
9	0.942	- 61.61
13	0.963	- 83.87
17	0.923	- 109.76
21	0.911	- 127.47
25	0.897	- 156.78
29	0.796	- 176.32
33	0.634	- 204.03
37	0.589	- 220.06

or IV-2 depending upon whether the case was a 2-step or 1-step test, and the correct phase was obtained by adding the correction factor for the phase, to the phase obtained in (1), from the appropriate table.

The tests were run for six periods of 256 bit, 2-step, MFBS and seventeen periods of 128 bit, 1-step, MFBS. An error was made in implementing the 2-step MFBS during the fourth period. The operator failed to move the rods at the proper time. This period was omitted for the data analysis purposes. The rest of the data were analyzed to give the frequency response, coherence function, and standard deviation.

FOURCO[14] and HFFT[15] computer codes were used to calculate the frequency response results. Both codes gave almost identical values. The slight differences are due to the different methods, used to calculate the Fourier coefficients in the codes. They are explained briefly in the Experimental Procedures chapter (Chapter III). Since the absolute values of gain are not available, the frequency response results were normalized at the third harmonic. The normalization factors are shown in Table IV-3.

The Bode plots for the reactor power (neutron level) to reactivity transfer function are shown in Figures IV-10. The experimental gain is in excellent agreement with the theoretical results. The plots of the phase have similar shapes, but the experimental values for the 2-step test are 10° to 27° less than the theoretical values in the frequency range of 0.0245 rad/sec to 0.3 rad/sec.

TABLE IV-3

NORMALIZATION FACTORS FOR REACTIVITY TESTS

Figure Number	2-Step Test	1-Step Test
IV-10	80.0	217.5
IV-11	80.0	216.5
IV-12A	4.45	22.2
IV-12B	4.45	22.2
IV-13	2.37	7.26
IV-14	1.83	3.9

The polar plot of the reactor power to reactivity frequency response is shown in Figure IV-11. The experimental and theoretical results are not as inconsistent as they seem to be. Here, the imaginary values of the experimental results are smaller and the real values are larger than the theoretical values at the corresponding frequencies. This is consistent with the agreement in gain (GAIN = $(Re^2 + Im^2)^{1/2}$) and the negative phase shift (PHASE = $\tan^{-1}$ (Im/Re)) observed between the experimental and the theoretical results shown in the Bode plots (Figures IV-10).

The coherence function for the reactor power to reactivity transfer function is shown in Figure IV-10. It was calculated using HFFT. As expected, the coherence function is very close to unity for the 2-step MFBS, and it is lower (between 0.86 and 0.96 at all points except one) for the 1-step MFBS signal. Here, the signal-to-noise ratio is lower than in the 2-step MFBS because the reactivity input for the 2-step test is about twice as large as in the 1-step test.

Other frequency response results and coherence functions for some of the important variables are shown in Figures IV-12 through IV-14. Most of the results are in good agreement with the theoretical results.

Since the time constants for the thermocouples used measuring temperatures in the loop are large, the effects of thermocouple dynamics were taken into account in calculating cold leg temperature to reactivity frequency response. The corrected results are shown in Figure IV-12B. Here, the thermocouple time constant was taken to

be 3 seconds.[18] Since the harmonic frequencies are low ($\leq$ 0.3025 rad/sec) the effects of thermocouple response on the experimental results is not very significant.

In the case of the cold leg temperature, we observe a slight disagreement in predicted and experimental results. The break frequency predicted by the model is 0.1 rad/sec, while the experimentally observed break frequency is about 0.05 rad/sec. Here, the break frequencies were obtained by visual inspection. The phase is in good agreement with the experimental results, except the phase shift of about 35° at high frequencies. This could be due to transport lags not considered in the model.[19] The coherence function for the cold leg temperature/reactivity frequency response is above 0.74 for the 2-step test while it is too low for reliable results in the case of 1-step test. Here, the input signal is not strong enough to overcome the effect of uncorrelated system noise.

The model has been able to predict both steam pressure and pressurizer pressure signals fairly accurately.

Figures IV-15 through IV-18 contain information on the standard deviations of neutron level, RC cold leg temperature, steam pressure, and pressurizer pressure. Each of five periods of data was analyzed separately. Results from these analyses were used to calculate standard deviations. The standard deviation was calculated using the following formula[20]

$$\sigma = \sum_{i=1}^{N} (x_i - \bar{x})^2/(N - 1) \qquad (6)$$

where

σ = standard deviation

N = number of data periods

x_i = value for each period

$\bar{X}$ = average x_i

The plots of the standard deviations are shown on a different scale than the frequency response plots, since the frequency response results were normalized to agree with the theoretical results at a selected frequency. For most of the harmonics, the standard deviation for the reactor power to rod position transfer function is within 10 percent of the average values of the gain. The phase shows more deviations from the average values. For the other signals, the standard deviation of the phase is around 10 percent while the gain shows more deviations.

II. STEAM FLOW PERTURBATION TESTS

The steam flow perturbation tests were performed using the main steam valve. A 64-bit MFBS signal with 20 second bit duration and steam valve step tests were used to obtain the frequency response results. The same approach was used in the data analysis as in the case of the reactivity perturbation tests except the first stage turbine pressure was used as an input signal. Since the first stage turbine pressure is proportional to the steam flow rate and also to the plant load, this will enable us to study both the steam generator dynamics and the load following capability of the PWR steam supply system.

The main purpose of the steam valve step test was to obtain results that emphasize the steam generator characteristics. Plots of the step tests are shown in Figures IV-19, IV-20, and IV-21. Most

of the results except the steam pressure, steam flow rate, and the cold leg temperature contain too much noise to be of value.

A time delay of about 9 to 14 sec was observed between the opening of the steam throttle valve and the response of RC cold leg temperature signal. The time delay is much longer than the transport time which is about 2 to 3 seconds. The pressurizer pressure is shown in Figure IV-21. The pressure changes because of volume changes of the primary water in the steam generator that accompany water temperature changes. Because the pressure sensors are fast, there is no concern with sensor dynamics in the case of the pressure signal. The pressure signal is noisy, but these results suggest a time delay in the response, giving added confidence in the delay indicated by the cold leg temperature response.

A similar time delay in the cold leg temperature was observed by G. Frei, et al.[21] in measurements on the Stade PWR in Germany. The simplified steam generator model used in the analysis or none of the other steam generator dynamic models known explain the sluggishness of the primary side coolant temperature. The steam generator model used in Reference 21 simulates the delay using an emperical pure time delay.

The delay phenomenon requires further study, but several possible factors in the process are:

1. Reactor coolant transport time which is about 2 to 3 seconds.
2. The tube and piping metals and the secondary water in the steam generator has fairly large thermal capacity which also contributes to the delay.

3. Pressure changes accompany the load changes, causing shrink or swell. For example, when the throttle valve is opened, the steam pressure decreases causing submerged bubbles to expand. This causes the boundary between the subcooled liquid section and boiling section to rise temporarily before the increased boiling rate causes the level to drop. This temporary rise causes a larger fraction of the heat transfer to be metal-to-liquid rather than nucleate boiling. This may reduce the overall metal-to-secondary heat transfer coefficient until the swell transient is completed. This effect has an opposite influence on heat transfer than the increased temperature difference that accompanies a pressure decrease. This compensation might result in a reduced effect on the primary fluid temperature until the level starts to drop.[18]

Results obtained from the 64 bit steam valve MFBS are shown in Figures IV-22 through IV-24. The frequency response results and the coherence functions for some of the important system variables are shown in Figures IV-25 through IV-28. The frequency response results were normalized at a frequency of 0.0147 rad/sec.

Most of the results are in good agreement with theoretical results. RC cold leg temperature shows considerable sluggishness which can be observed both in the time domain (Figure IV-23) and in the frequency domain (Figure IV-26) confirming our observation in the steam valve step tests. Figure IV-26 also shows considerable phase shift, about 60° at 0.0147 rad/sec to about 90° at 0.13 rad/sec.

Here, the pressurizer model fails to predict the results at low frequencies, below 0.02 rad/sec. The gain for the experimental results seems to be dropping while the model predicts it to be constant. A possible reason for such behavior could be the automatic control system which is not included in the model. The automatic control system plays an important role in controlling the pressure at low frequencies. Also, examination of the time response plots (Figures IV-21 and IV-23) shows that the pressurizer pressure initially moves in the same direction as the turbine first stage pressure, but after reacting its maximum value, it starts moving in the other direction, even when the turbine pressure is still unchanged.

The plots of the standard deviations of the results for three periods of data are included in Figures IV-29 through IV-32. The deviations in the gain are within 13 percent of the average values except for the reactor power and cold leg temperature.

CHAPTER V

CONCLUSIONS

The purpose of this work was to analyze and interpret experimental measurements of the frequency response of a large PWR type steam supply system using binary signals. The experimental frequency response and theoretical results (predicted with a preliminary simple model) are in fair agreement for most cases.

The coherence functions for the 1-step MFBS were very low except in the case of the neutron level signal. This is due to small reactivity input. The input signals with larger perturbations increase the signal-to-noise ratio and increase the confidence in the experimental results. The 2-step test and the steam valve tests gave good results except the problem of obtaining absolute values of the gain. The gain was normalized to agree with the theoretical predictions at a selected frequency.

During the steam flow perturbation tests, a considerable time delay was observed between opening (and closing) of the steam valve and the response of the RC cold leg temperature. Further study should be made of this to determine the cause. A further effort also needs to be made to study the low frequency pressurizer pressure results and the phase shifts in some of the signals.

Dynamic testing provides information on the adequacy of the model and in evaluating the performance of the nuclear systems. The experience gained in this work suggests that the binary signals should

play an important role in performing the dynamic tests on the commercial power reactors.

LIST OF REFERENCES

LIST OF REFERENCES

1. Kerlin, T. W., Frequency Response Testing in Nuclear Reactors, Academic Press, New York (1974).

2. Leech, W. D., "HTGR Dynamic Modeling and Testing," Proceedings of Power Plant Dynamics, Control and Testing, Knoxville, Tennessee (October 1973).

3. Mashe, George, System Summary of Westinghouse Pressurized Water Reactor Power Plant, Westinghouse Nuclear Energy Systems, Pittsburgh, Pennsylvania (1971).

4. Final Facility Description and Safety Analysis Report, Vol. 1, H. B. Robinson Unit No. 2, Carolina Power and Light Company.

5. Schultz, M. A., Control of Nuclear Reactors and Power Plants, McGraw Hill Book Company, New York (1961).

6. RESAR, Reference Safety Analysis Report, Vol. 1, Westinghouse Nuclear Energy System, Pittsburgh, Pennsylvania (1970).

7. Ali, M. R., Personal communication (November 1973).

8. Pressurized Water Reactor Technology, Vol. 1, Babcock and Wilcox Company, Lynchburg, Virginia (1971).

9. Thomas, A. W., and J. A. Findaly, "PRE - A Pressurized Transient Program for the Philco 2000 Computer," KAPL Report, KAPL-M-EC-7, UL-32 (1961).

10. Glasstone, S., and A. Sesonske, Nuclear Reactor Engineering, Van Nostrand Reinhold Company, New York (1962).

11. Katz, E. M., Personal communication (June 1973).

12. Kerlin, T. W., "Frequency Response Testing," Nuclear Safety 8(4): 339-345 (1967).

13. Buckner, M. R., "Optimum Binary Signals for Frequency Response Testing," Doctoral Dissertation, Nuclear Engineering Department, The University of Tennessee, Knoxville, Tennessee (1970).

14. Ball, S. J., "A Digital Filtering Technique for Efficient Fourier Transform Calculations," USAEC Report, ORNL-TM-1778, Oak Ridge National Laboratory (1967).

15. Chang, S. I., "HFFT - A Method for Digital Fourier Analysis," Nuclear Engineering Department, The University of Tennessee, Knoxville, Tennessee (1973).

16. Samulon, H. A., "Spectrum Analysis of Transient Response Curves," Proceedings of Institute of Radio Engineers, Inc., Vol. 39, No. 2: 175-186 (February 1951).

17. Bendat, J. S. and A. G. Pierson, Measurement and Analysis of Random Data, John Wiley and Sons, Inc., New York (1966).

18. Kerlin, T. W., Personal communication, (November 1973).

19. Ball, S. J., Personal communication, (September 1973).

20. Sololnikoff, I. S. and R. M. Redheffer, Mathematics for Physics and Morden Engineering, McGraw-Hill Book Company, New York (1958).

21. Frei, G., J. Weber, and F. Hirmer, "Dynamics Behavior of 660 Mw Nuclear Power Station," Proceedings of the International Conference on Boiler Dynamics and Control in Nuclear Power Stations, British Nuclear Energy Society, 5.1 - 5.6 (March 1973).

22. Kerlin, T. W., "Class Notes on System Dynamics (NE 5210)," The University of Tennessee Nuclear Engineering Department (1971).

APPENDICES

APPENDIX A

REACTOR MODEL

The differential equations used in the reactor model are:

Reactor power;

$$\frac{d\delta P}{dt} = -\frac{\beta_T}{\Lambda}\delta P + \sum_{i=1}^{6} \lambda_i \delta C_i + \frac{\alpha_f P_0}{\Lambda}\delta T_f + \frac{\alpha_c P_0}{2\Lambda}\delta \theta_{c1}$$

$$+ \frac{\alpha_c P_0}{2\Lambda}\delta \theta_{c2} + \frac{\alpha_p P_0}{\Lambda}\delta P_p + \frac{P_0}{\Lambda}\delta\rho_{ext} \qquad \text{(A-1)}$$

where,

P = reactor power, Mwt

β_T = total delayed neutron fraction

Λ = prompt neutron generation time, sec

λ_i = delayed neutron decay constant for ith group, sec^{-1}

C_i = ith group delayed neutron precursor concentration

α_f = Doppler coefficient, ($\delta\rho$/°F)

P_0 = steady state reactor power, Mwt

T_f = fuel temperature, °F

α_c = moderator temperature coefficient of reactivity, ($\delta\rho$/°F)

θ_c = reactor coolant temperature, °F

α_p = moderator pressure coefficient, ($\delta\rho$/psi)

P_p = pressurizer pressure, psia

$\delta\rho_{ext}$ = external reactivity, due to control rod movement

Delayed neutron precursors,

$$\frac{d\delta C_i}{dt} = \frac{\beta_i}{\Lambda} \delta P - \lambda_i \delta C_i \qquad i = 1, 2, \ldots, 6 \tag{A-2}$$

where β_i = delayed neutron fraction for the ith group

Average fuel temperature,

$$\frac{d\delta T_f}{dt} = \frac{P_f}{(M C_p)_f} \delta P - \frac{(hA)_{f-c}}{(M C_p)_f} (\delta T_f - \delta \theta_{cl}) \tag{A-3}$$

where

P_f = fraction of power generated in the fuel

M = mass of fuel, lbm

C_p = specific heat, mw - sec/lbm°F

h = overall heat transfer coefficient from fuel to coolant, mw/ft^2°F

A = heat transfer area in the core, ft^2

Reactor coolant temperatures:

Lower plenum coolant temperature,

$$\frac{d\delta\theta_{\ell.p.}}{dt} = \frac{W}{M_{\ell.p.}} \delta\theta_{c.\ell.} - \frac{W}{M_{\ell.p.}} \delta\theta_{\ell.p.} \tag{A-4}$$

$\theta_{\ell.p.}$ = reactor coolant temperature in the lower plenum, °F

W = reactor coolant mass flow rate, lb/sec

$M_{\ell.p.}$ = mass of coolant in the lower plenum, lb

$\theta_{c.\ell.}$ = reactor coolant cold leg temperature, °F

Average coolant temperature in the core, (The schematic drawing of heat transfer from fuel to coolant is shown in Figure II-7.)

$$\frac{d\delta\theta_{c1}}{dt} = \frac{P_{c1}}{(M\,C_p)_c}\ \delta P + \frac{(hA)_{f-c}}{(M\,C_p)_c}\ (\delta T_f - \delta\theta_{c1})$$

$$- \left(\frac{2W}{M}\right)_c\ (\delta\theta_{c1} - \delta\theta_{\ell.p.}) \qquad \text{(A-5)}$$

P_c = fraction of power generated in the coolant

M = mass of coolant in the core, lb.

Core outlet coolant temperature,

$$\frac{d\delta\theta_{c2}}{dt} = \frac{P_{c2}}{(M\,C_p)_c}\ \delta P + \frac{(hA)_{f-c}}{(M\,C_p)_c}\ (\delta T_f - \delta\theta_{c1})$$

$$- \left(\frac{2W}{M}\right)\ (\delta\theta_{c2} - \delta\theta_{c1}) \qquad \text{(A-6)}$$

Upper plenum coolant temperature,

$$\frac{d\delta\theta_{u.p.}}{dt} = \frac{W}{M_{u.p.}}\ \delta\theta_{c2} - \frac{W}{M_{u.p.}}\ \delta\theta_{u.p.} \qquad \text{(A-7)}$$

$\theta_{u.p.}$ = reactor coolant temperature in the upper plenum, °F

$M_{u.p.}$ = mass of coolant in the upper plenum, lb

The reactor is coupled to the steam generator using the following equation,

$$\frac{d\delta\theta_{h.L.}}{dt} = \frac{1}{\tau_{h.L.}}\ \delta\theta_{u.p.} - \frac{1}{\tau_{h.L.}}\ \delta\theta_{h.L.} \qquad \text{(A-8)}$$

$\theta_{h.L.}$ = coolant hot leg temperature, °F

$\tau_{h.L.}$ = coolant residence time in the hot leg, sec

The responses of the reactor for the step input in reactivity, and reactor coolant inlet temperature are shown in Figures A-1 and A-2.

APPENDIX B

STEAM GENERATOR MODEL

The equations used in the steam generator model are:

Primary side coolant temperature,

$$\frac{d\delta T_p}{dt} = \frac{W_p}{M_p}\delta\theta_{i.p.} - \frac{h_{pm}\,A_{pm}}{M_p\,C_p}(\delta T_p - \delta T_m) - \frac{W_p}{M_p}\delta T_p \qquad \text{(B-1)}$$

T_p = primary side coolant temperature, °F

W_p = primary coolant flow rate, lb/sec

M_p = mass of the primary coolant in the steam generator, lb

h_{pm} = primary side to U-tube metal heat transfer coefficient, Btu/sec-ft^2 °F

A_{pm} = primary side to U-tube metal heat transfer area, ft^2

T_m = U-tube metal temperature, °F

$\theta_{i.p.}$ = reactor coolant temperature in the inlet plenum, °F

U-tube metal temperature,

$$\frac{d\delta T_m}{dt} = \frac{h_{pm}\,A_{pm}}{M_m\,C_{pm}}(\delta T_p - \delta T_m) - \frac{h_{ms}\,A_{ms}}{M_m\,C_{pm}} * \left[\delta T_m - \left(\frac{\partial T_{sat}}{\partial P_s}\right)\delta P_s\right] \qquad \text{(B-2)}$$

M_m = mass of U-tube metal, lb

h_{ms} = metal to secondary side heat transfer coefficient, Btu/sec-ft^2 °F

A_{ms} = metal to secondary side heat transfer area, ft^2

$\left(\frac{\partial T_{sat}}{\partial P_s}\right)$ = slope of saturation temperature to saturation pressure curve, °F/psia

P_s = saturation or steam pressure, psia

Derivation of steam pressure equation, mass balance:

Water:

$$\frac{d\delta M_w}{dt} = \delta W_i - \delta W_s \qquad \text{(B-3)}$$

M_w = mass of the secondary side water in the steam generator, lb

W_i = secondary side water flow rate, lb/sec

W_s = steam generation rate, lb/sec

Steam:

$$\frac{d\delta M_s}{dt} = \delta W_s - \delta W_{s,o} \qquad \text{(B-4)}$$

M_s = mass of steam in the steam generator, lb

$W_{s,o}$ = steam flow rate to the turbine, lb/sec

Assuming,

$$W_{s,o} \propto \sqrt{P_s - P_T}$$

where,

P_T = turbine 1st stage pressure, psia

$$W_{s,o} = \varepsilon \sqrt{P_s - P_T}$$

ε = orifice coefficient, lbm/(sec $psi^{1/2}$)

Linearizing

$$\delta W_{s,o} = \varepsilon' (\delta P_s - \delta P_T) \qquad \text{(B-5)}$$

where

$$\varepsilon' = \varepsilon^2 / 2W_{s,o}$$

substituting (B-5) into (B-4)

$$\frac{d\delta M_s}{dt} = \delta W_s - \varepsilon' (\delta P_s - \delta P_T) \tag{B-6}$$

Energy balance:

Assuming both secondary side water and steam are at saturation temperature corresponding to the steam pressure,

$$\frac{d\delta E}{dt} = h_{ms} A_{ms} (\delta T_m - \delta T_{sat}) + W_i C_p$$

$$* (\delta T_i - \delta T_{sat}) - h_s \delta W_{s,o} \tag{B-7}$$

E = secondary side heat content, Btu

T_i = secondary side water inlet temperature, °F

h_s = specific enthalpy

Equation of state (gas law)

$$P_s V_s = RM_s T_s \tag{B-8}$$

V_s = steam volume, ft^3

R = gas constant for steam, $(\frac{lbf - ft}{lbm - °F}) * z$

z = compressibility factor, (PV/RT)

Volume balance:

$$\delta V_w + \delta V_s = 0 \tag{B-9}$$

V_w = volume of secondary water, ft^3

From B-8 and B-9

$$\delta P_s = A \delta M_s + B \delta M_w \tag{B-10}$$

where

$$A = R\ T_s/(V_{s,o} - R\ M_{s,o}\ (\partial T_s/\partial P_s))$$

and

$$B = P_{s,o}/\rho_w\ (V_{s,o} - R\ M_{s,o}\ (\partial T_s/\partial P_s))$$

ρ_w = density of water, lb/ft^3

From B-10

$$\frac{d\delta P_s}{dt} = A\ \frac{d\delta M_s}{dt} + B\ \frac{d\delta M_w}{dt} \qquad \text{(B-11)}$$

substituting for δP_s (from B-10 into B-6)

$$\frac{d\delta M_s}{dt} = \delta W_s - \varepsilon'\ (A\ \delta M_s + B\ \delta M_w) + \varepsilon'\ \delta P_T. \qquad \text{(B-12)}$$

From B-3 and B-12

$$\frac{d\delta M_w}{dt} = \delta W_i - \{\varepsilon'\ (A\ \delta M_s + B\ \delta M_w) + \frac{d\delta M_s}{dt} - \varepsilon'\ \delta P_T\}. \qquad \text{(B-13)}$$

From B-11 and B-13

$$\frac{d\delta M_w}{dt}\ (1 - B/A) + \frac{1}{A}\ \frac{d\delta P_s}{dt} = \delta W_i - \varepsilon'\ \delta P_s + \varepsilon'\ \delta P_T. \qquad \text{(B-14)}$$

Taking

$$E = C_p\ M_w\ T_s + u_s\ M_s \text{ and}$$

differentiating

$$\frac{d\delta E}{dt} = C_p\ M_{w,o}\ \left(\frac{\partial T_s}{\partial P_s}\right)\ \frac{d\delta P_s}{dt} + C_p\ T_s\ \frac{d\delta M_w}{dt} + u_s\ \frac{d\delta M_s}{dt}\ . \qquad \text{(B-15)}$$

From B-15 and B-7

$$\frac{d\delta E}{dt} = C_p M_{w,o} \left(\frac{\partial T_s}{\partial P_s}\right) \frac{d\delta P_s}{dt} + C_p T_s \frac{d\delta M_w}{dt} + u_s \frac{d\delta M_s}{dt}$$

$$= h_{ms} A_{ms} \delta T_m - \{(h_{ms} A_{ms} + W_i C_p) \left(\frac{\partial T_s}{\partial P_s}\right)\}$$

$$* \delta P_s + W_i C_p \delta T_i - h_s \{\varepsilon' \delta P_s + \frac{1}{A} \frac{d\delta P_s}{dt}$$

$$- B/A \frac{d\delta M_w}{dt} - \varepsilon' \delta P_T\}. \qquad \text{(B-16)}$$

Simplifying B-16

$$\{C_p M_{w,o} \left(\frac{\partial T_s}{\partial P_s}\right) + \frac{h_s}{A}\} \frac{d\delta P_s}{dt} + \{C_p T_s - \frac{h_s B}{A}\}$$

$$* \frac{d\delta M_w}{dt} = h_{ms} A_{ms} \delta T_m - \{(h_{ms} A_{ms} + W_i C_p)$$

$$* \left(\frac{\partial T_s}{\partial P_s}\right) + h_s \varepsilon'\} \delta P_s + W_i C_p \delta T_i . \qquad \text{(B-17)}$$

From Equations B-14 and B-17, we can obtain a simple first order equation for the steam pressure

$$\{\frac{C_p M_w (\partial T_s/\partial P_s) + h_s A}{C_p T_s - h_s B/A} - \frac{1}{A - B}\} \frac{d\delta P_s}{dt}$$

$$= \{\frac{(h_{ms} A_{ms} + W C_p) * (\partial T_s/\partial P_s) + h_s \varepsilon'}{C_p T_s - h_s B/A} - \frac{\varepsilon'}{(1 - B/A)}\}$$

$$* \delta P_s + \frac{h_{ms} A_{ms}}{(C_p T_s - h_s B/A)} \delta T_m$$

$$+ \frac{W_i C_p}{(C_p T_s - h_s B/A)} \delta T_i - \frac{1}{(1 - B/A)} \delta W_{FW}$$

$$- \frac{\varepsilon'}{(1 - B/A)} \delta P_T \,. \qquad \text{(B-18)}$$

Temperatures in the inlet and outlet plenums of the steam generator are modeled using the following differential equations.

Inlet plenum:

$$\frac{d\delta\theta_{i.p.}}{dt} = \frac{W_p}{M_{i.p.}} \delta\theta_{h.L.} - \frac{W_p}{M_{i.p.}} \delta\theta_{i.p.} \qquad \text{(B-19)}$$

$\theta_{i.p.}$ = reactor coolant temperature in the inlet plenum, °F

$M_{i.p.}$ = mass of primary water in the inlet plenum, lbm

Outlet plenum:

$$\frac{d\delta\theta_{o.p.}}{dt} = \frac{W_p}{M_{o.p.}} \delta T_p - \frac{W_p}{M_{o.p.}} \delta\theta_{o.p.} \qquad \text{(B-20)}$$

$\theta_{o.p.}$ = reactor coolant temperature in the outlet plenum, °F

$M_{o.p.}$ = mass of primary water in the outlet plenum, lbm.

The response of isolated steam generator for the step input in the primary side temperature and lst stage turbine pressure are shown in Figures B-l and B-2.

The steam generator is coupled to the reactor using the following equation.

$$\frac{d\delta\theta_{c.\ell.}}{dt} = - \frac{1}{\tau_{c.\ell.}} \delta\theta_{c.\ell.} + \frac{1}{\tau_{c.\ell.}} \delta T_p \qquad \text{(B-21)}$$

$\theta_{c.\ell.}$ = reactor coolant cold leg temperature, °F

$\tau_{c.\ell.}$ = coolant residence time in the cold leg, sec

APPENDIX C

PRESSURIZER MODEL

The pressurizer pressure equation is derived from the mass, energy, and volume balance on the water and steam in the pressurizer. The derivation is shown below.

The following assumptions were made in deriving the pressurizer pressure equation:

1. Both water and steam in the pressurizer are always at the saturation temperature corresponding to the reactor coolant pressure.
2. No heat losses through the pressurizer wall and pipings.
3. The automatic control system including the relief valve and the safety valves are omitted to simplify the model.

A schematic of the pressurizer is shown in Figure C-1.

Mass balance:

Water:

$$\frac{d\delta M_w}{dt} = \delta W_{w,i} + \delta W_{sp} - \delta W_s \qquad \text{(C-1)}$$

M_w = mass of water in the pressurizer, lb

$W_{w,i}$ = mass flow rate to or from the primary loop, lb/sec

W_{sp} = spray flow rate, lb/sec

W_s = steam generation rate, or condensation rate, lb/sec

Steam:

$$\frac{d\delta M_s}{dt} = \delta W_s \qquad \text{(C-2)}$$

Energy balance:

$$\frac{dE_w}{dt} = q + W_{w,i}\, h_{w,i} + W_{sp}\, h_{sp} - W_s h_s + P\dot{V}_w \qquad \text{(C-3)}$$

q = heat input from the electric heaters, btu/sec

h = enthalpy, btu/lb

P = pressure, psia

V_w = volume of water, ft^3

$$\frac{dE_s}{dt} = W_s h_s - P\dot{V}_s \qquad \text{(C-4)}$$

Volume balance:

$$\delta V_w + \delta V_s = \delta V_T = 0 \qquad \text{(C-5)}$$

V_s = steam volume, ft^3

Substituting the following equalities in Equation C-3 and linearizing

$$E = H - PV = U = Mu$$

$$\delta u = (\partial u/\partial P)\, \delta P$$

$$\delta v_w = (\partial v_w/\partial P_w)\, \delta P_w$$

$$h_{fg} = h_s - h_w$$

$$\delta h = C_p\, \delta T$$

$$\delta T_w = (\partial T_w/\partial P_w)\, \delta P_w$$

v_w = specific volume of water, ft^3/lb

h_{fg} = heat of vaporization, btu/lb

T_w = water temperature, °F.

Assuming

$$T_w = T_s = T_{sat}$$

$$P_p = P_w = P_s = P_{sat}$$

T_s = steam temperature, °F

P_s = steam pressure, psia

P_{sat} = saturation pressure corresponding to the saturation temperature

$$\{M_{w,o} \left(\frac{\partial u_w}{\partial P_p}\right) + M_{w,o} P_{p,o} \left(\frac{\partial v_w}{\partial P_p}\right)\} \frac{d\delta P_p}{dt} = \delta q$$

$$+ (h_{w,i} - h_w + P_p v_w)_o \delta W_{w,i} + (h_{sp} - h_w$$

$$+ P_p v_w)_o \delta W_{sp} - (h_{fg} + P_p v_w)_o \delta W_s$$

$$+ W_{w,o} C_p \delta T_{w,i} + W_{sp,o} C_p \delta T_{sp} + [W_{w,o} \{-C_p$$

$$* (\partial T_w/\partial P_p) + P_{p,o} (\partial v_w/\partial P_p) + v_{w,o}\}$$

$$+ W_{sp,o} \{-C_p (\partial T_w/\partial P_p) + P_{p,o} \left(\frac{\partial v_w}{\partial P_p}\right) + v_{w,o}$$

$$- \{P_{p,o} (\partial v_w/\partial P_p) + v_{w,o}\} W_{s,o}] \delta P_p. \qquad \text{(C-6)}$$

Equation of state (gas law)

$$P_s V_s = R M_s T_s \qquad \text{(C-7)}$$

R = Gas constant for the steam, lb_f - ft/lbm - °F.

From (C-5) and (C-7)

$$\delta P_s = A\ \delta M_s + B\ \delta M_w \tag{C-8}$$

where,

$$A = R\ T_s/(V_{s,o} - R\ M_{s,o}\ (\partial T_s/\partial P_s)) \text{ and}$$

$$B = P_{s,o}/\rho_w\ (V_{s,o} - R\ M_{s,o}\ (\partial T_s/\partial P_s)).$$

From (C-8)

$$\frac{d\delta P_s}{dt} = A\ \frac{d\delta M_s}{dt} + B\ \frac{d\delta M_w}{dt}\ . \tag{C-9}$$

From (C-9) and (C-2)

$$\delta W_s = \frac{1}{A}\ \frac{d\delta P_p}{dt} - B/A\ \frac{d\delta M_w}{dt} \tag{C-10}$$

substituting (C-10) in (C-1)

$$\frac{d\delta M_w}{dt}\ (1 - B/A) + \frac{1}{A}\ \frac{d\delta P_p}{dt} = \delta W_{w,i} + \delta W_{sp}$$

or

$$\frac{d\delta M_w}{dt} = \frac{(\delta W_{w,i} + \delta W_{sp})}{(1 - B/A)} - \left(\frac{1}{(A-B)}\right)\ \frac{d\delta P_p}{dt}\ . \tag{C-11}$$

From (C-7), (C-10), and (C-11)

$$\{M_{w,o}\ \left(\frac{\partial u_w}{\partial P_p}\right) + M_{w,o}\ P_{p,o}\ \left(\frac{\partial v_w}{\partial P_p}\right) + \frac{(h_{fg} + Pv_w)_o}{A}$$

$$+ \frac{(h_{fg} + Pv_w)_{,o} \; B}{A(A-B)}\} \; \frac{d\delta P_p}{dt} =$$

$$[W_{w,o} \{-C_p \; (\partial T_w / \partial P_p) + P_{p,o} \; (\frac{\partial v_w}{\partial P_p}) + v_{w,o}\}$$

$$+ W_{sp,o} \{-C_p \; (\partial T_w / \partial P_p) + P_{p,o} \; (\frac{\partial v_w}{\partial P_p}) + v_{w,o}\}$$

$$- W_{s,o} \{P_{p,o} \; (\frac{\partial v_w}{\partial P_p}) + v_{w,o}\}] \; \delta P_p$$

$$+ \delta q + \{h_{w,i} - h_{w,o} + P_{p,o} \; v_{w,o} +$$

$$\frac{B \; (h_{fg} + Pv_w)_o}{A - B}\} \; \delta W_w + \{h_{sp,o}$$

$$- h_{w,o} + P_{p,o} \; v_{w,o} + \frac{B \; (h_{fg} + P_p \; v_w)_o}{A - B}\}$$

$$* \; \delta W_{sp} + C_p \; W_{w,o} \; \delta T_{w,i} + C_p \; W_{sp,o} \; \delta T_{sp} \; . \qquad \text{(C-12)}$$

δW_w in Equation (C-12) represents insurge into the pressurizer or outsurge from the pressure depending upon the increase or decrease in the primary side coolant temperature, and it is equal to

$$\delta W_w = \sum_{i=1}^{N} V_i \beta_i \; \frac{\delta \theta_{c,i}}{dt} \qquad \text{(C-13)}$$

The index i represents the location of reactor coolant nodes at various points in the loop and

β_i = slope of coolant density vs. coolant temperature curve, lbm/ft^3, °F

V_i = steady state coolant volume corresponding to the ith node.

The response of the pressurizer for the step changes in the surge rate, δW_w, spray rate, δW_{sp}, and heat input rate, δq, are shown in Figures C-2 through C-4 .

APPENDIX D

OVERALL SYSTEM MODEL

The overall system consisting of equations from the reactor, steam generator, and pressurizer models can be represented, using the state variable approach,[22] as follows:

$$\frac{d\bar{X}}{dt} = \bar{\bar{A}}\,\bar{X} + \bar{f}$$

where

$$\bar{X} = \begin{bmatrix} \delta P \\ \delta C_1 \\ \delta C_2 \\ \delta C_3 \\ \delta C_4 \\ \delta C_5 \\ \delta C_6 \\ \delta T_f \\ \delta \theta C1 \\ \delta \theta C2 \\ \delta \theta_{u.p.} \\ \delta \theta_{i.p.} \\ \delta T_p \\ \delta T_m \\ \delta P_s \end{bmatrix}$$

(continued on next page)

$\delta\theta_{o.p.}$

$\delta\theta_{L.P.}$

$\delta\theta_{h.L.}$

$\delta\theta_{c.L.}$

δP_p

$\bar{\bar{A}}$ = constant coefficient matrix

$\bar{f}$ = forcing vector

Nonzero elements of the coefficient matrix are given in Table D-1. The nonzero elements of the forcing vector must also be specified for each type of perturbation. The forcing vector is 1.475×10^{-4} $\delta\rho$ in row 1 for a reactivity perturbation, -0.17024 δP_T in row 15 for a turbine pressure change, -0.03076 δW_{FW} for a feedwater flow change, and 0.05327 $\delta\theta_{FW}$ for a feedwater temperature perturbation. The system can also be perturbed by -7.989×10^{-3} δW_{SP} in row 20 for spray flow rate change and 2.1726×10^{-4} δq for electric heat input change in the pressurizer.

The response of the overall system consisting of a reactor, a steam generator, and a pressurizer using the above A-matrix is shown in Figures D-1 through D-6 (pp. 118 - 123).

TABLE D-1

NONZERO ELEMENTS OF $\bar{\bar{A}}$ MATRIX

Row Number	Column Number	Elements	Obtained From Equation
1	1	-400.000	A-1
1	2	0.0125	A-1
1	3	0.0305	A-1
1	4	0.11100	A-1
1	5	0.30100	A-1
1	6	1.140	A-1
1	7	3.010	A-1
1	8	-1781.000	A-1
1	9	-13700.000	A-1
1	10	-13700.000	A-1
1	20	411.00	A-1
2	1	13.1250	A-2
2	2	-0.0125	A-2
3	1	87.500	A-2
3	3	-0.0305	A-2
4	1	78.125	A-2
4	4	-0.11100	A-2
5	1	158.125	A-2
5	5	-3.010	A-2
6	1	46.250	A-2
6	6	-1.140	A-2

TABLE D-1 (continued)

Row Number	Column Number	Elements	Obtained From Equation
7	1	16.8750	A-2
7	7	-3.010	A-2
8	1	0.0756	A-3
8	8	-0.16466	A-3
8	9	0.16466	A-3
9	1	0.00039	A-5
9	8	0.05707	A-5
9	9	-2.4403	A-5
9	17	2.3832	A-5
10	1	0.00039	A-6
10	8	0.05707	A-6
10	9	2.3262	A-6
10	10	-2.3832	A-6
11	10	0.33645	A-7
11	11	-0.33645	A-7
12	12	-1.4500	B-19
12	18	1.4500	B-19
13	12	0.2238	B-1
13	13	-0.76642	B-1
13	14	0.53819	B-1
14	13	3.07017	B-2
14	14	-5.3657	B-2
14	15	0.332720	B-2

TABLE D-1 (continued)

Row Number	Column Number	Elements	Obtained From Equation
15	14	1.3500	B-18
15	15	-0.4480	B-18
16	13	1.4500	B-20
16	16	-1.4500	B-20
17	17	-0.5160	A-4
17	19	0.5160	A-4
18	11	2.500	A-8
18	18	-2.500	A-8
19	16	1.4800	B-21
19	19	-1.4800	B-21
20	8	0.020707	C-12 and C-13
20	9	-0.020707	C-12 and C-13
20	10	0.01057	C-12 and C-13
20	11	0.24516	C-12 and C-13
20	12	-0.13296	C-12 and C-13
20	13	-0.51964	C-12 and C-12
20	14	0.64821	C-12 and C-13
20	16	-0.118330	C-12 and C-13
20	17	+0.12321	C-12 and C-13
20	18	-0.28554	C-12 and C-13
20	19	0.02401	C-12 and C-13
20	20	$-1.9130 * 10^{-6}$	C-12

APPENDIX E

FIGURES

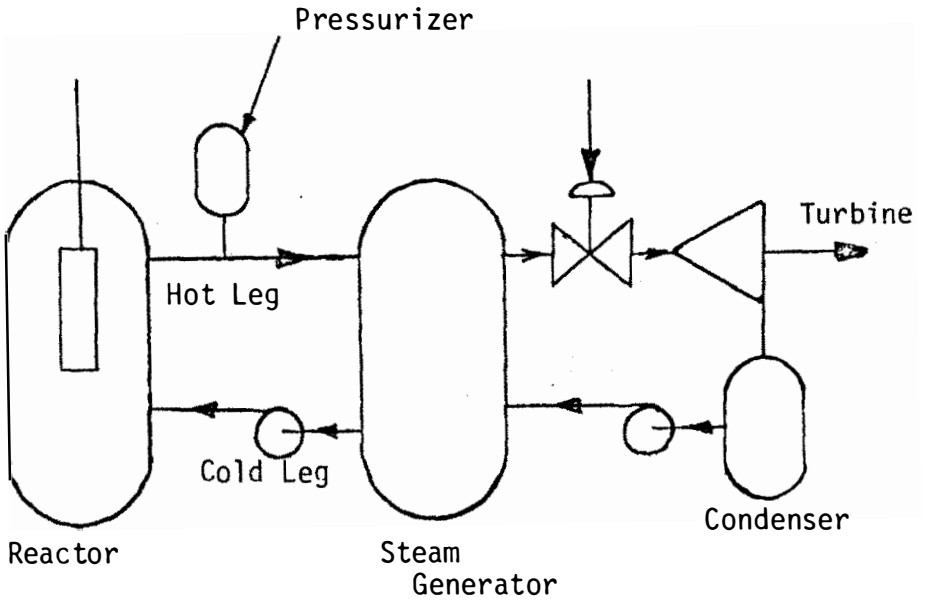

FIGURE II-1. Reactor Coolant Loop Flow Diagram.

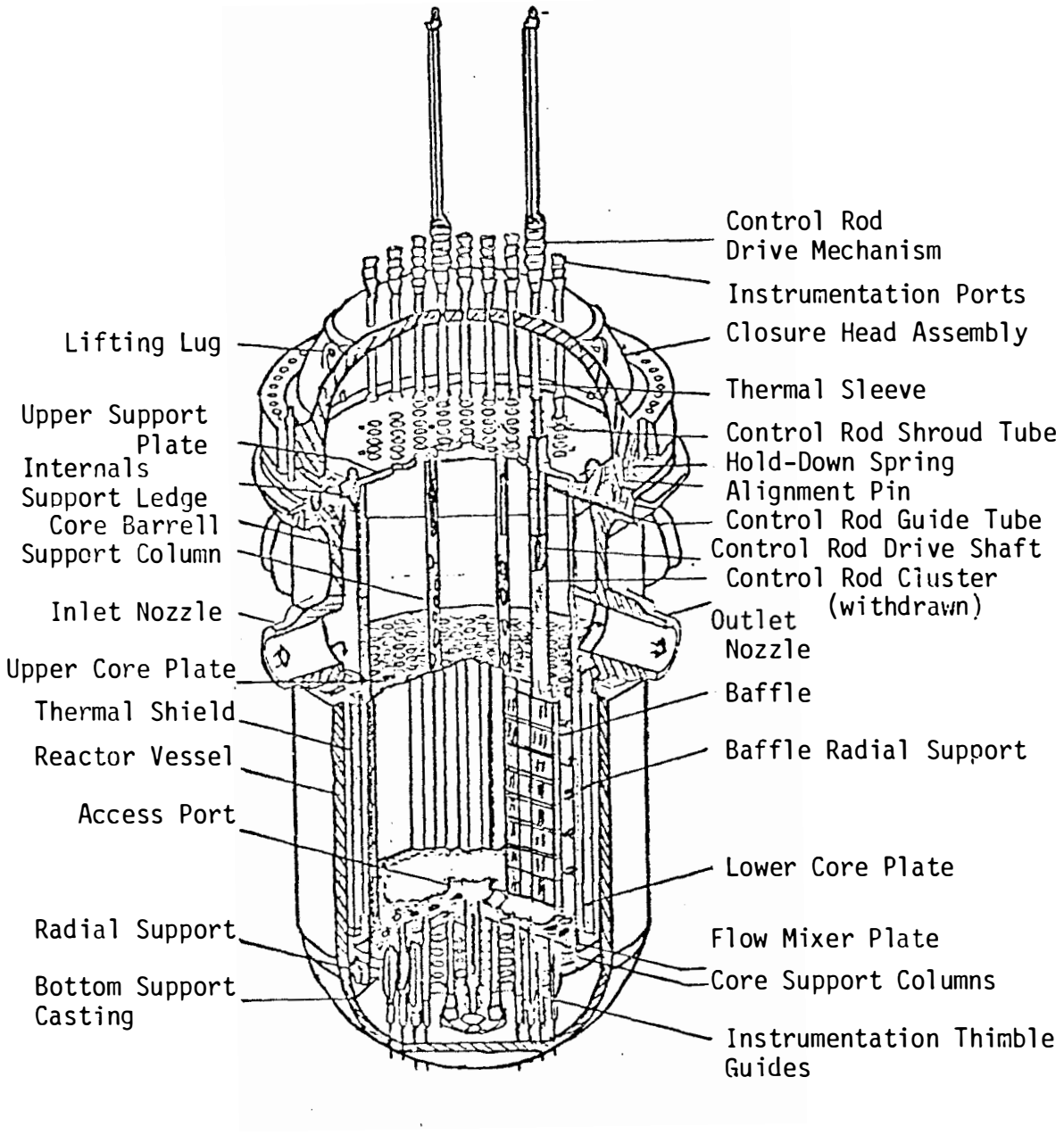

FIGURE II-2. Reactor Vessel Internals.

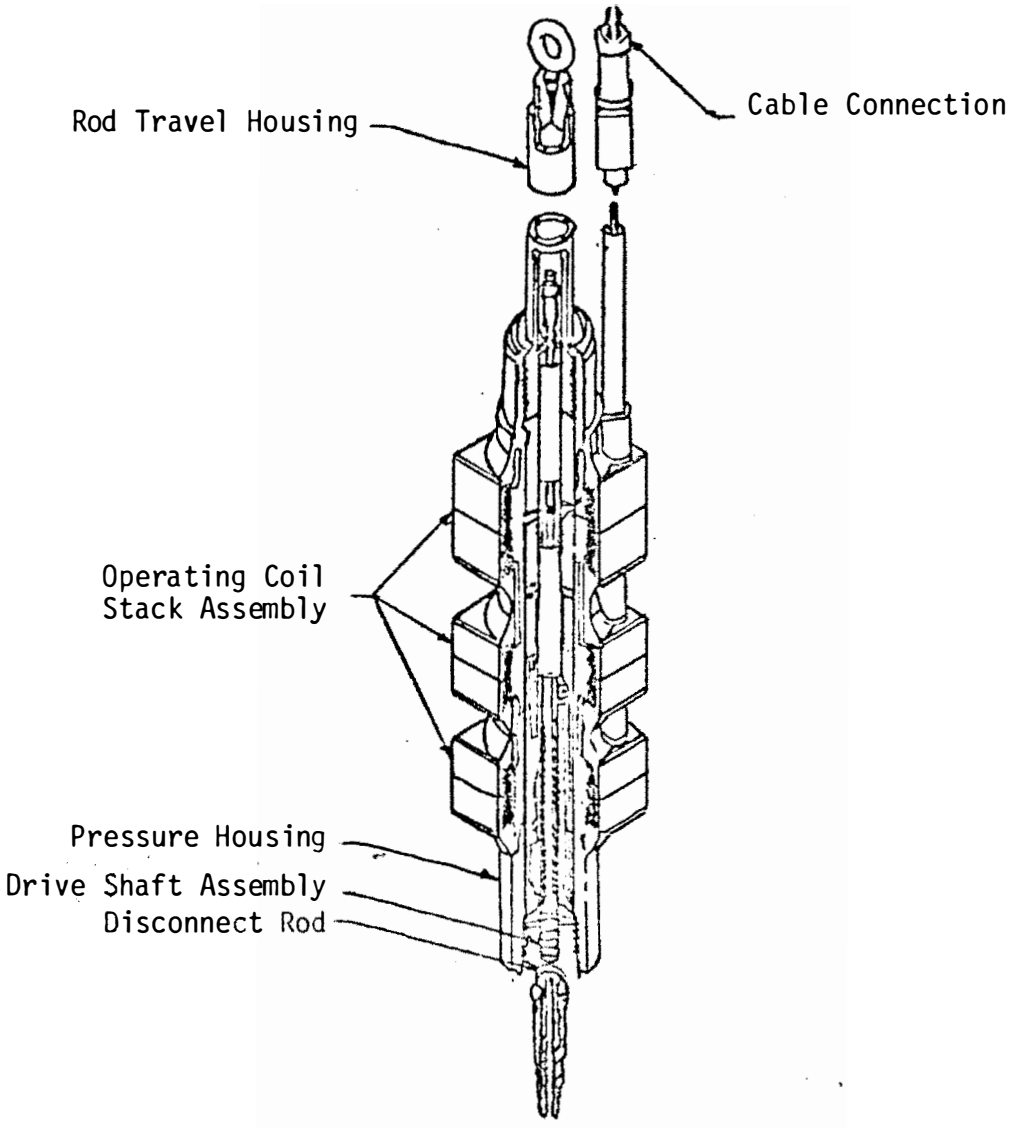

FIGURE II-3. Rod Cluster Control Drive Mechanism Assembly.

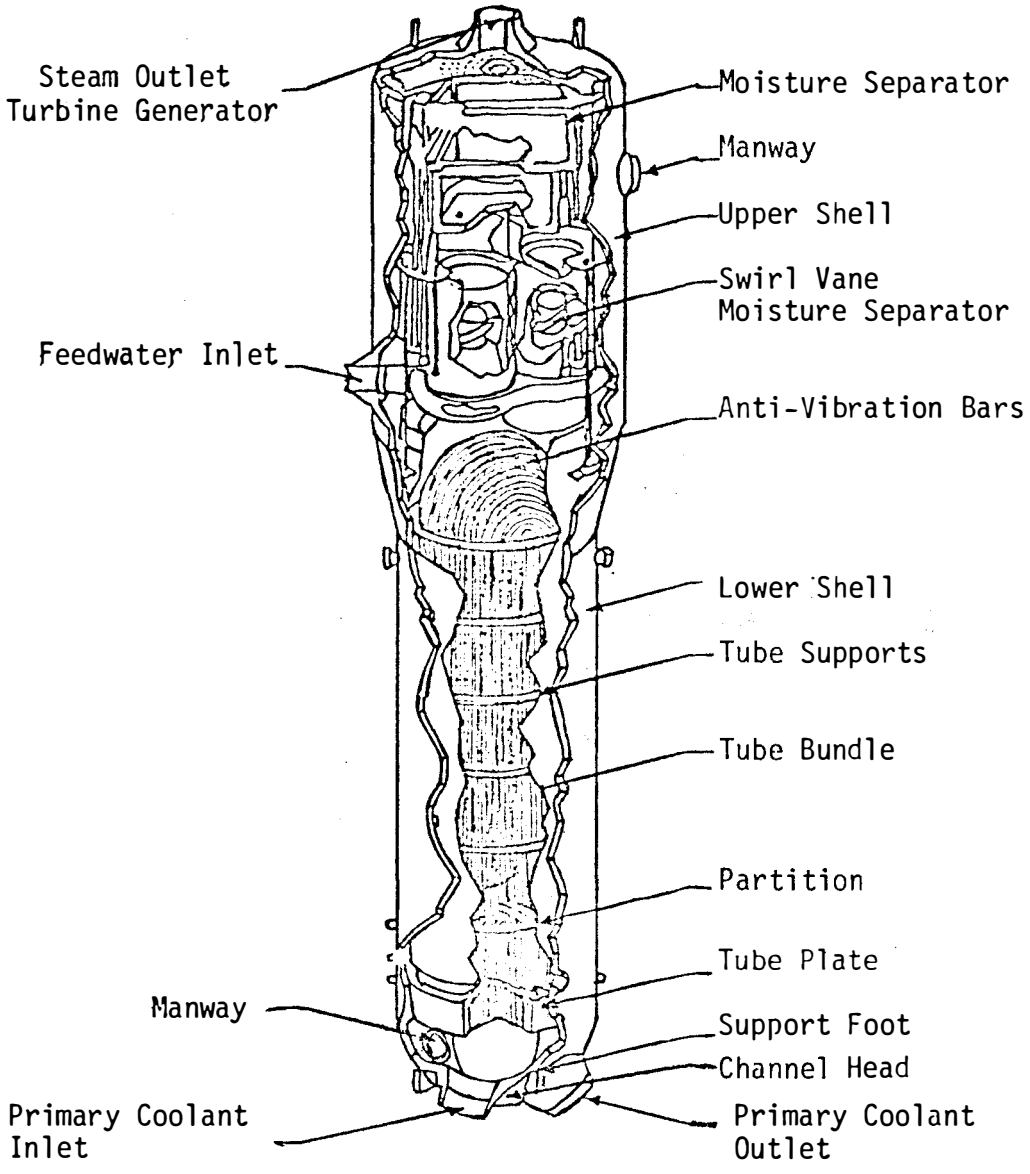

FIGURE II-4. Steam Generator.

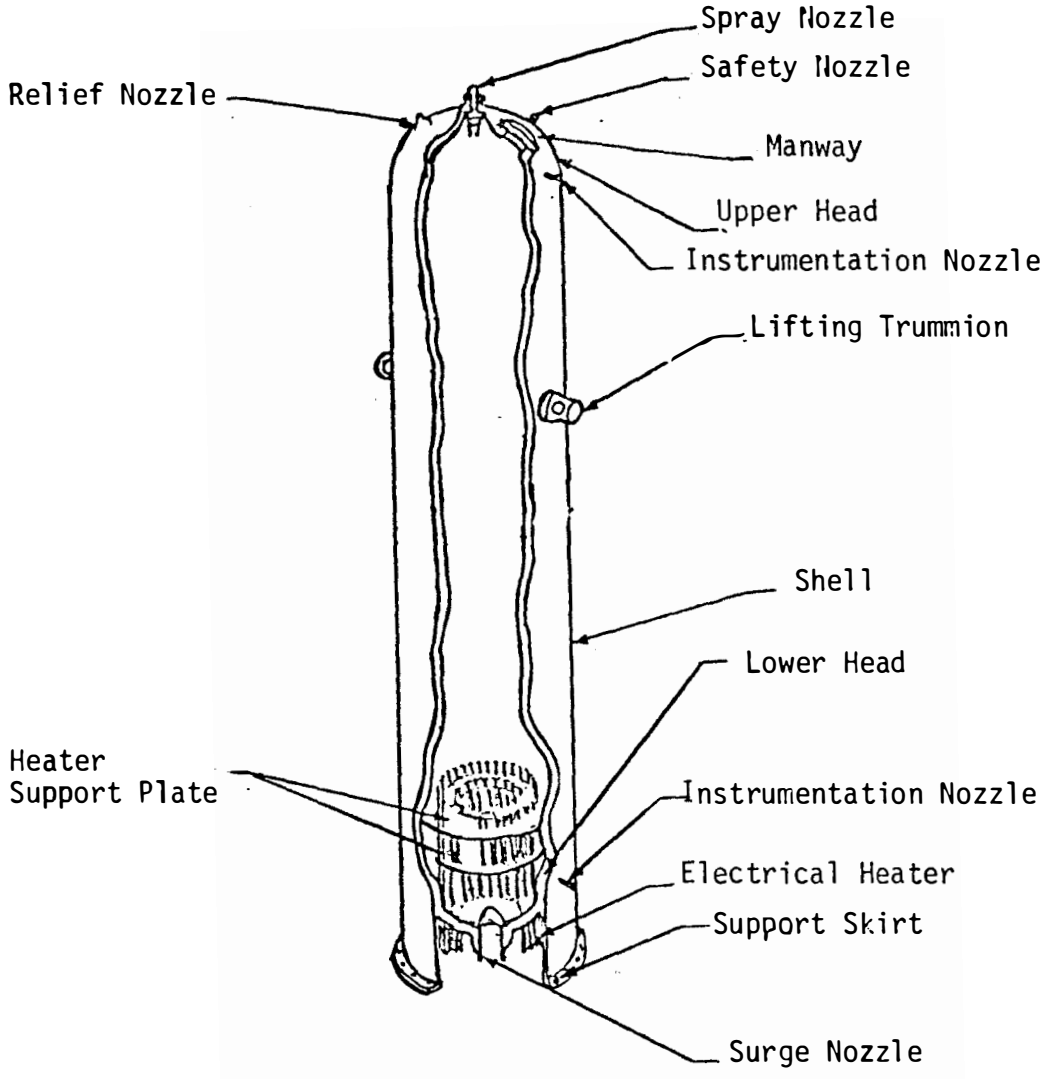

FIGURE II-5. Pressurizer.

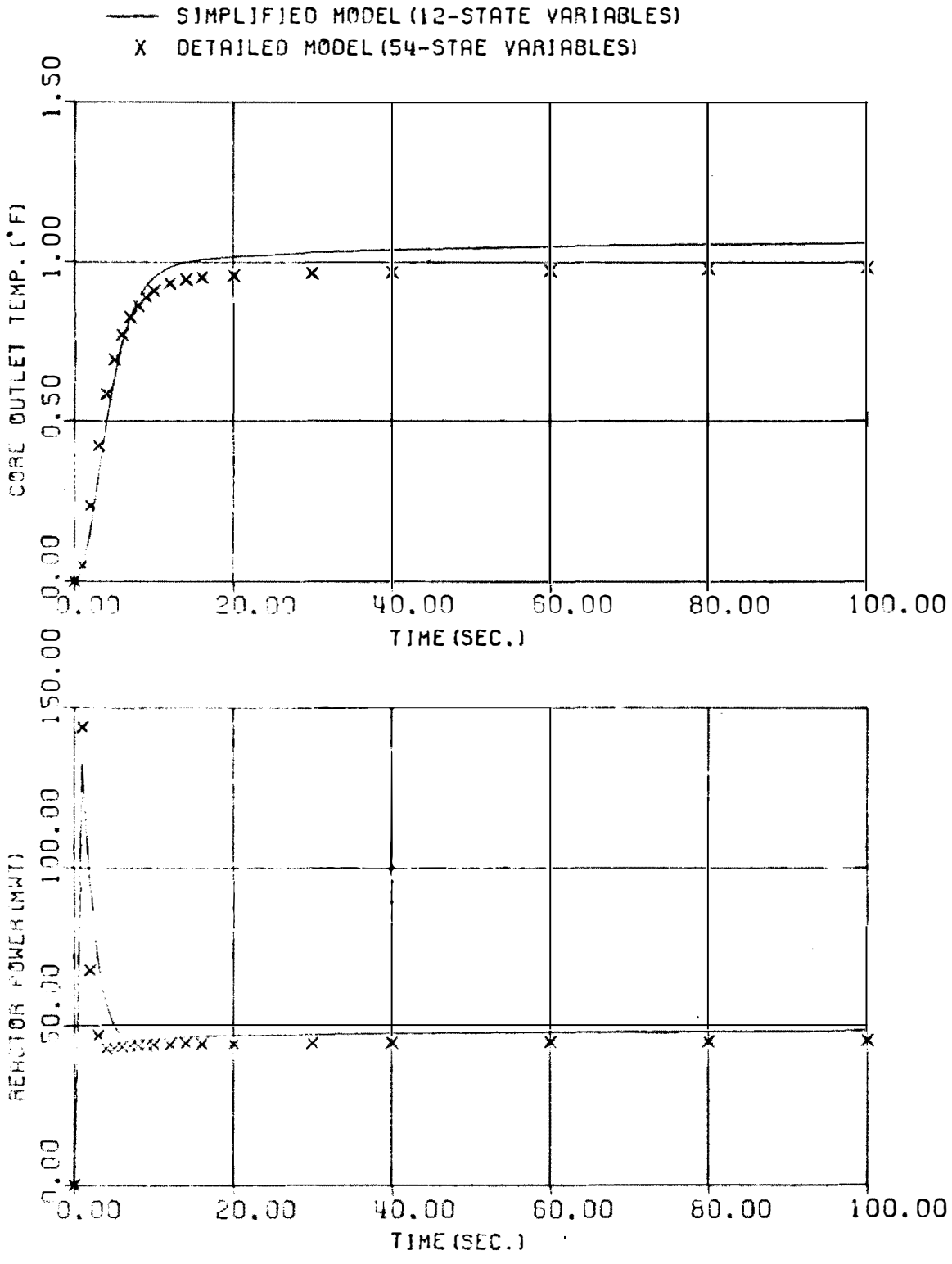

FIGURE II-6. A COMPARISION OF THE SIMPLIFIED AND THE DETAIL REACTOR MODEL FOR 0.071$ STEP CHANGE IN REACTIVITY

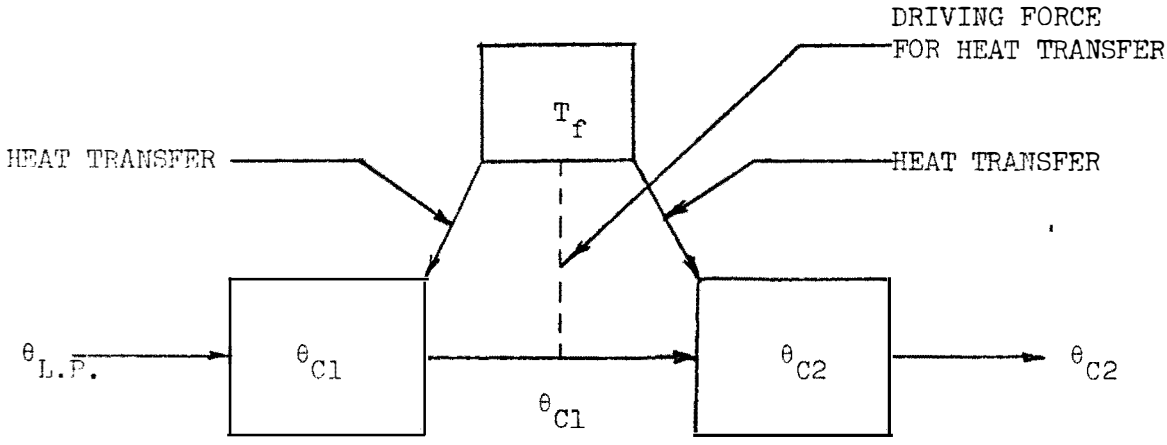

FIGURE II-7. Schematic Drawing of Heat Transfer Process From Fuel to Coolant.

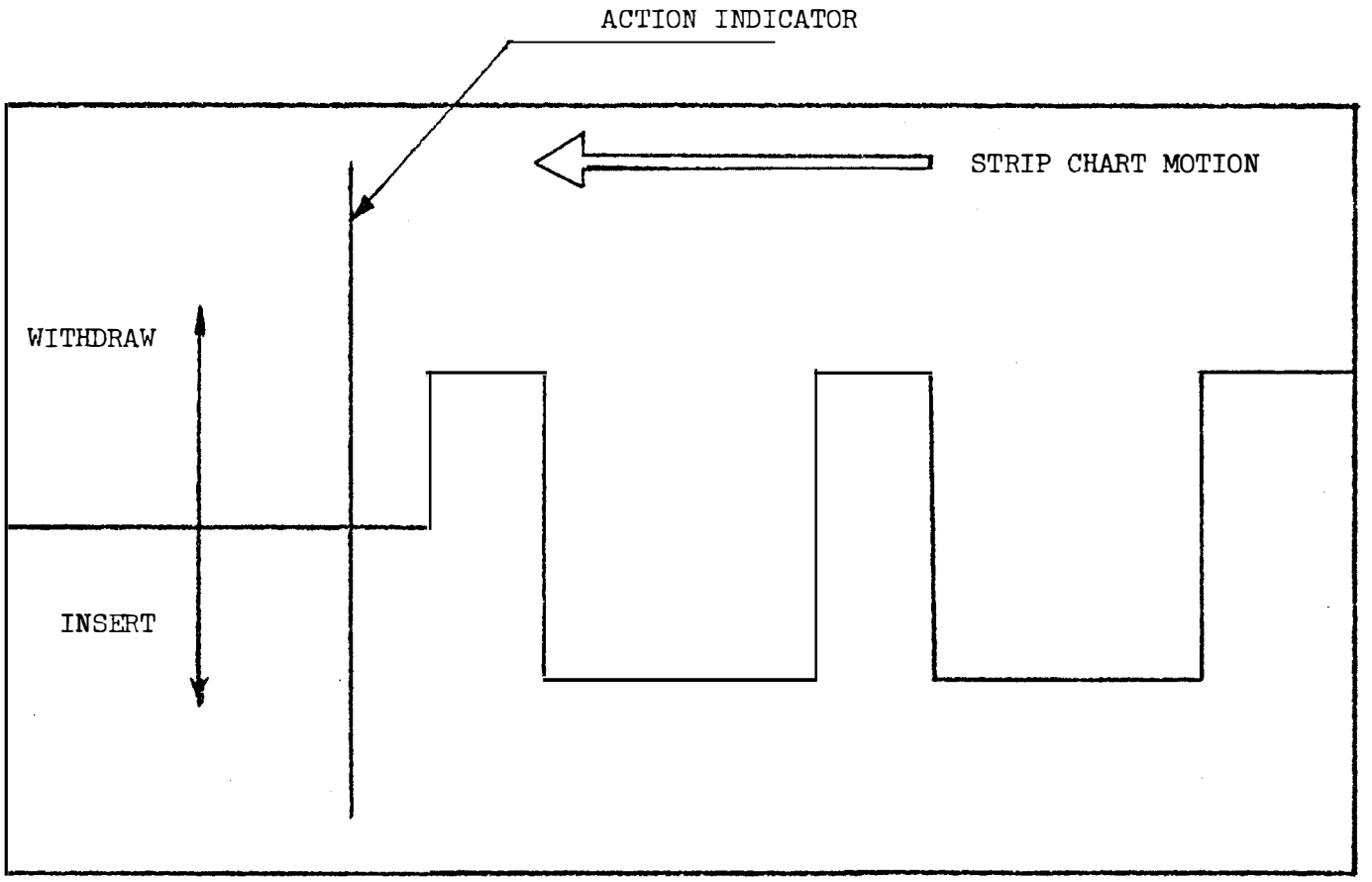

FIGURE III-1. Strip Chart Recorder Set Up for the Input Signal.

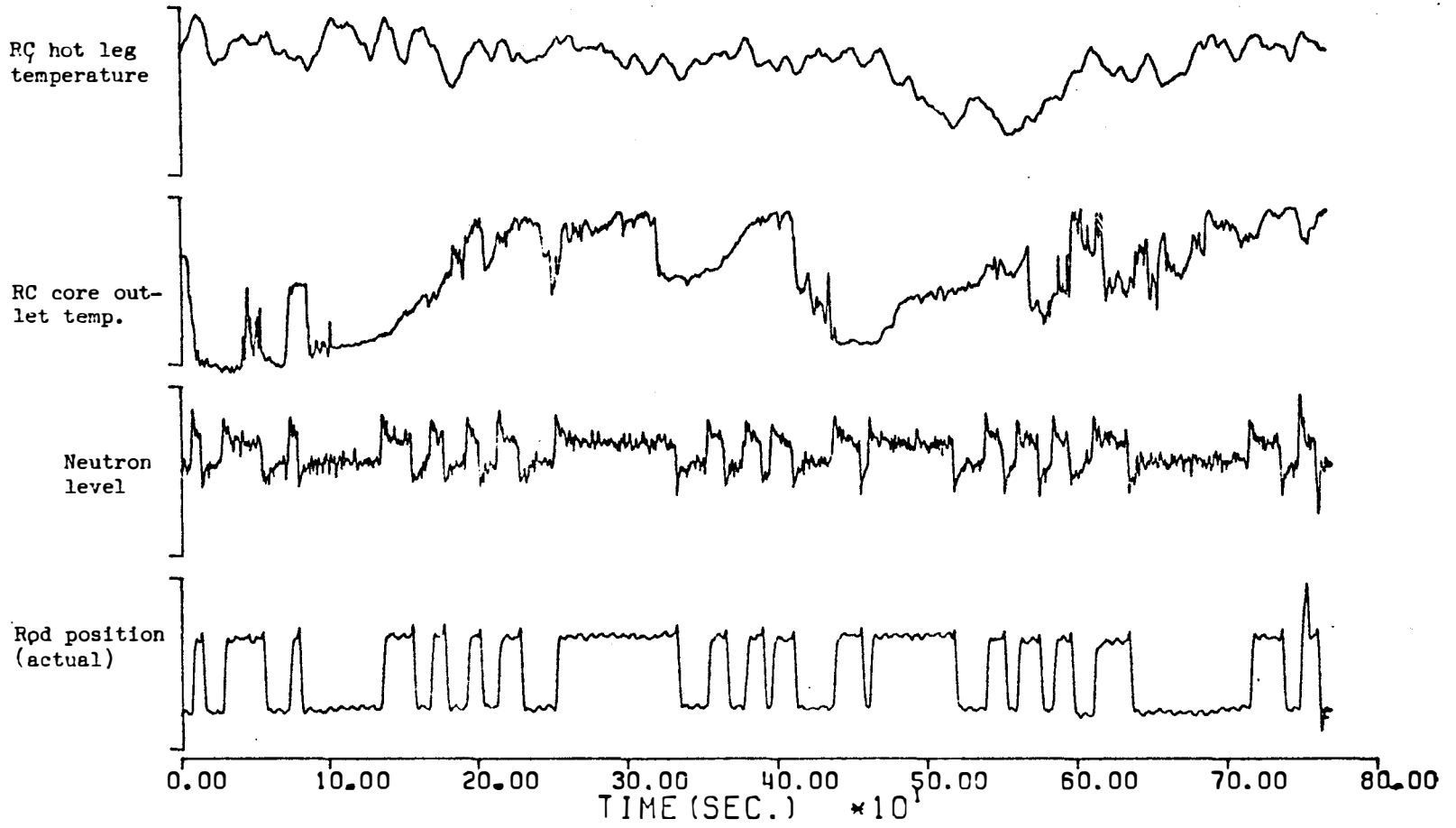

FIGURE IV-1. Responses of Neutron Level, RC Core Outlet Temperature, and RC Hot Leg Temperature Along with the Actual (Measured by LVDT) Rod Position Signal.

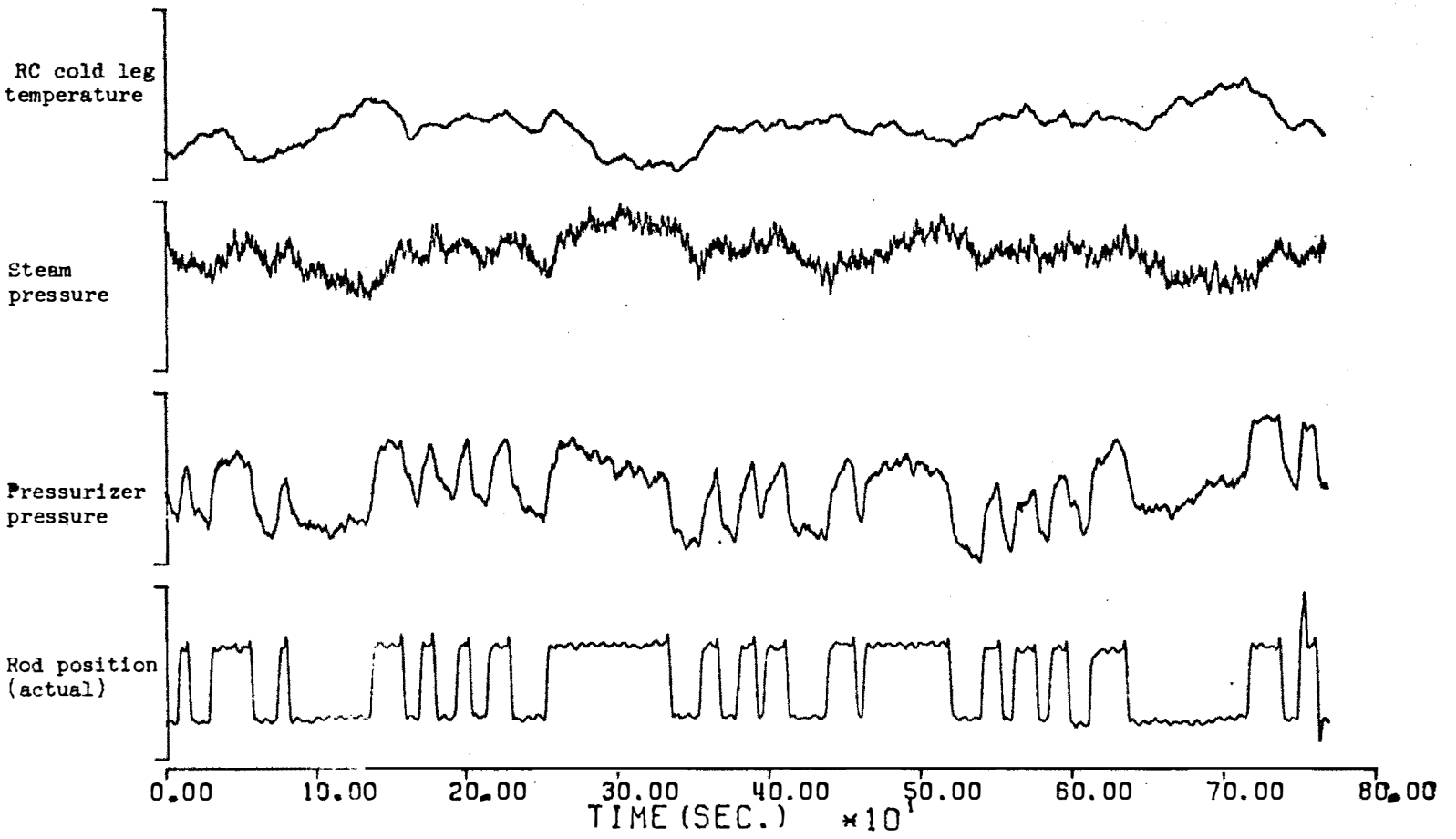

FIGURE IV-2. Responses of Pressurizer Pressure, Steam Pressure, and RC Cold Leg Temperature Along with the Actual (Measured by LVDT) Rod Position Signal.

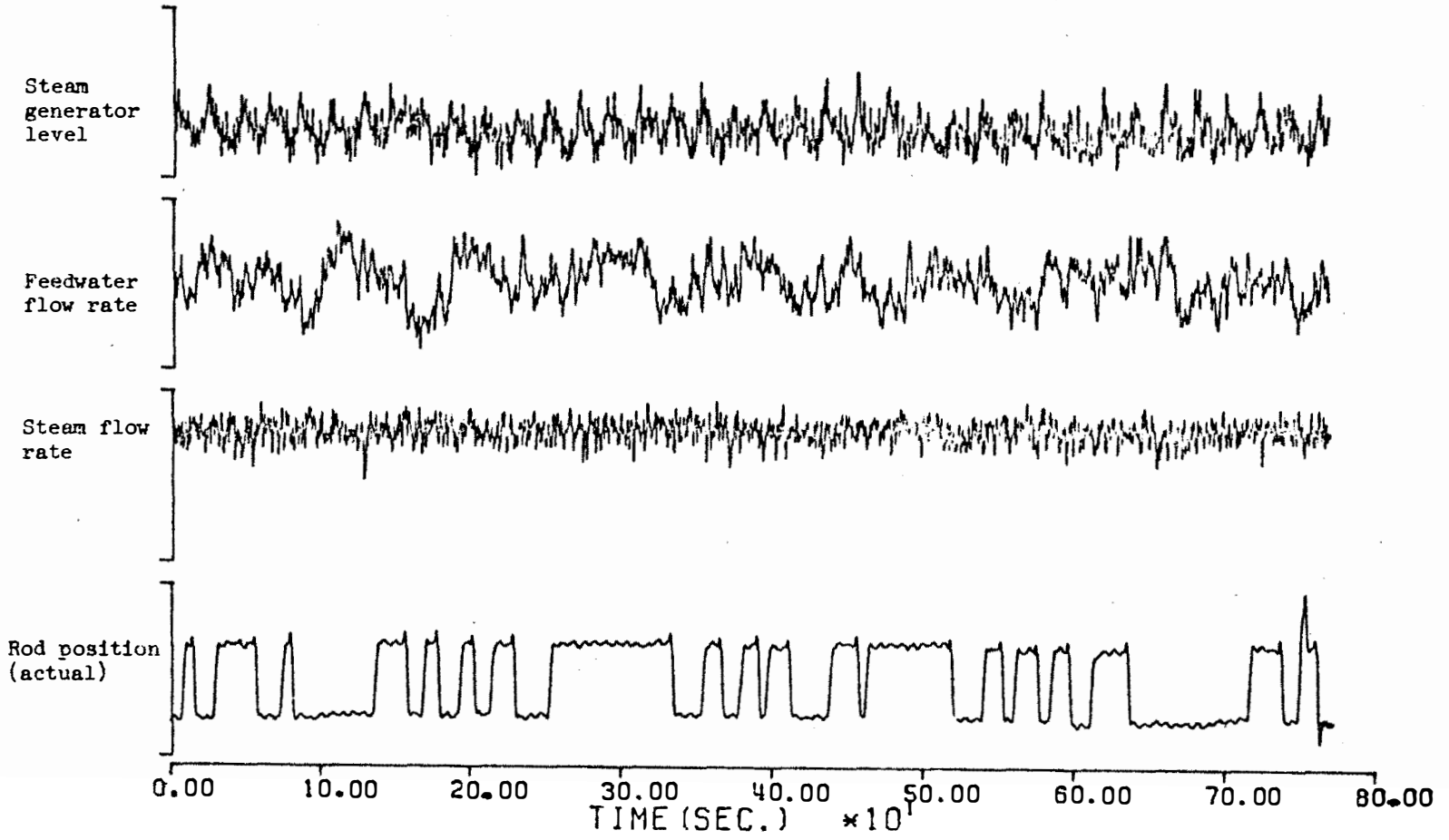

FIGURE IV-3. Responses of Steam Flow Rate, Feedwater Flow Rate, and Steam Generator Level Along with the Actual (Measured by LVDT) Rod Position.

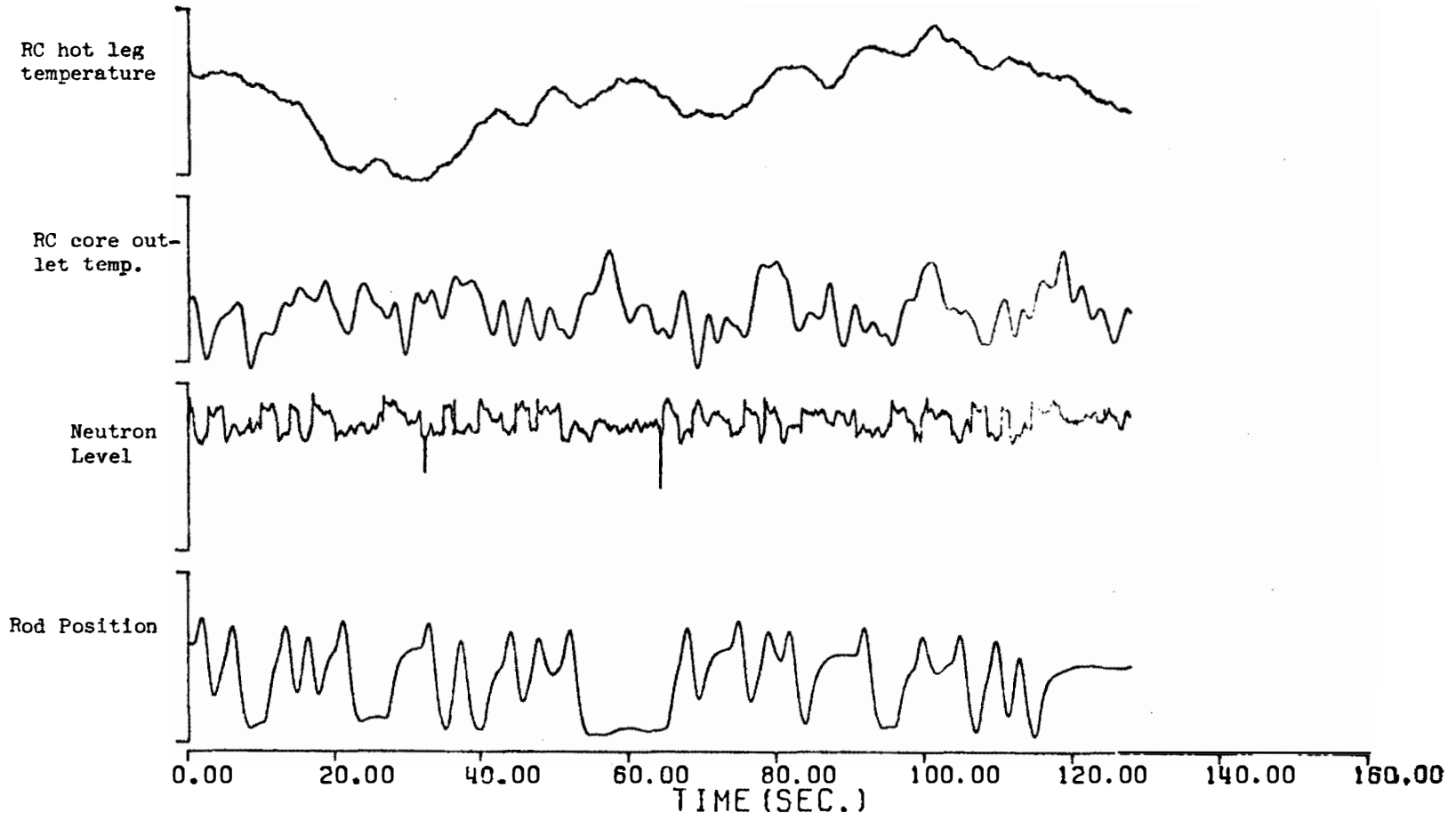

FIGURE IV-4. Response of Neutron Level, RC Core Outlet Temperature, and RC Hot Leg Temperature Along with the 128 Bit, 1-Step, MFBS Signal.

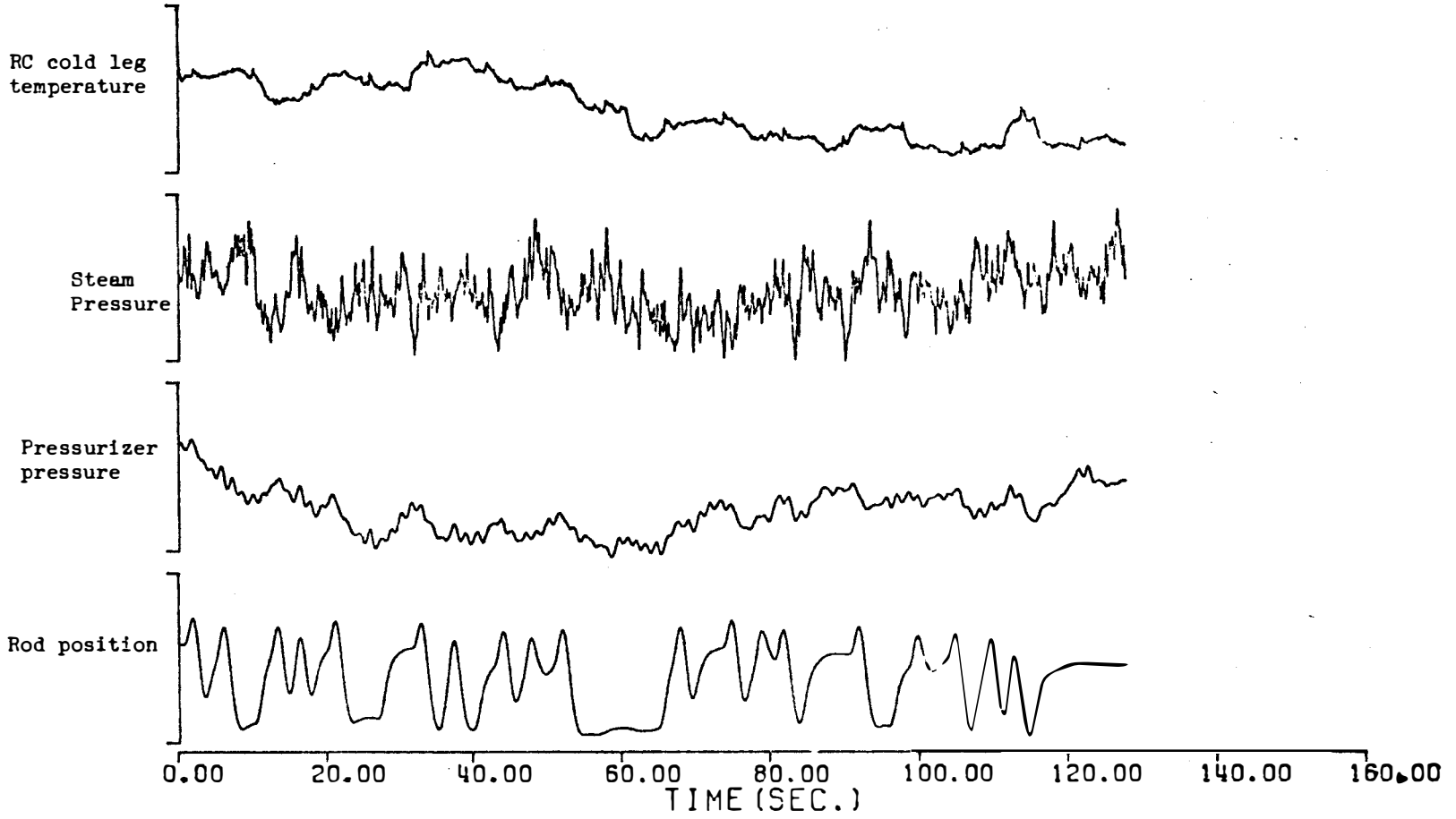

FIGURE IV-5. Response of Pressurizer Pressure, Steam Pressure, and RC Cold Leg Temperature Along with the 128-Bit, 1-Step, MFBS Signal.

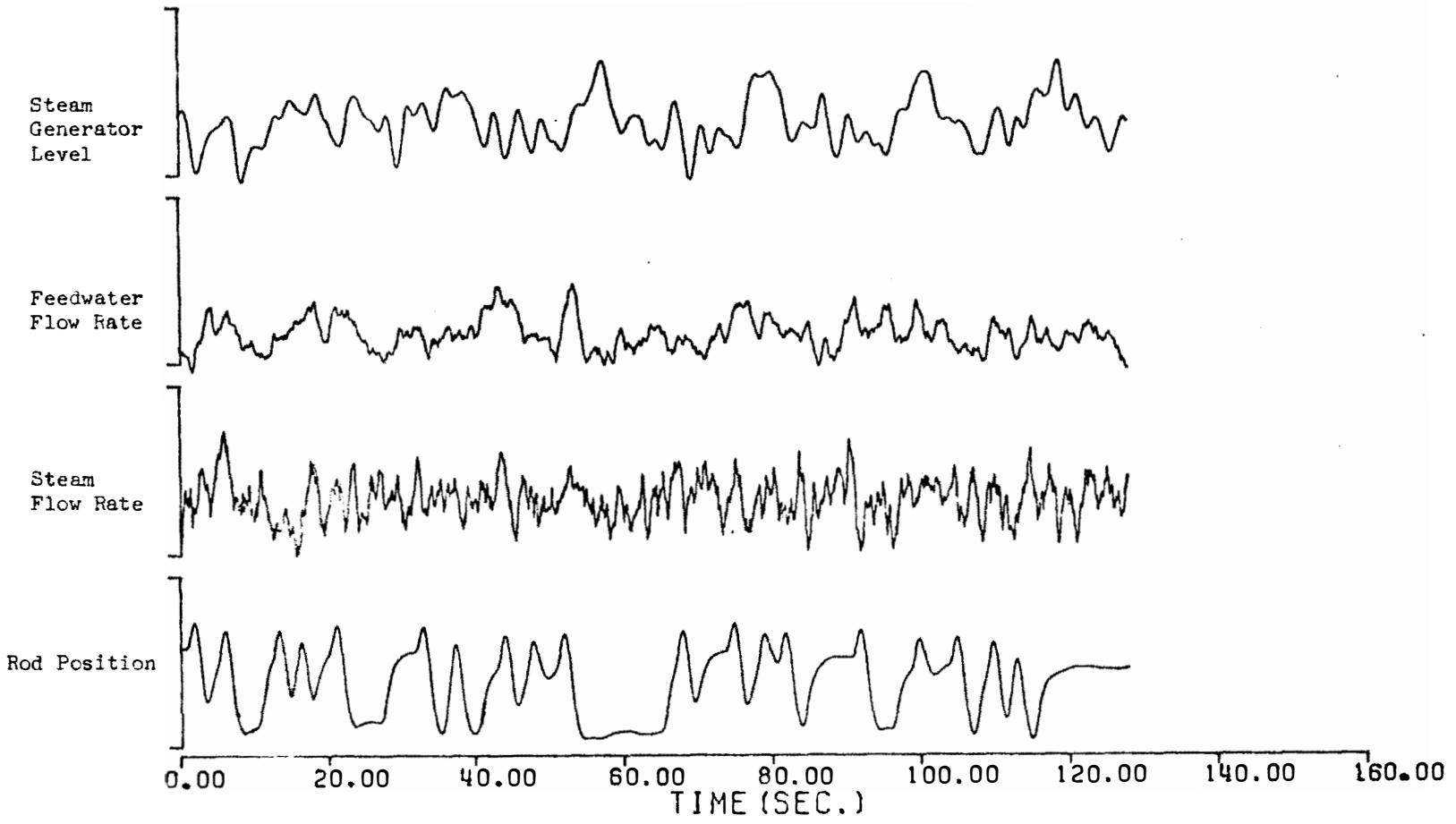

FIGURE IV-6. Response of Steam Flow Rate, Feedwater Flow Rate, and Steam Generator Level Along with 128-Bit, 1-Step, MFBS Signal.

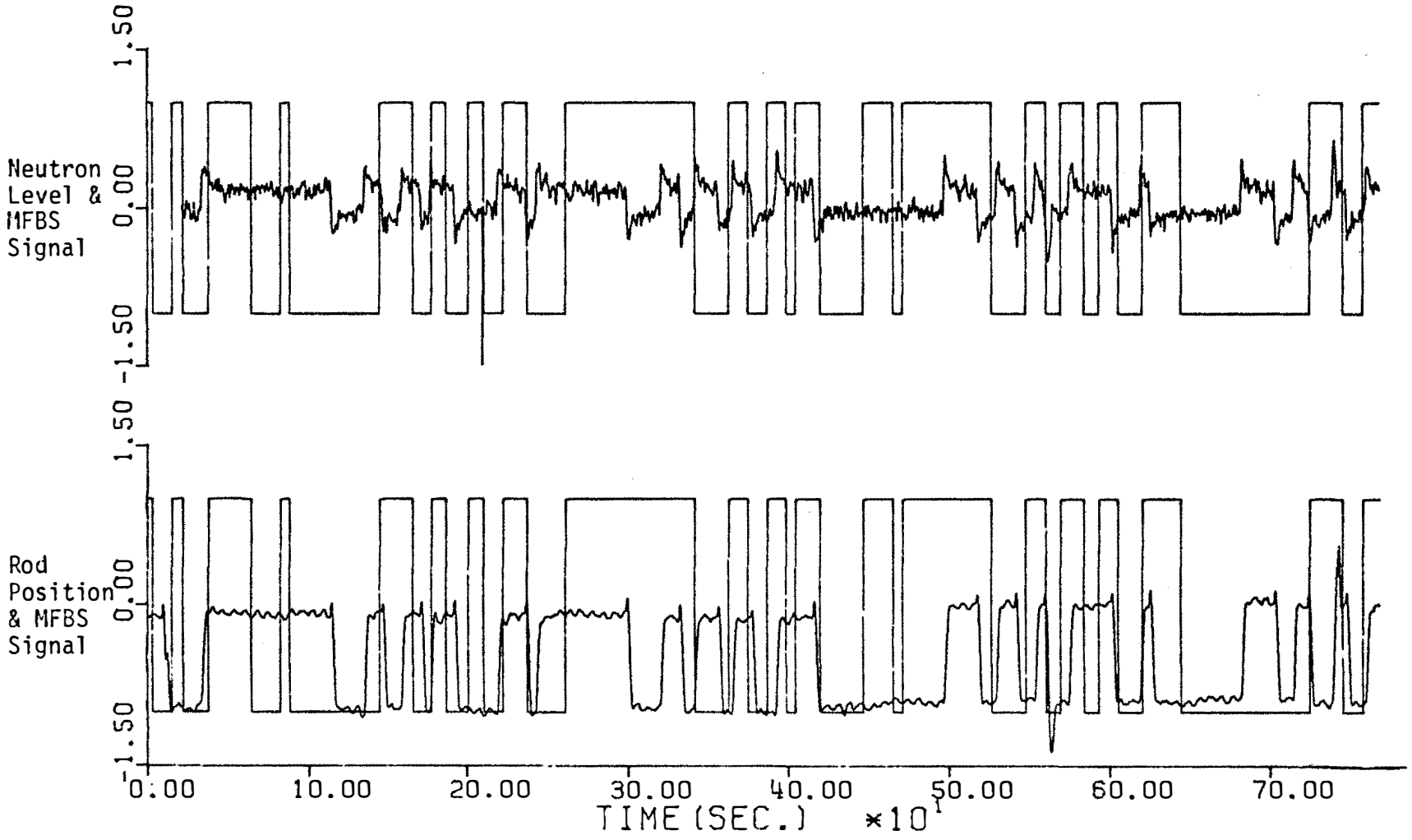

FIGURE IV-7. Neutron Level and Rod Position Signals with 256-Bit, 2-Step, MFBS Signal Superimposed.

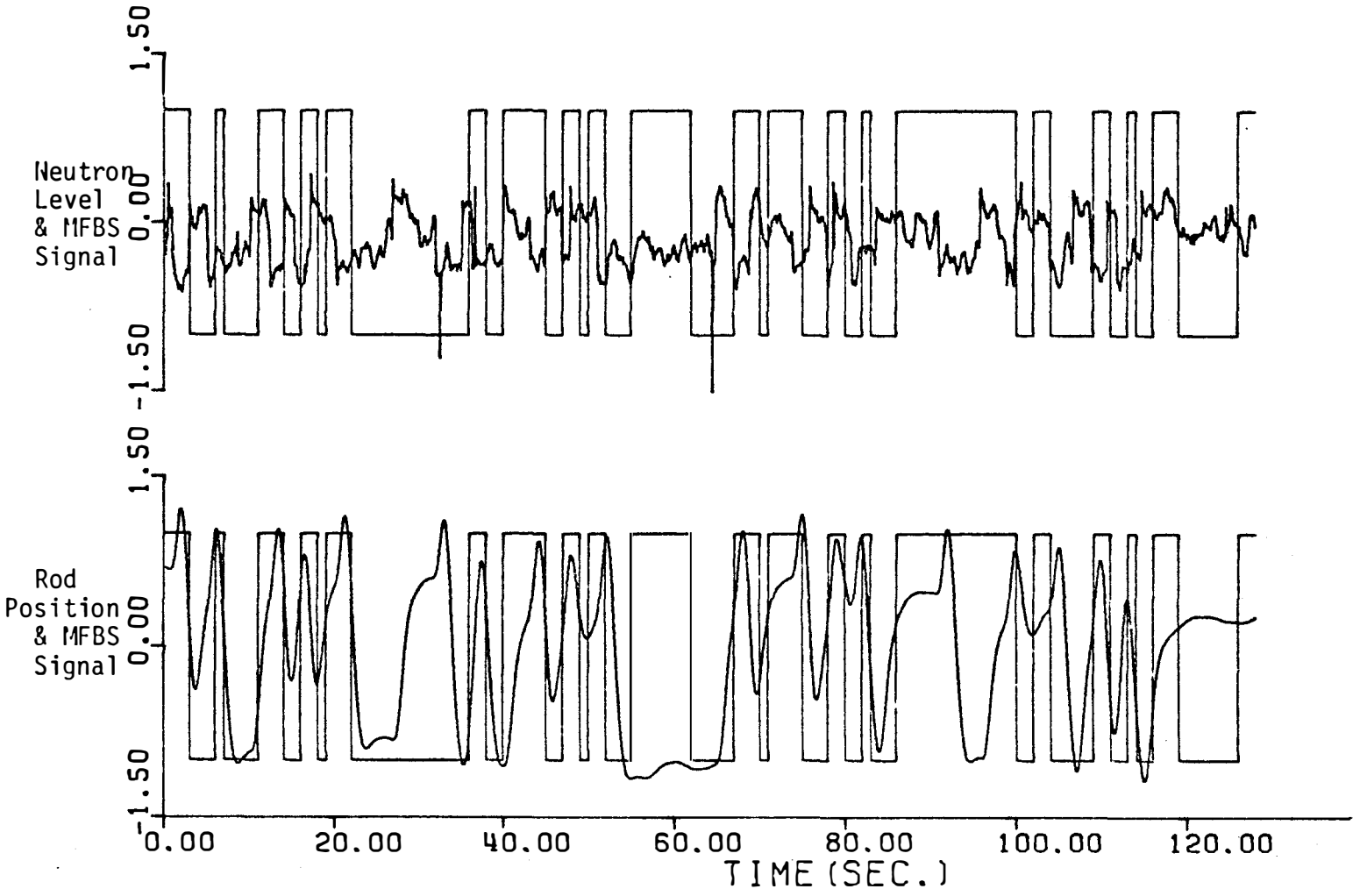

FIGURE IV-8. Neutron Level and Rod Position Signals with 128-Bit, 1-Step, MFBS Signal Superimposed.

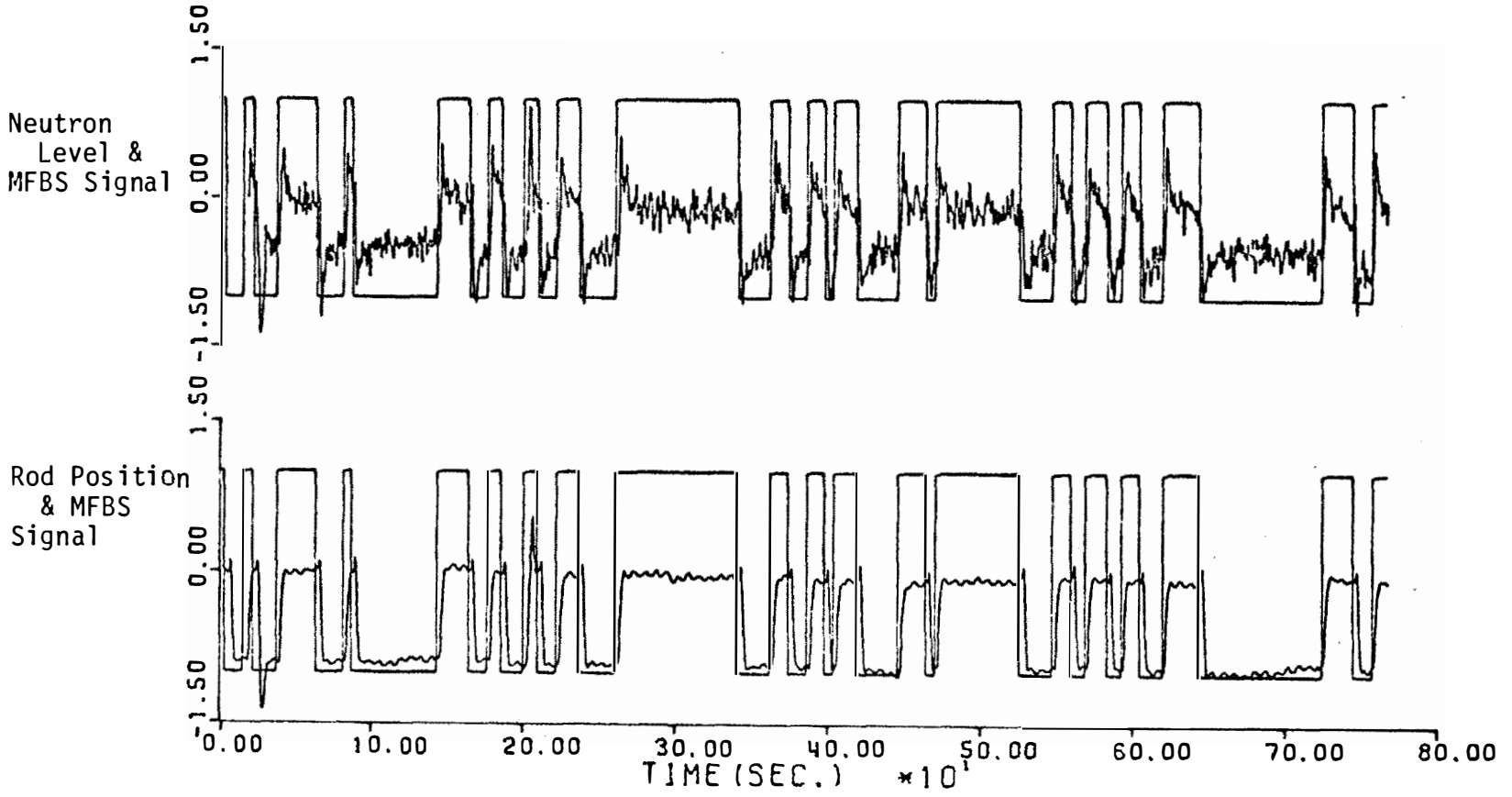

Part A - 2-Step. Part B - 1-Step.

FIGURE IV-9. Adjusted Neutron Level and Rod Position Signals with the Modified MFBS, 2-Step, Signal Superimposed.

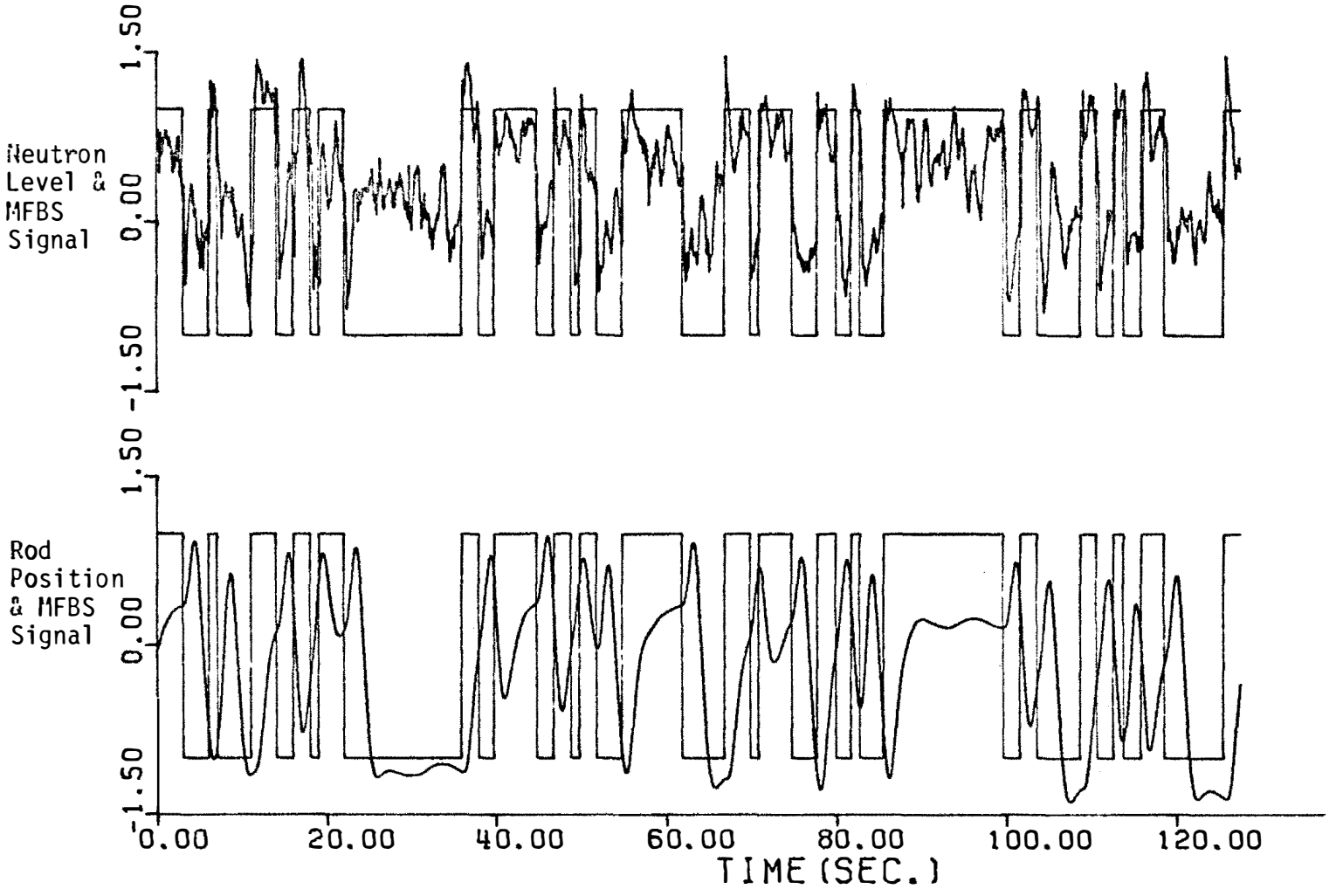

FIGURE IV-9. (Continued).

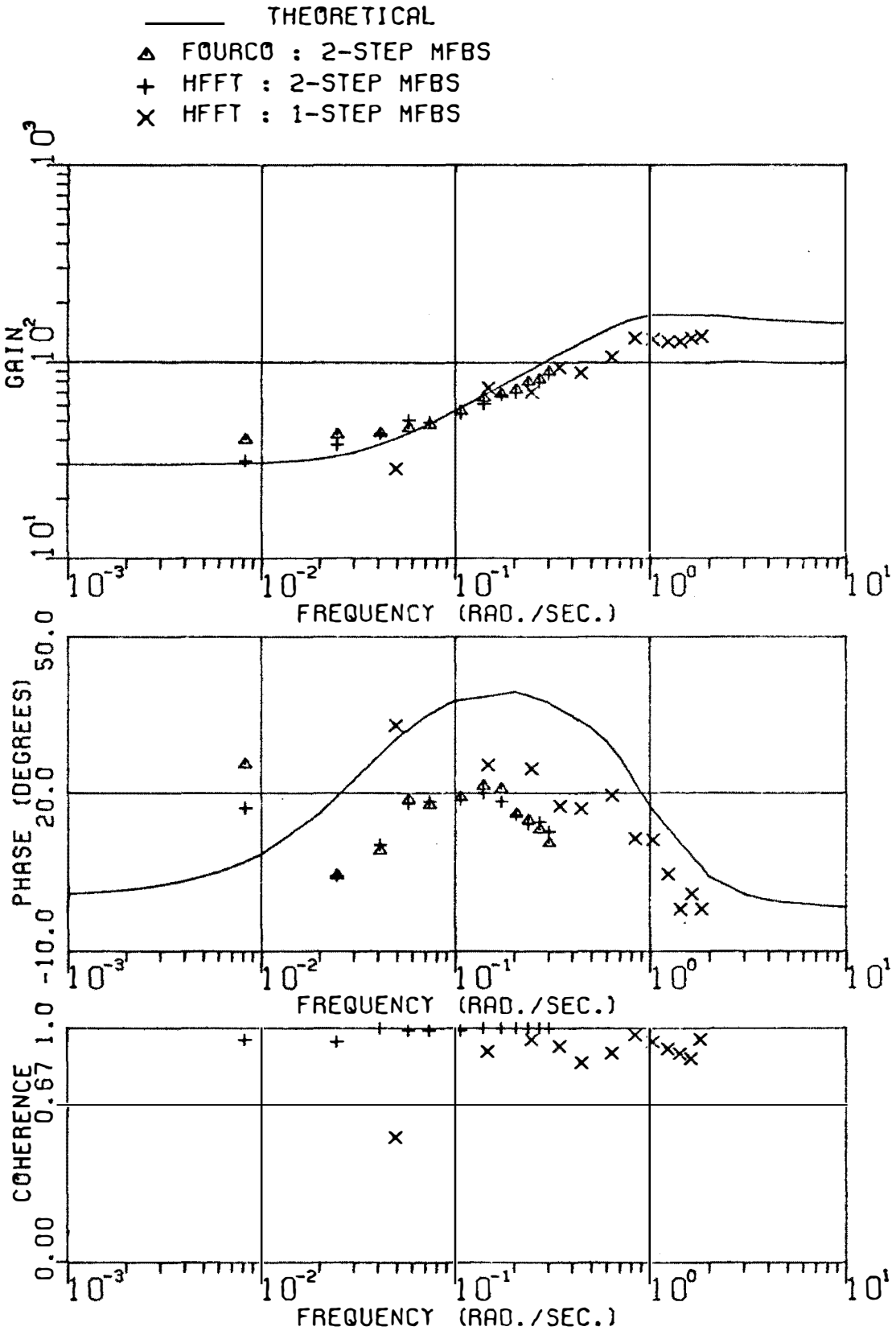

FIGURE IV-10. REACTOR POWER TO REACTIVITY TRANSFER FUNCTION

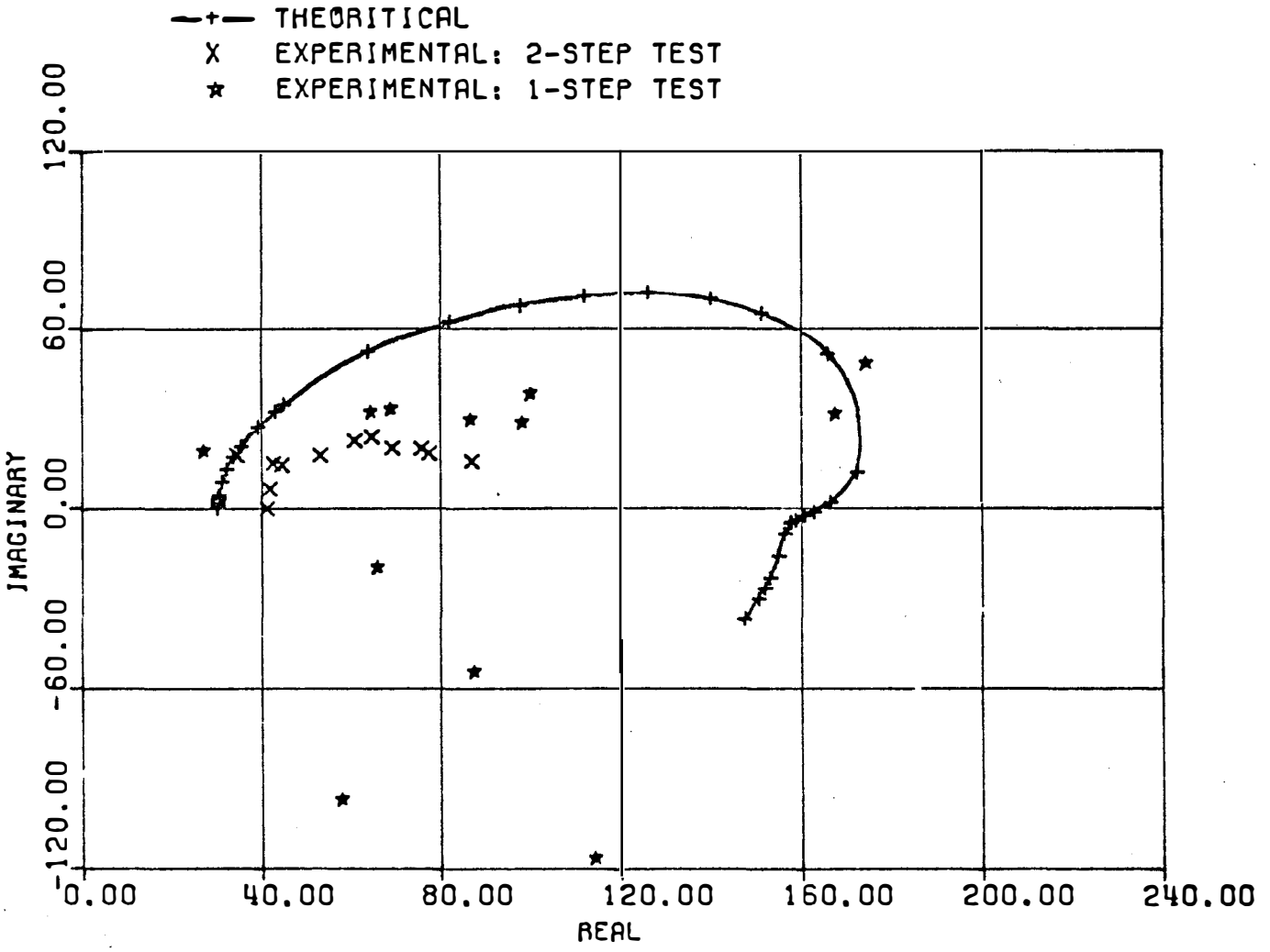

FIGURE IV-11. POLAR PLOT OF REACTOR POWER TO REACTIVITY TRANSFER FUNCTION

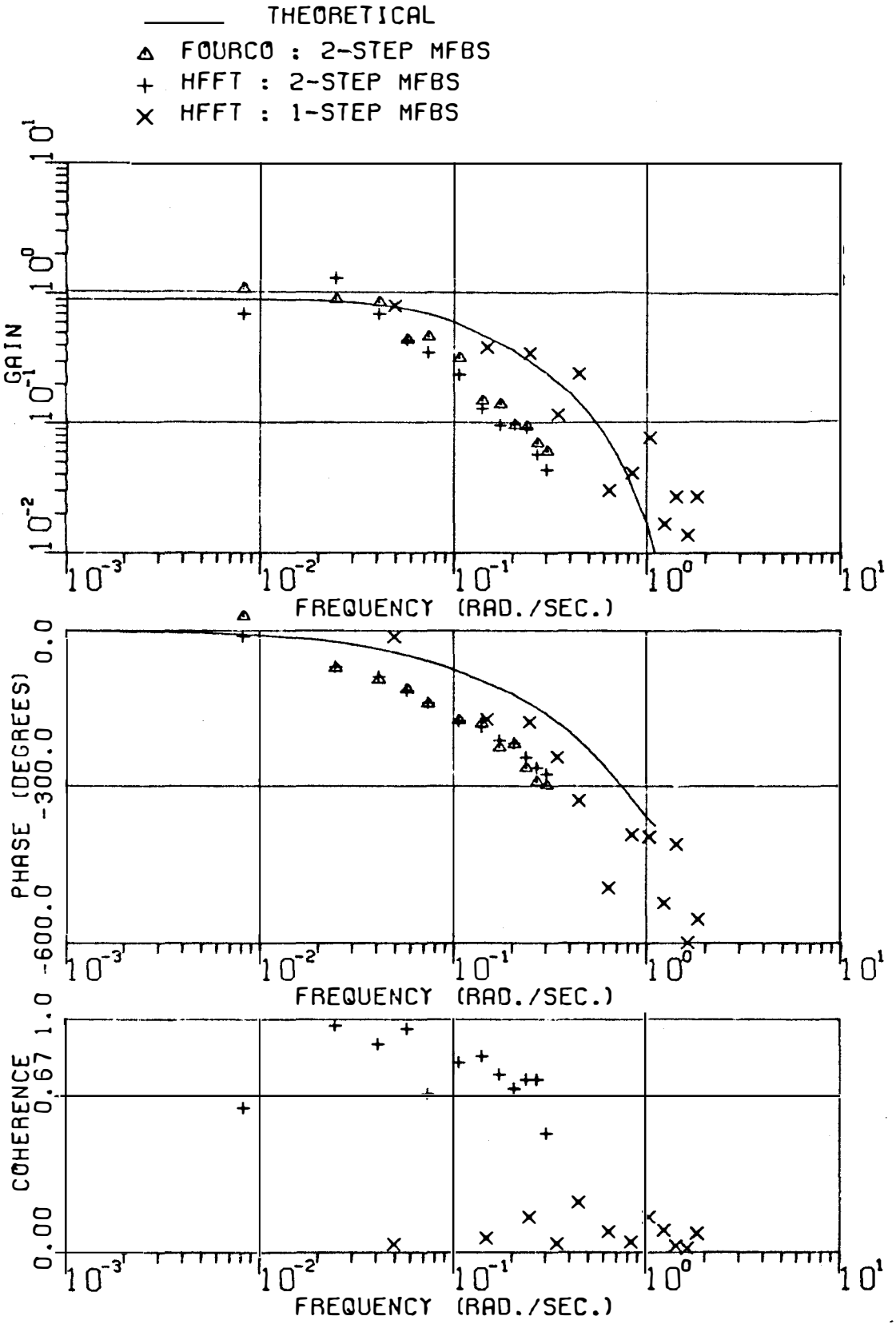

FIGURE IV-12. Cold Leg Temperature to Reactivity Transfer Function.

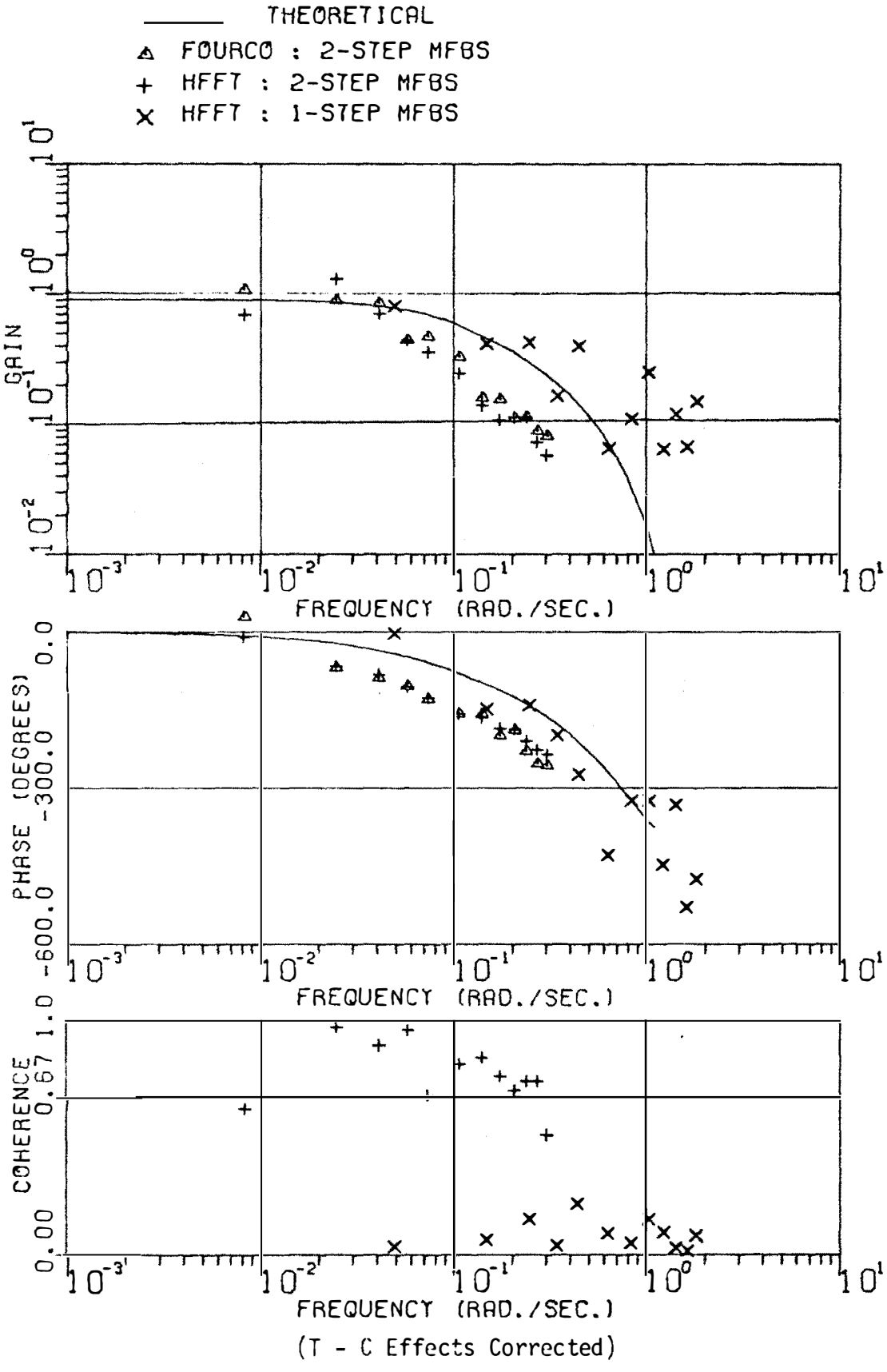

FIGURE IV-12. (Continued).

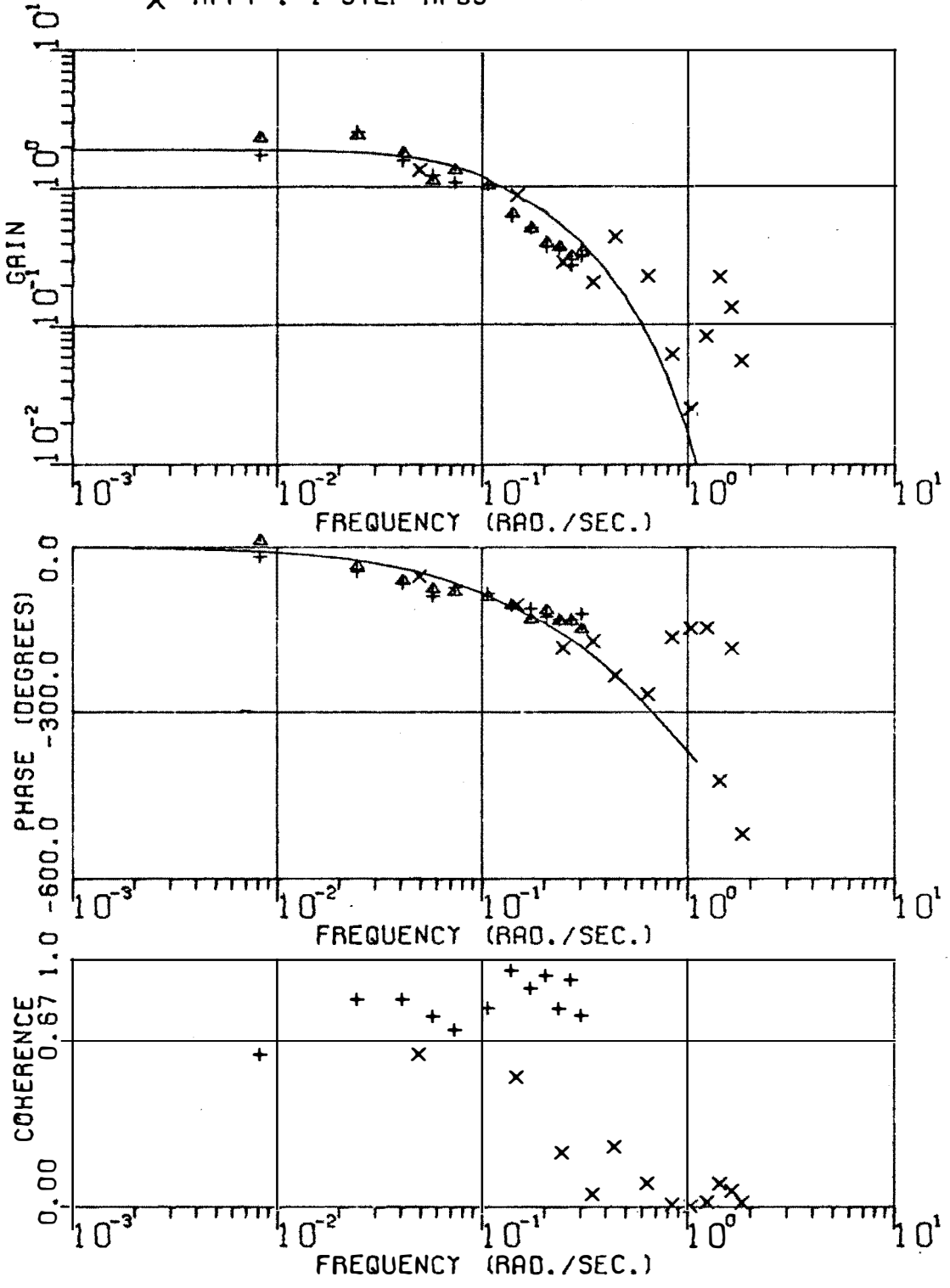

FIGURE IV-13. STEAM PRESSURE TO REACTIVITY TRANSFER FUNCTION

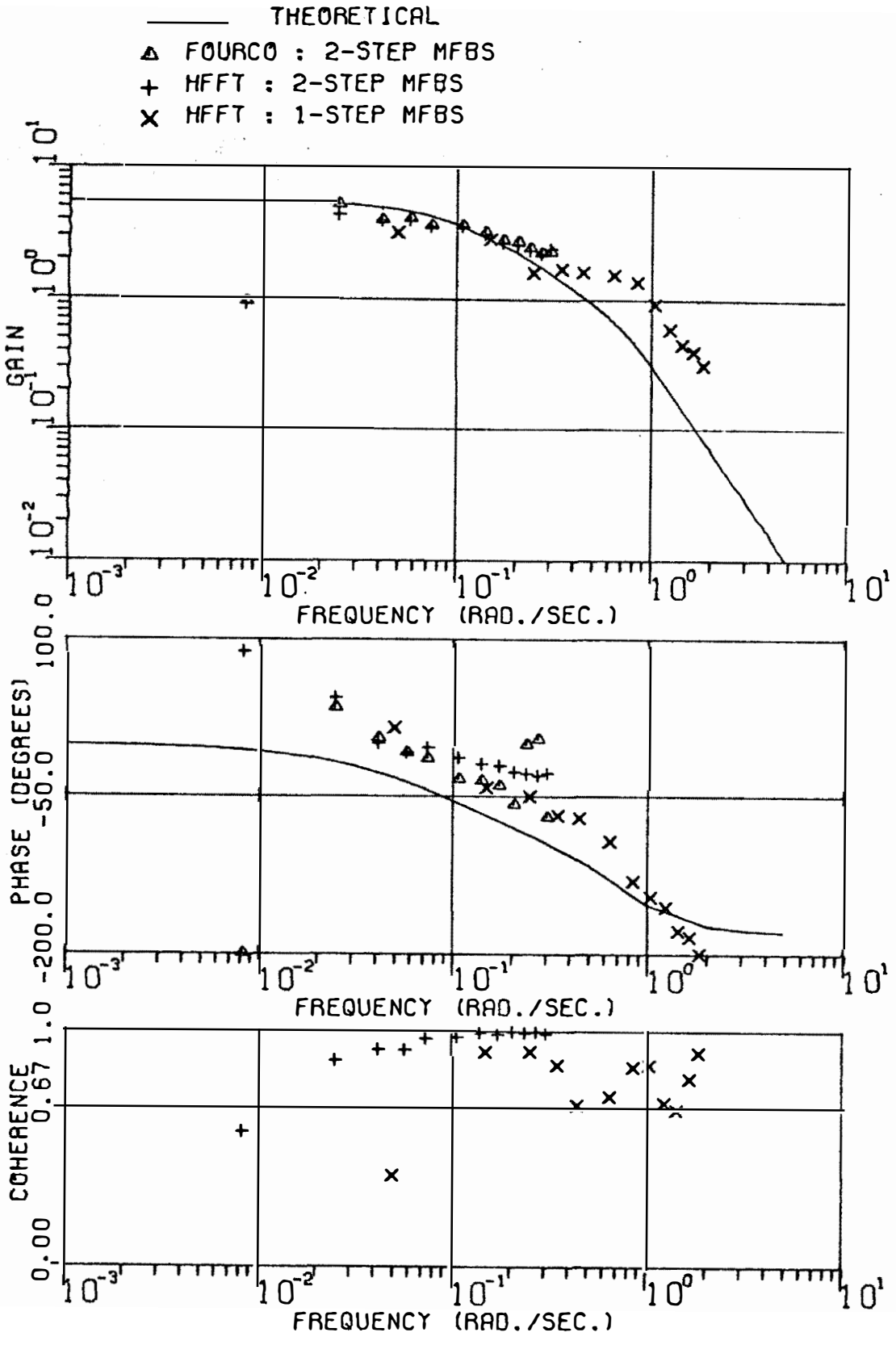

FIGURE IV-14. PRESSURIZER PRESS. TO REACTIVITY TRANSFER FUNCTION

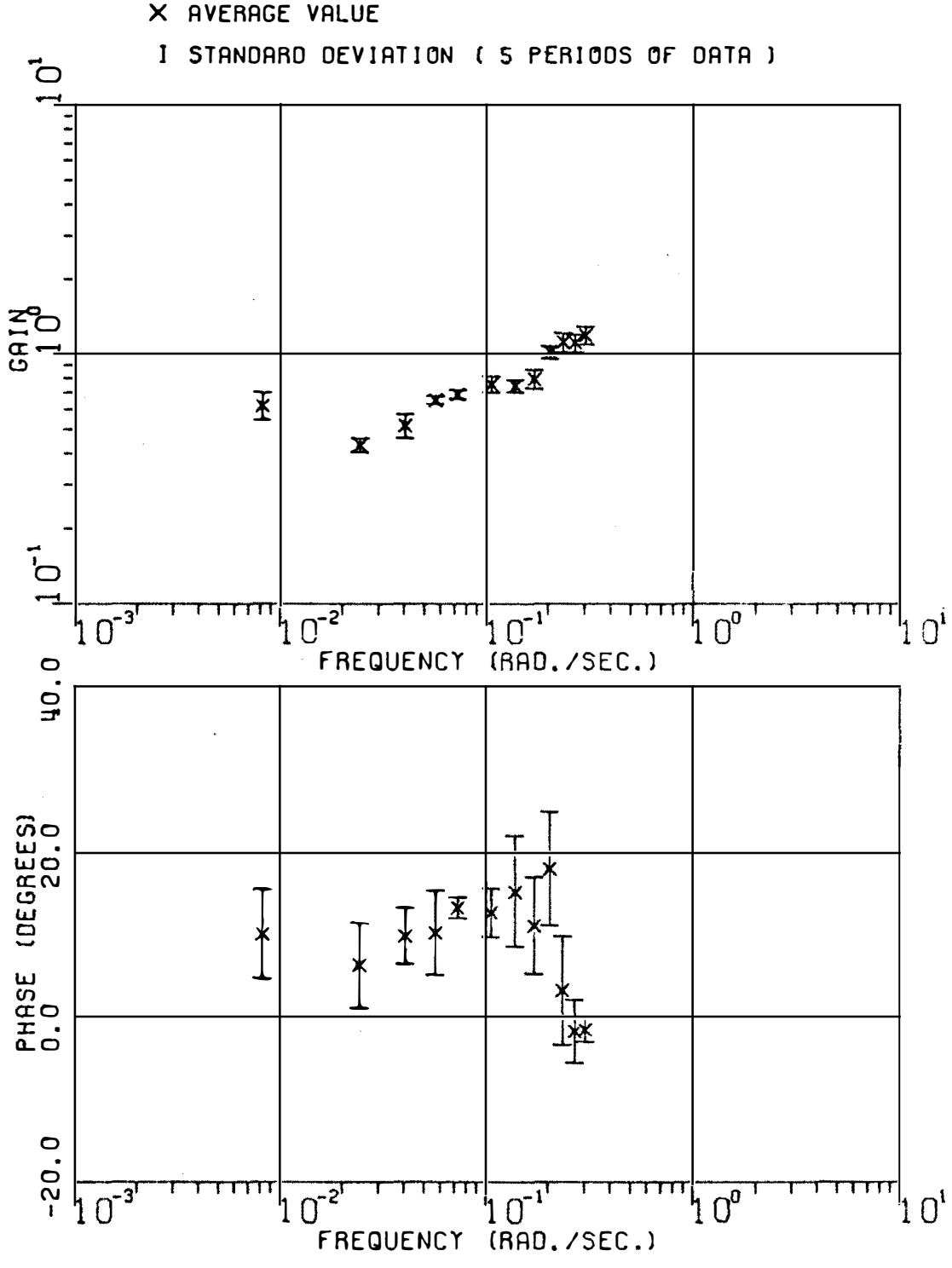

FIGURE IV-15. STANDARD DEVIATIONS OF REACTOR POWER TO REACTIVITY TRANSFER FUNCTION RESULTS

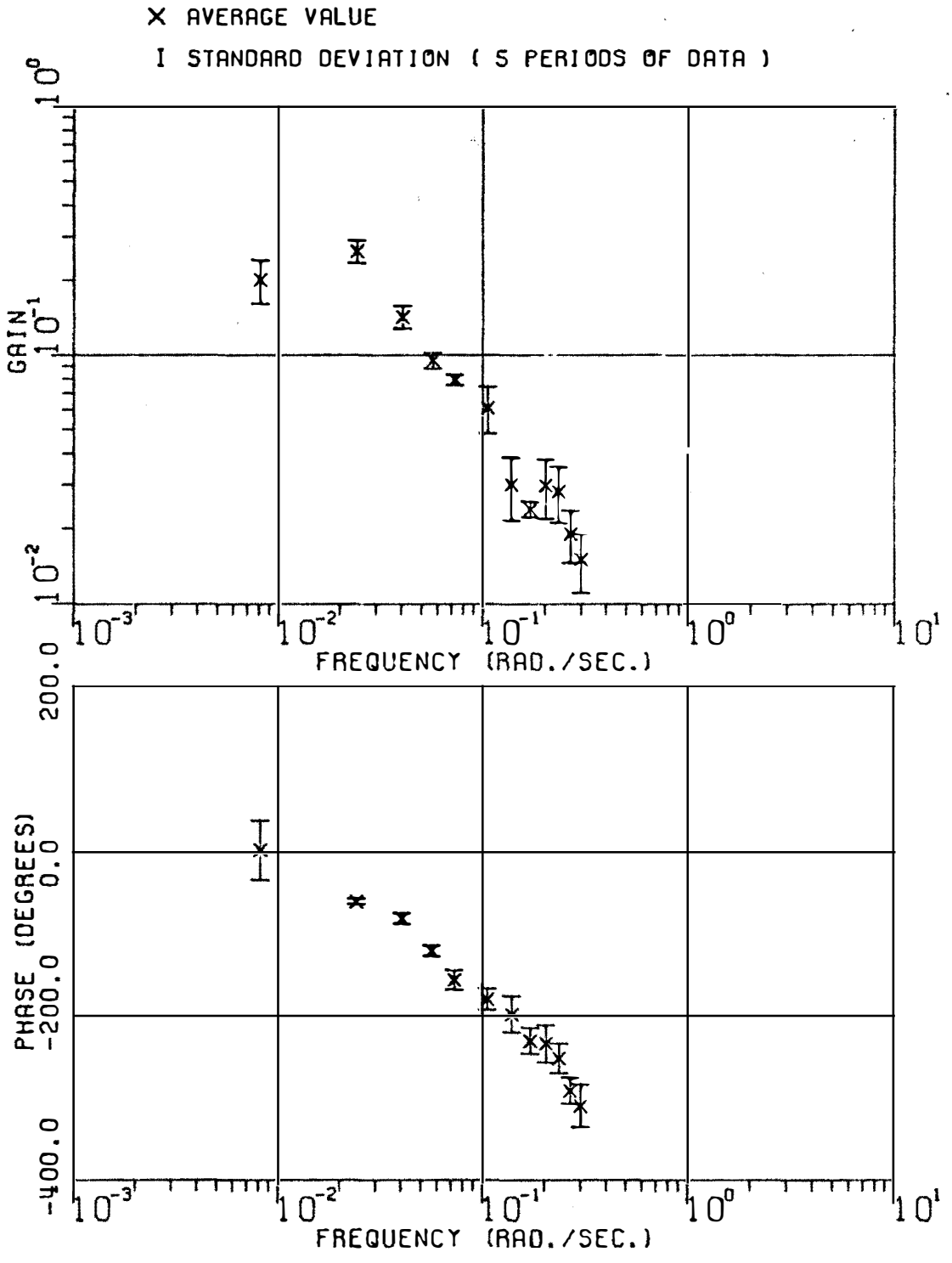

FIGURE IV-16. STANDARD DEVIATIONS OF COLD LEG TEMPERATURE TO REACTIVITY TRANSFER FUNCTION RESULTS

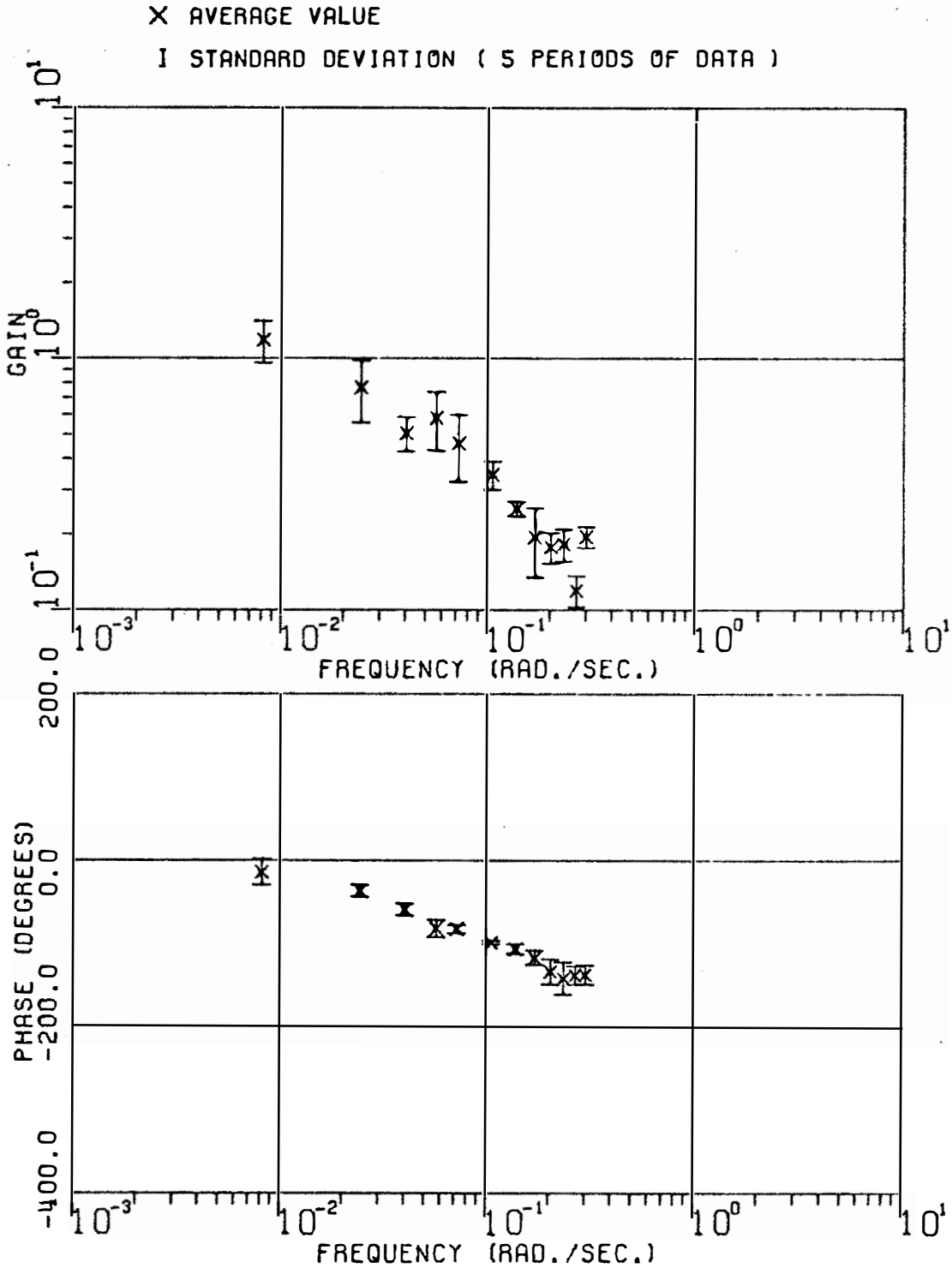

FIGURE IV-17. STANDARD DEVIATIONS OF STEAM PRESSURE TO REACTIVITY TRANSFER FUNCTION RESULTS

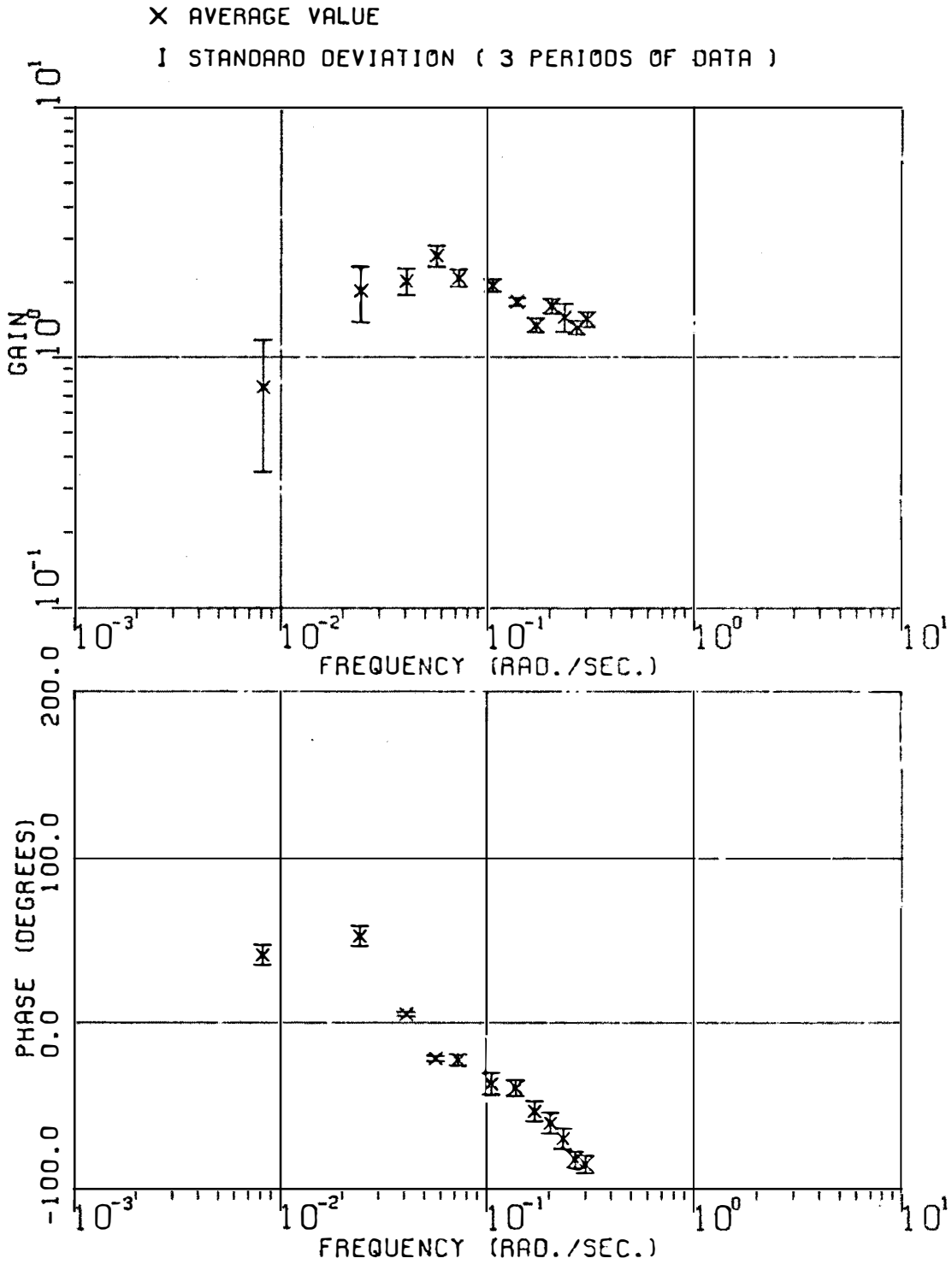

FIGURE IV-18. STANDARD DEVIATIONS OF PRESSURIZER PRESSURE TO REACTIVITY TRANSFER FUNCTION RESULTS

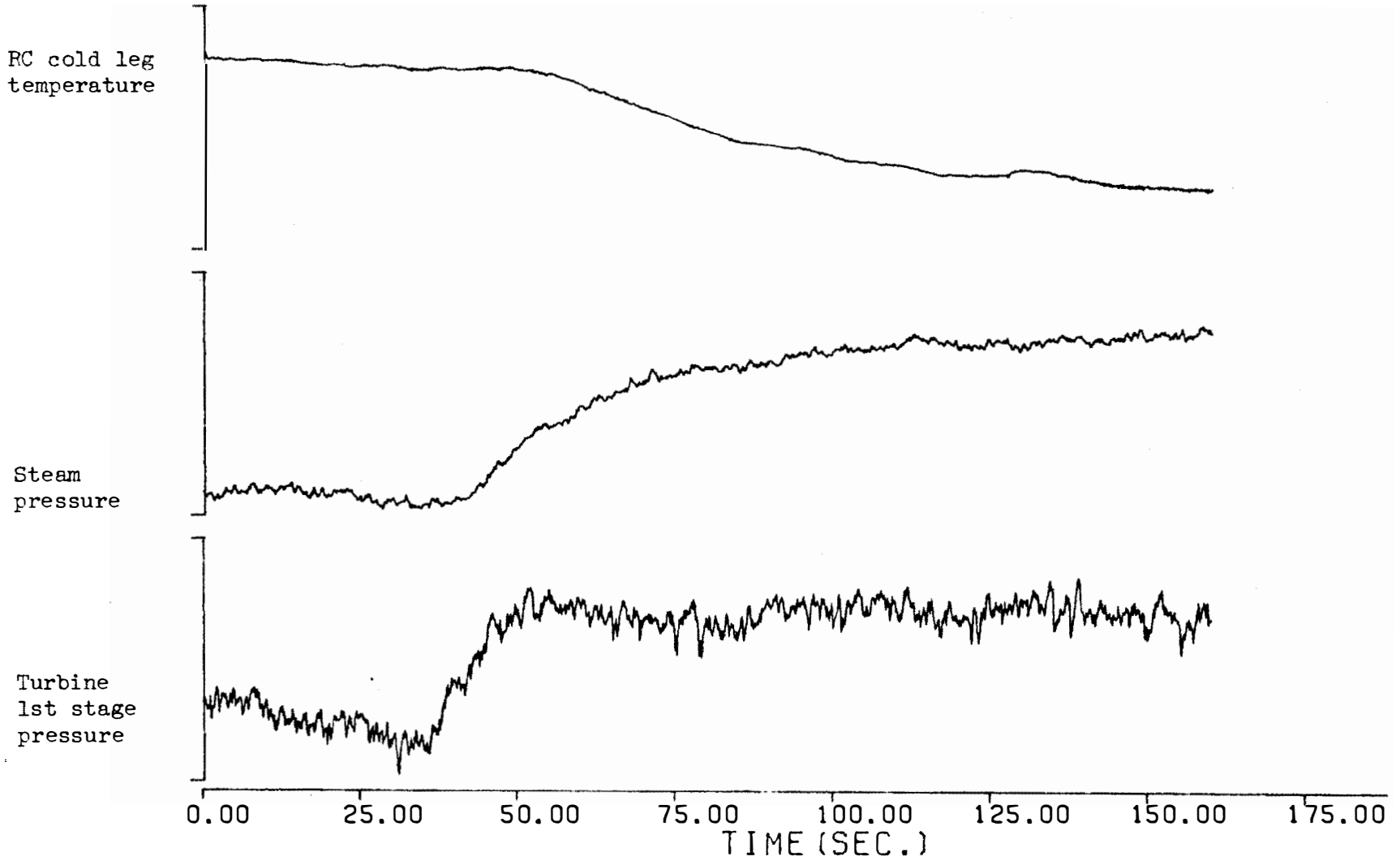

FIGURE IV-19. Responses of Steam Pressure and RC Cold Leg Temperature to a Step Change (Positive Step) in the Turbine 1-st Stage Pressure.

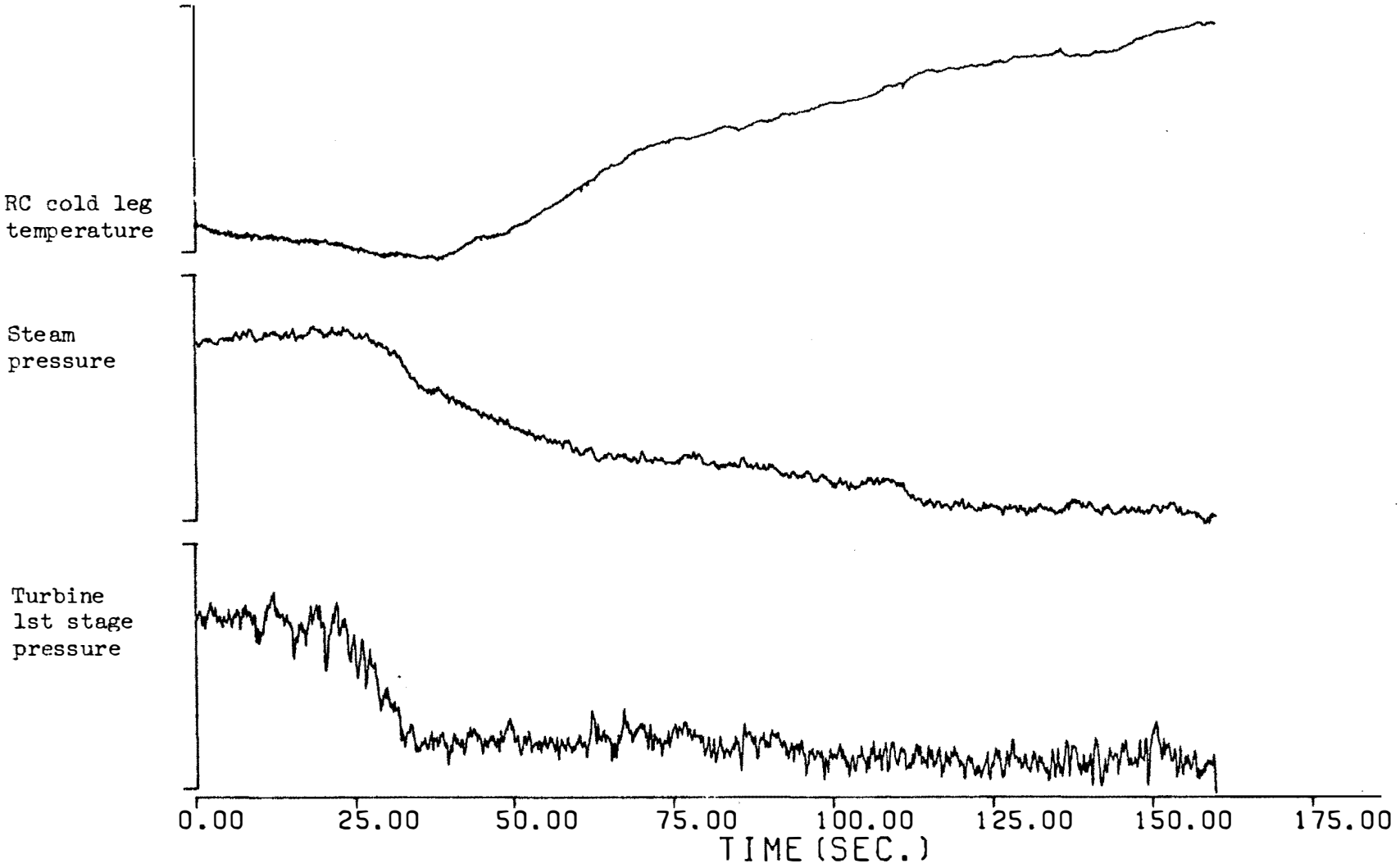

FIGURE IV-20. Responses of the Steam Pressure and RC Cold Leg Temperature to a Step Change (negative step) in the Turbine 1-st Stage Pressure.

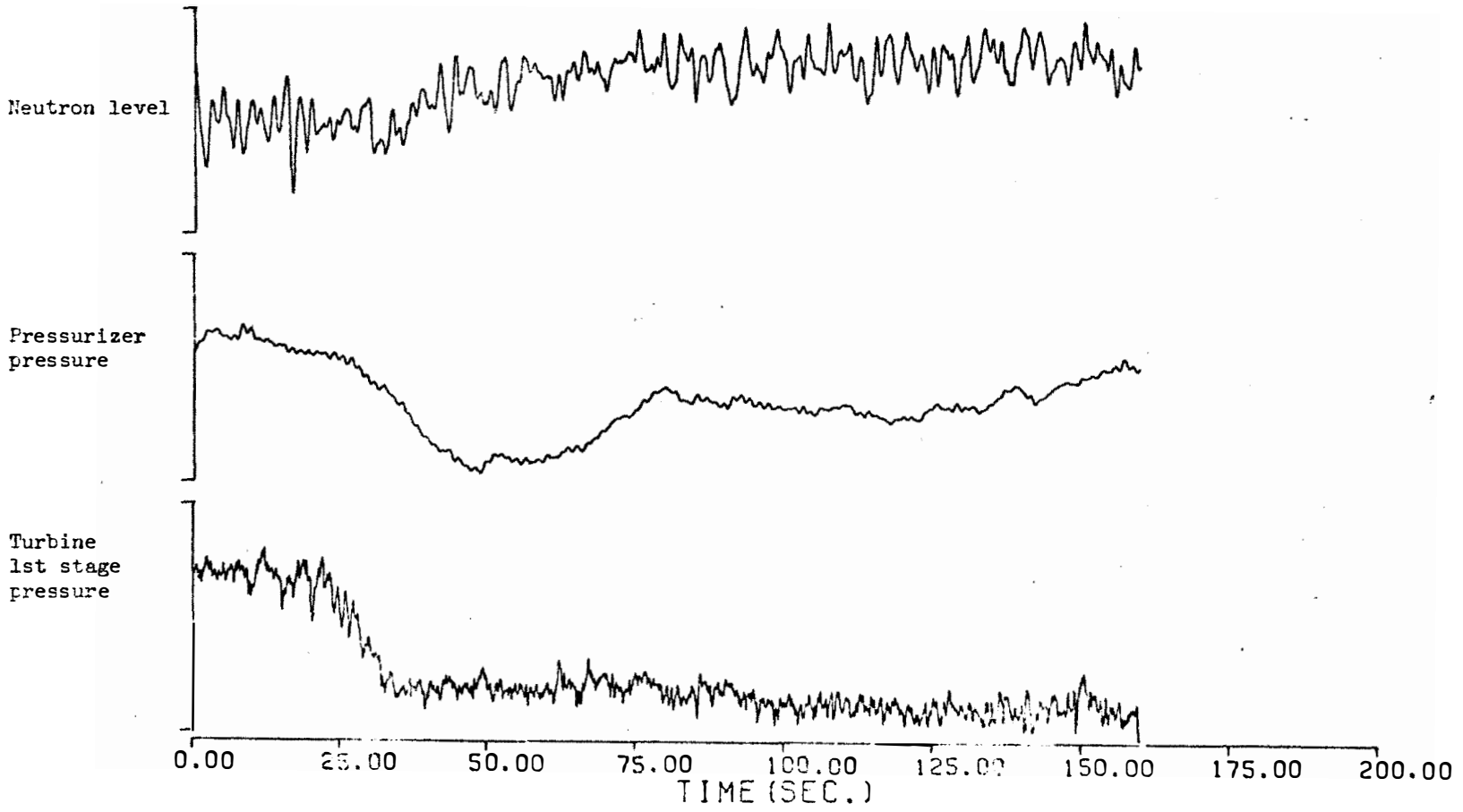

FIGURE IV-21. Responses of Pressurizer Pressure and Neutron Level to a Step Change in the Turbine 1-st Stage Pressure.

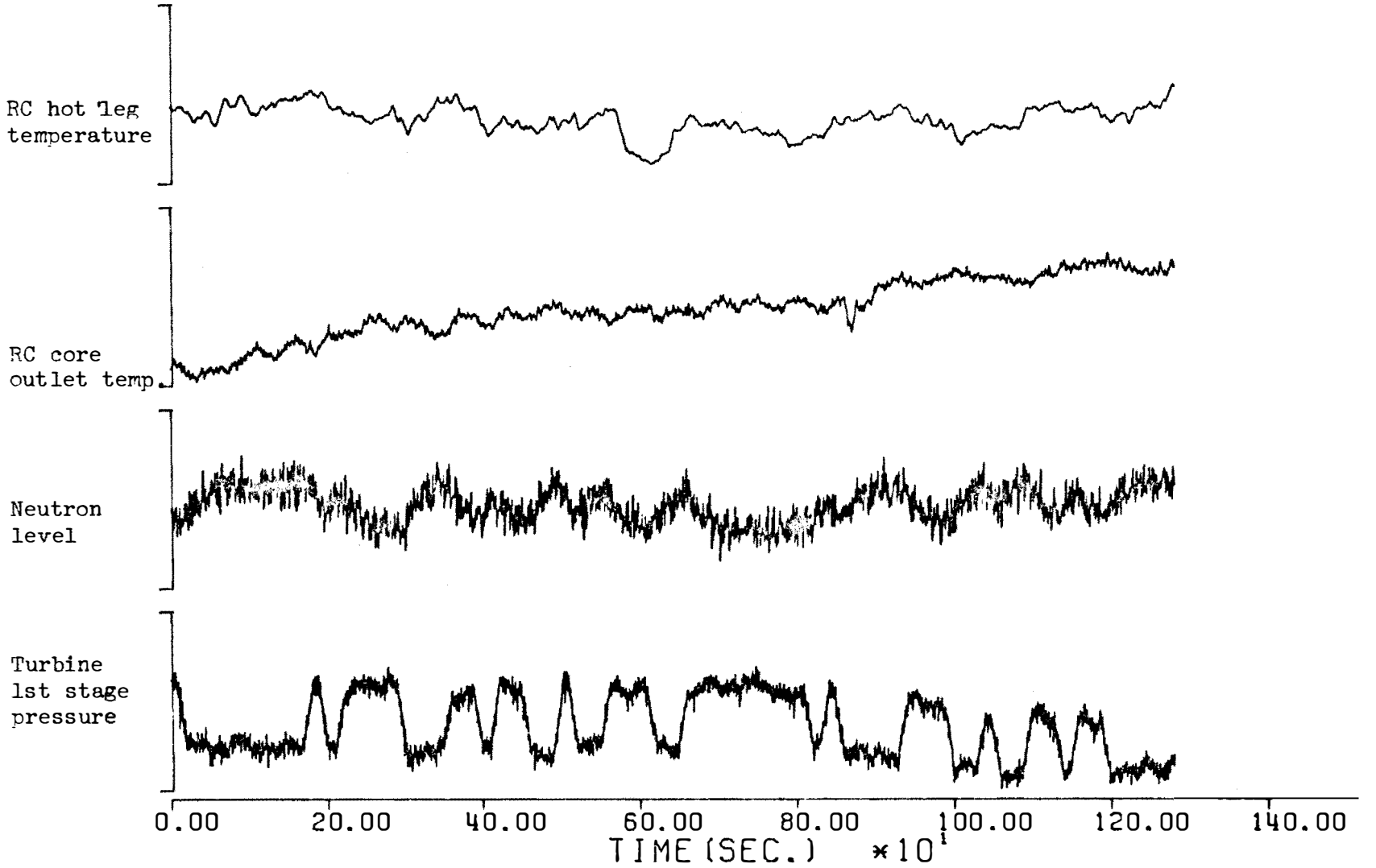

FIGURE IV-22. Responses of Neutron Level, RC Core Outlet Temperature, and RC Hot Leg Temperature Along with the 64-Bit MFBS Signal.

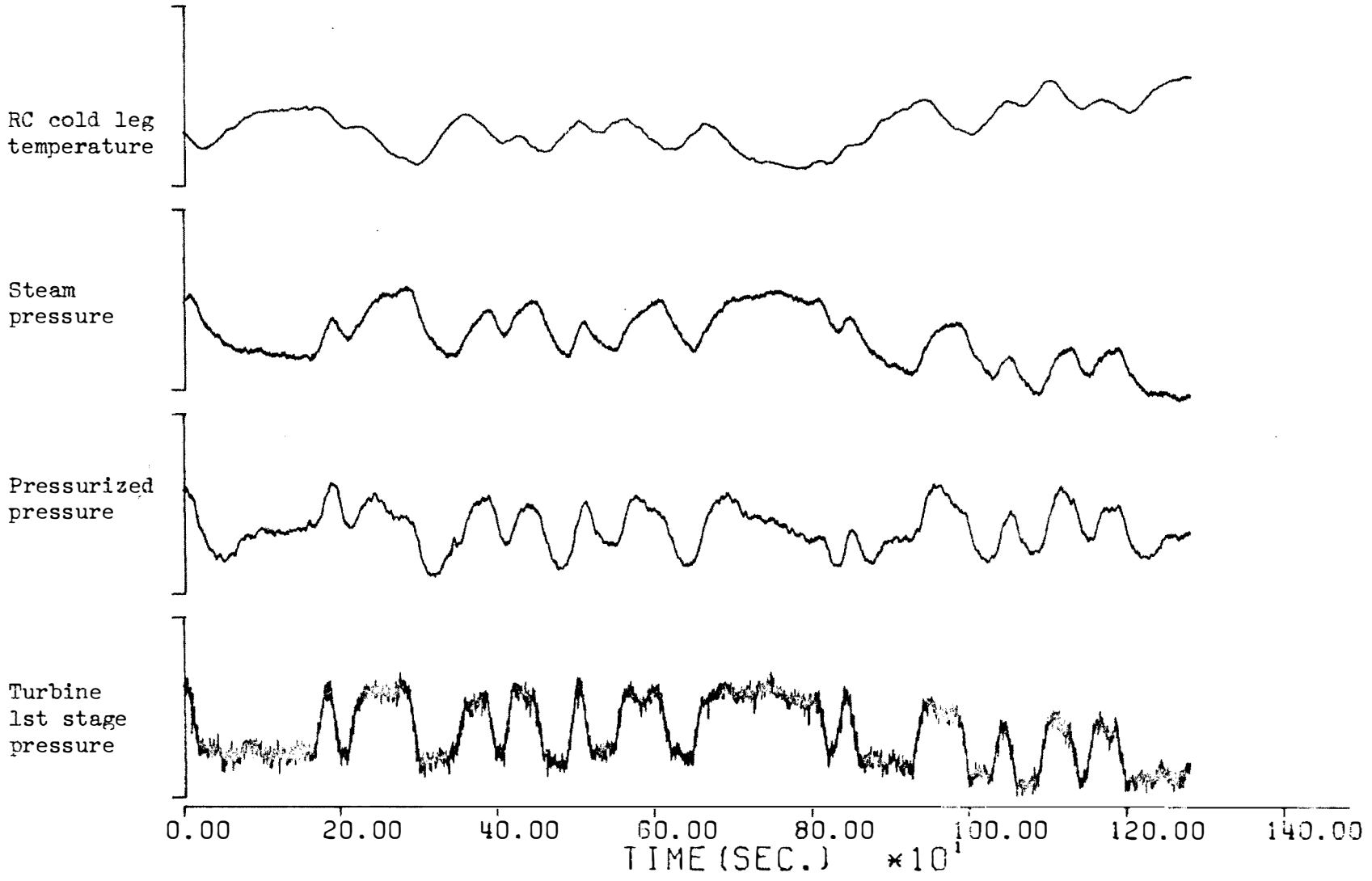

FIGURE IV-23. Responses of Pressurizer Pressure, Steam Pressure, and RC Cold Leg Temperature Along with the 64-Bit MFBS Signal.

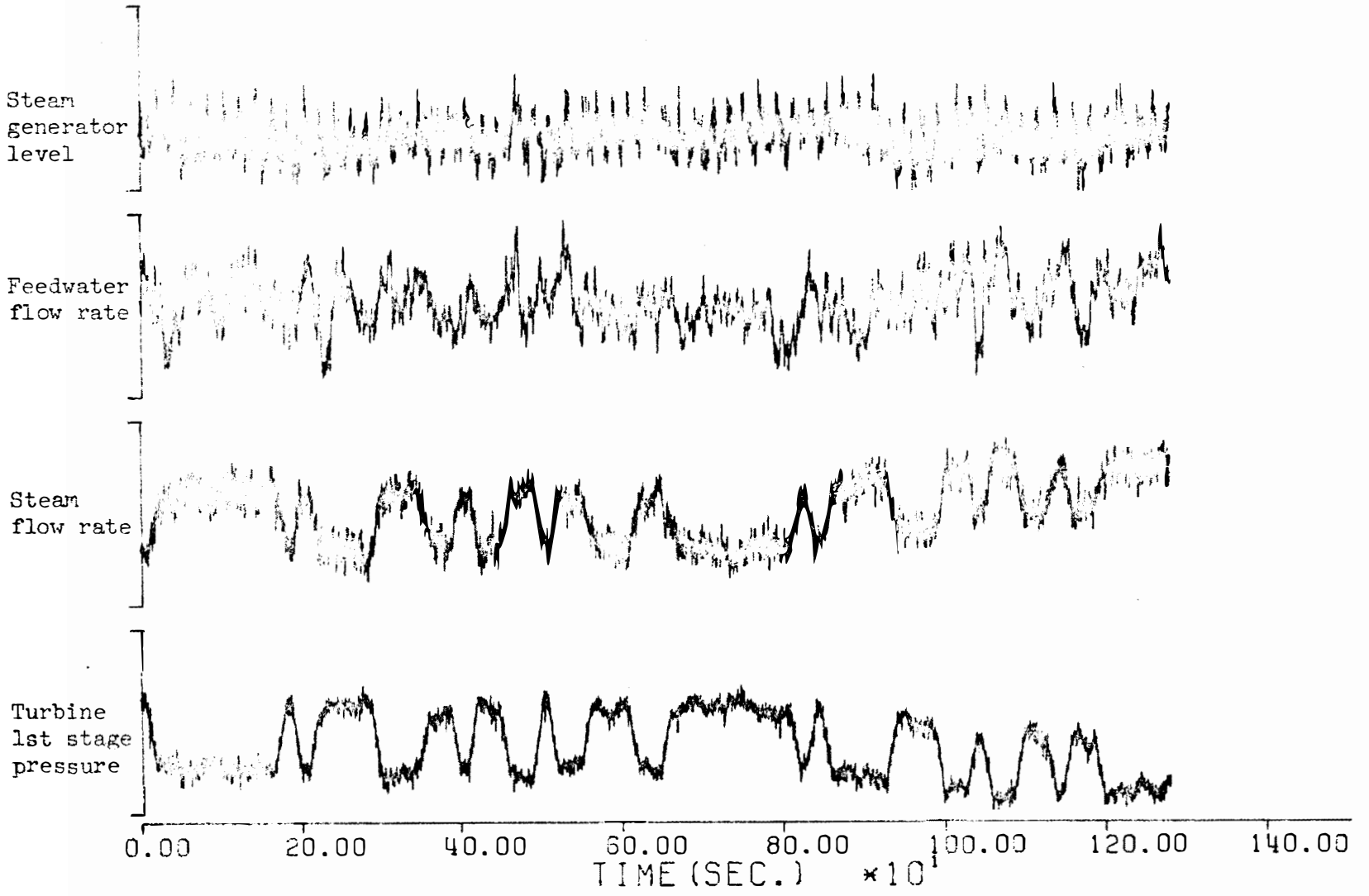

FIGURE IV-24. Responses of Steam Flow Rate, Feedwater Flow Rate, and Steam Generator Level Along with the 64-Bit MFBS Signal.

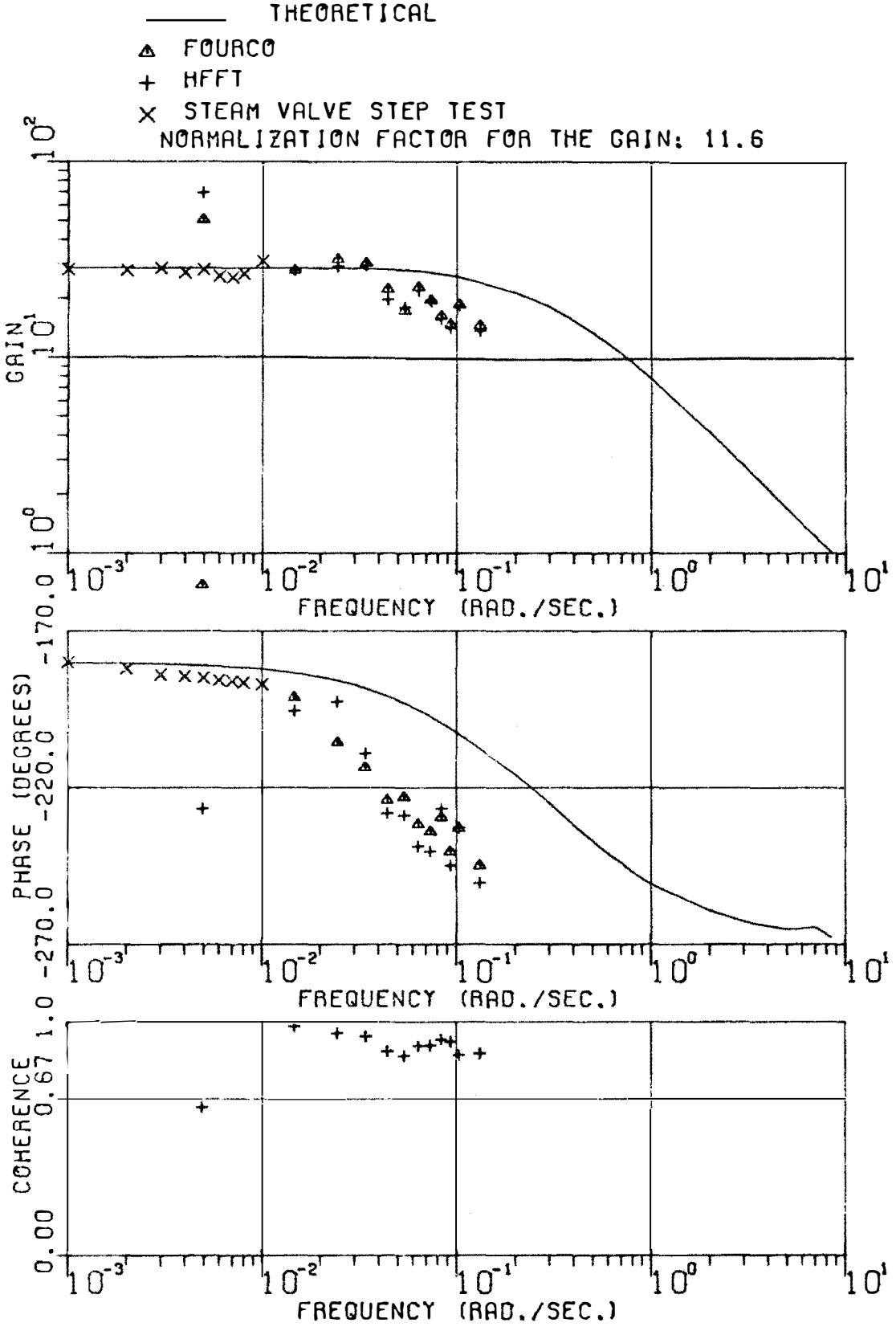

FIGURE IV-25. STEAM PRESSURE TO TURBINE (1-ST STAGE) PRESSURE TRANSFER FUNCTION

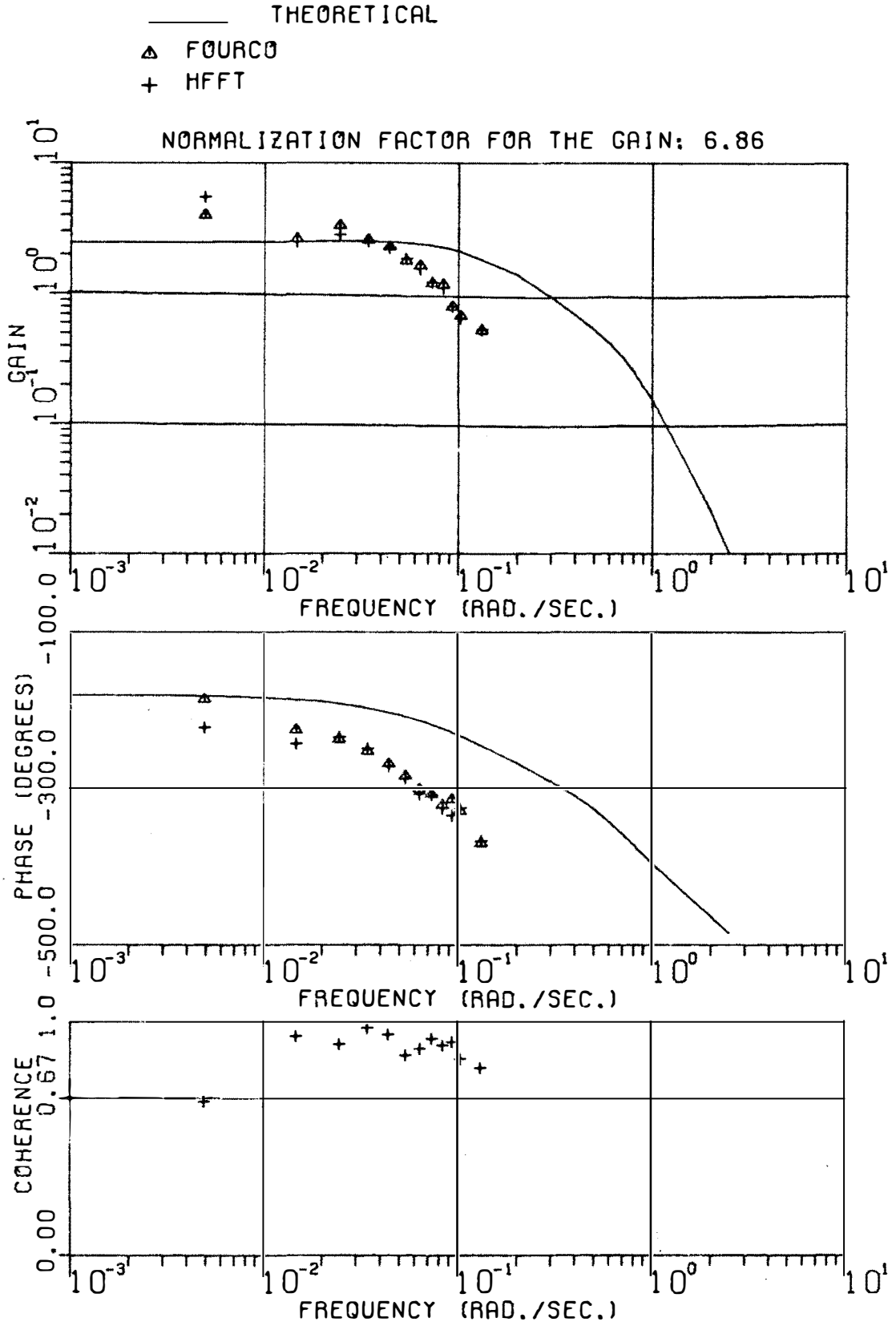

FIGURE IV-26. COLD LEG TEMPERATURE TO TURBINE (1-ST STAGE) PRESSURE TRANSFER FUNCTION

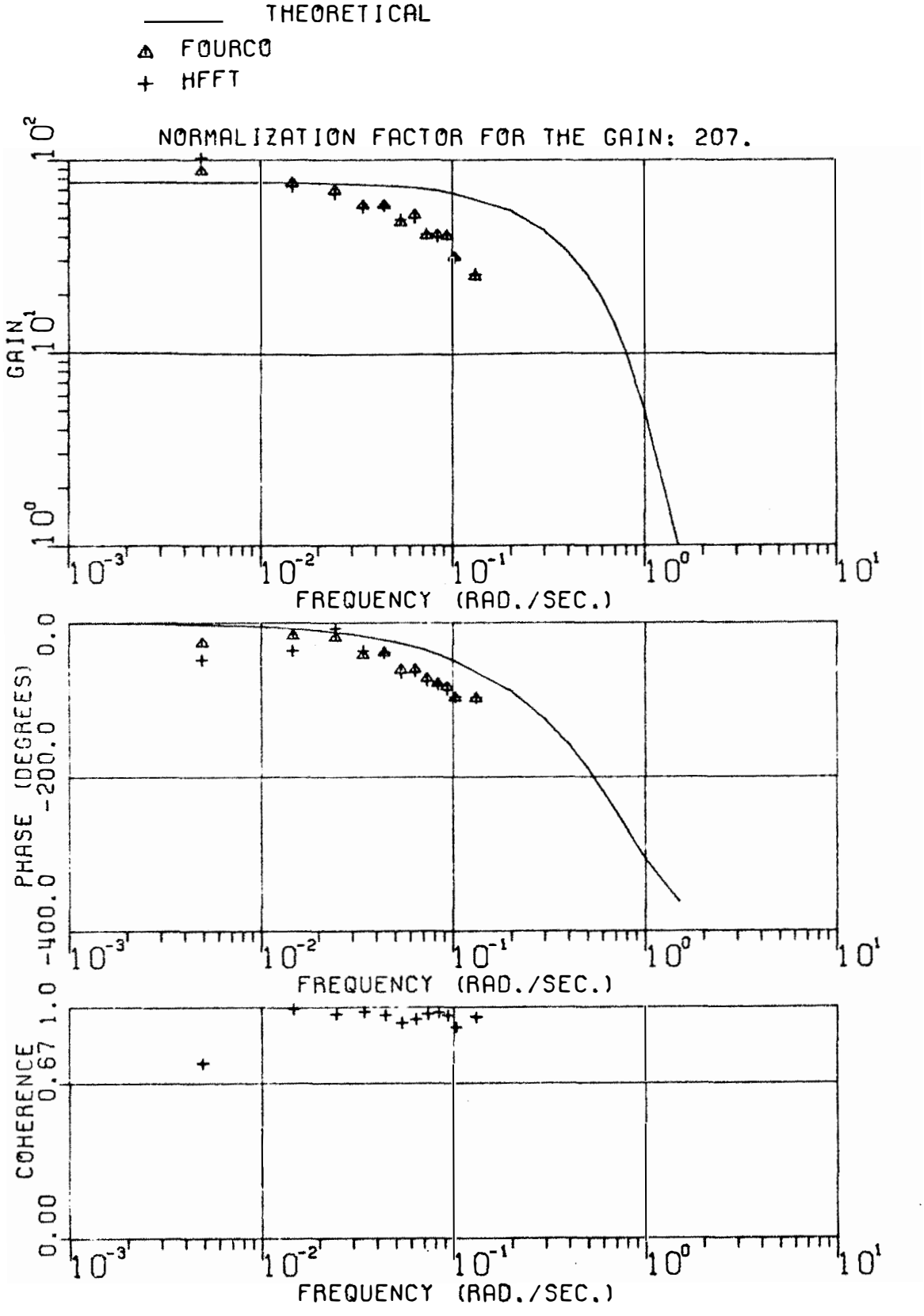

FIGURE IV-27. REACTOR POWER TO TURBINE (1-ST STAGE) PRESSURE TRANSFER FUNCTION

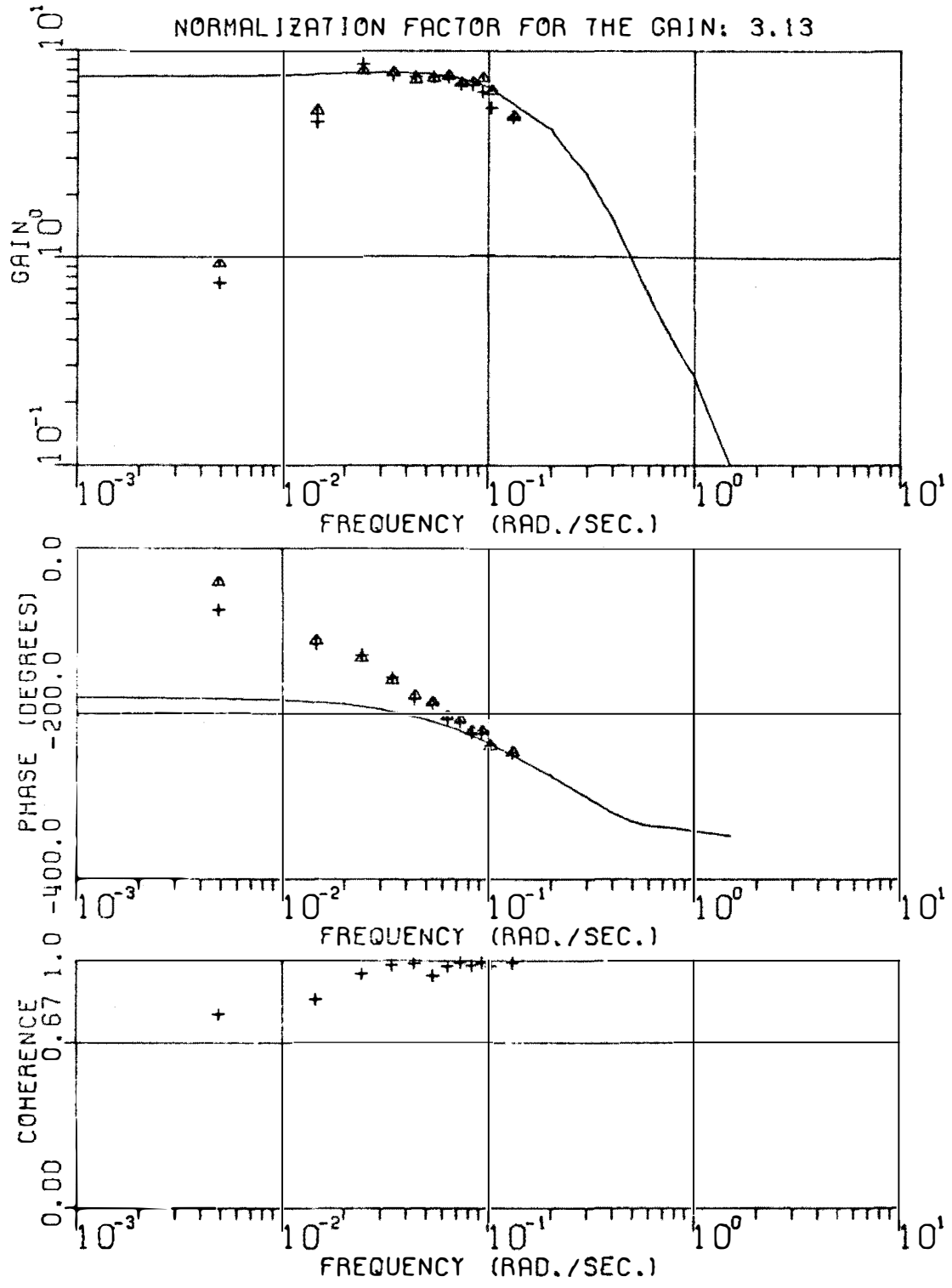

FIGURE IV-28. PRESSURIZER PRESSURE TO TURBINE (1-ST STAGE) PRESSURE TRANSFER FUNCTION

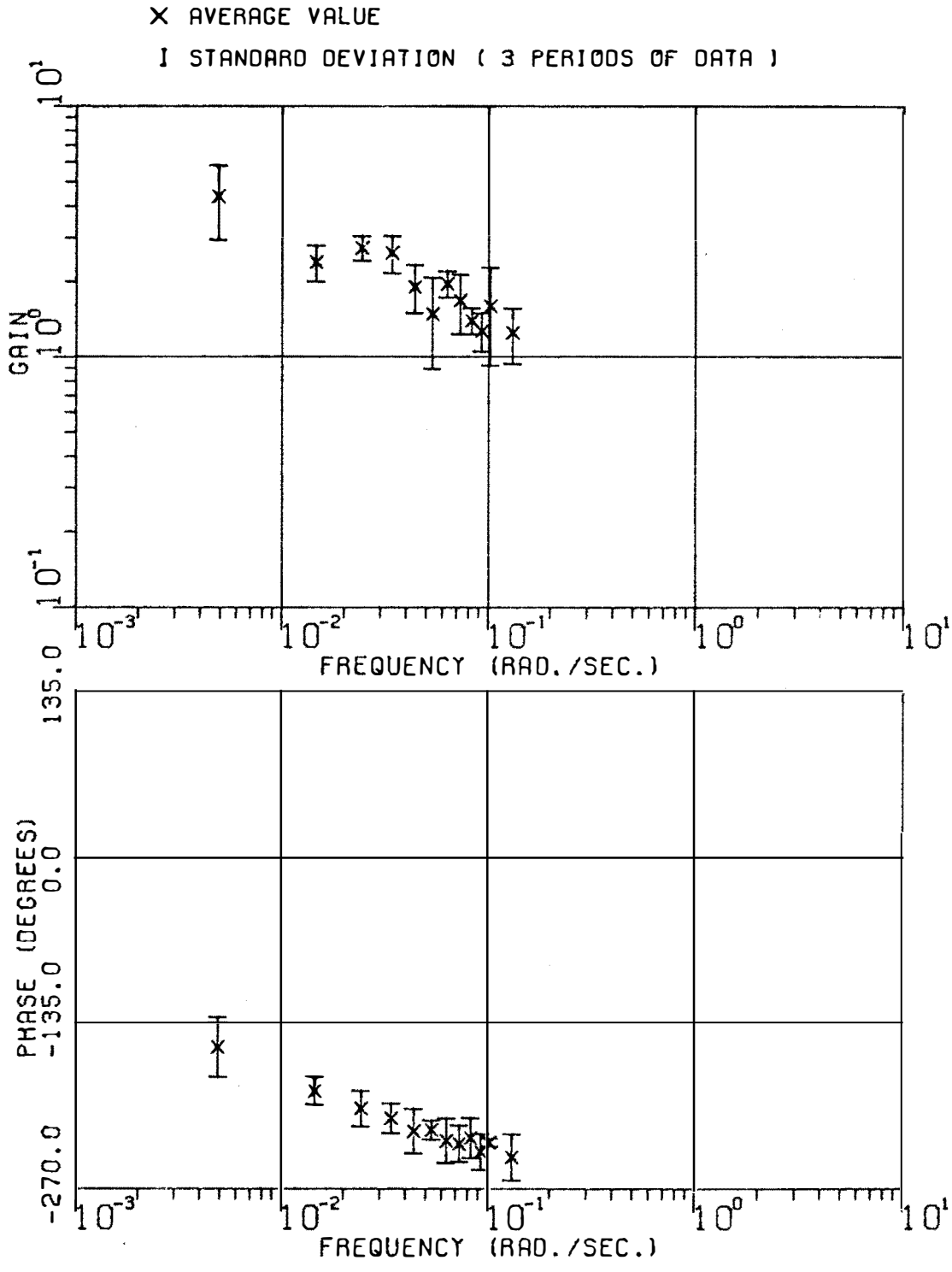

FIGURE IV-29. STANDARD DEVIATIONS OF STEAM PRESSURE TO TURBINE (1-ST STAGE) PRESSURE TRANSFER FUNCTION RESULTS

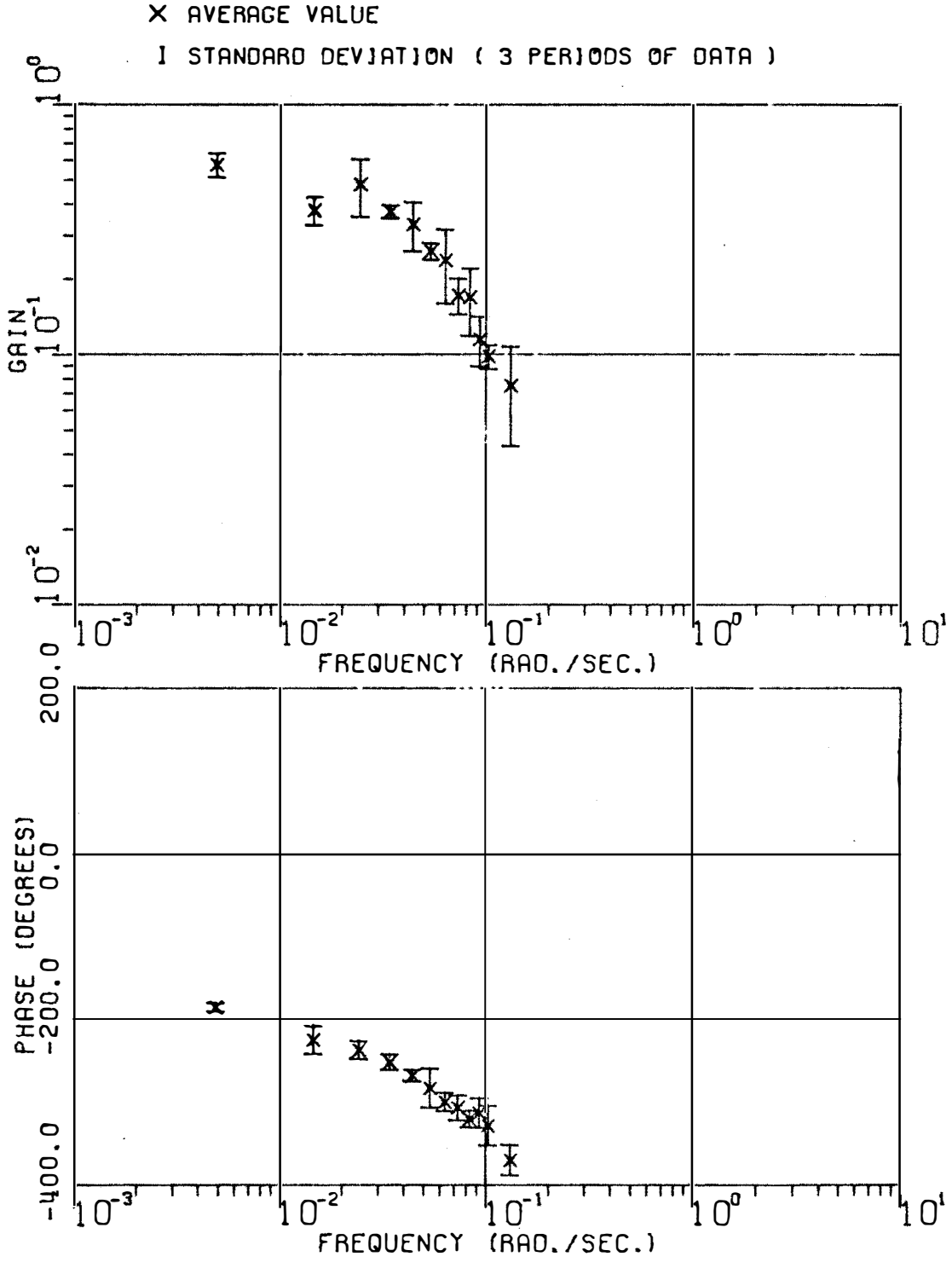

FIGURE IV-30. STANDARD DEVIATIONS OF COLD LEG TEMP. TO TURBINE (1-ST STAGE) PRESSURE TRANSFER FUNCTION RESULTS

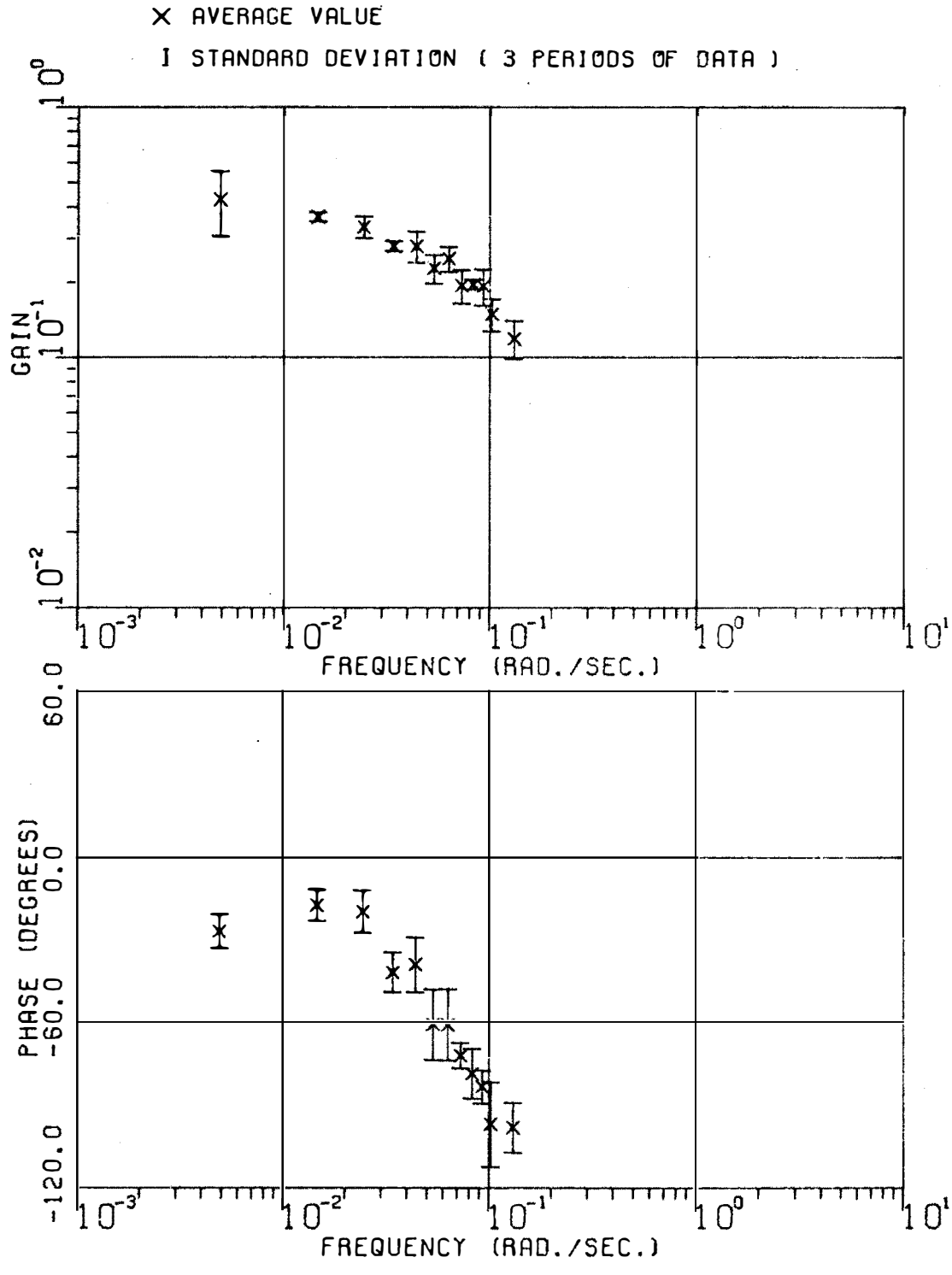

FIGURE IV-31. STANDARD DEVIATIONS OF REACTOR POWER TO TURBINE (1-ST STAGE) PRESSURE TRANSFER FUNCTION RESULTS

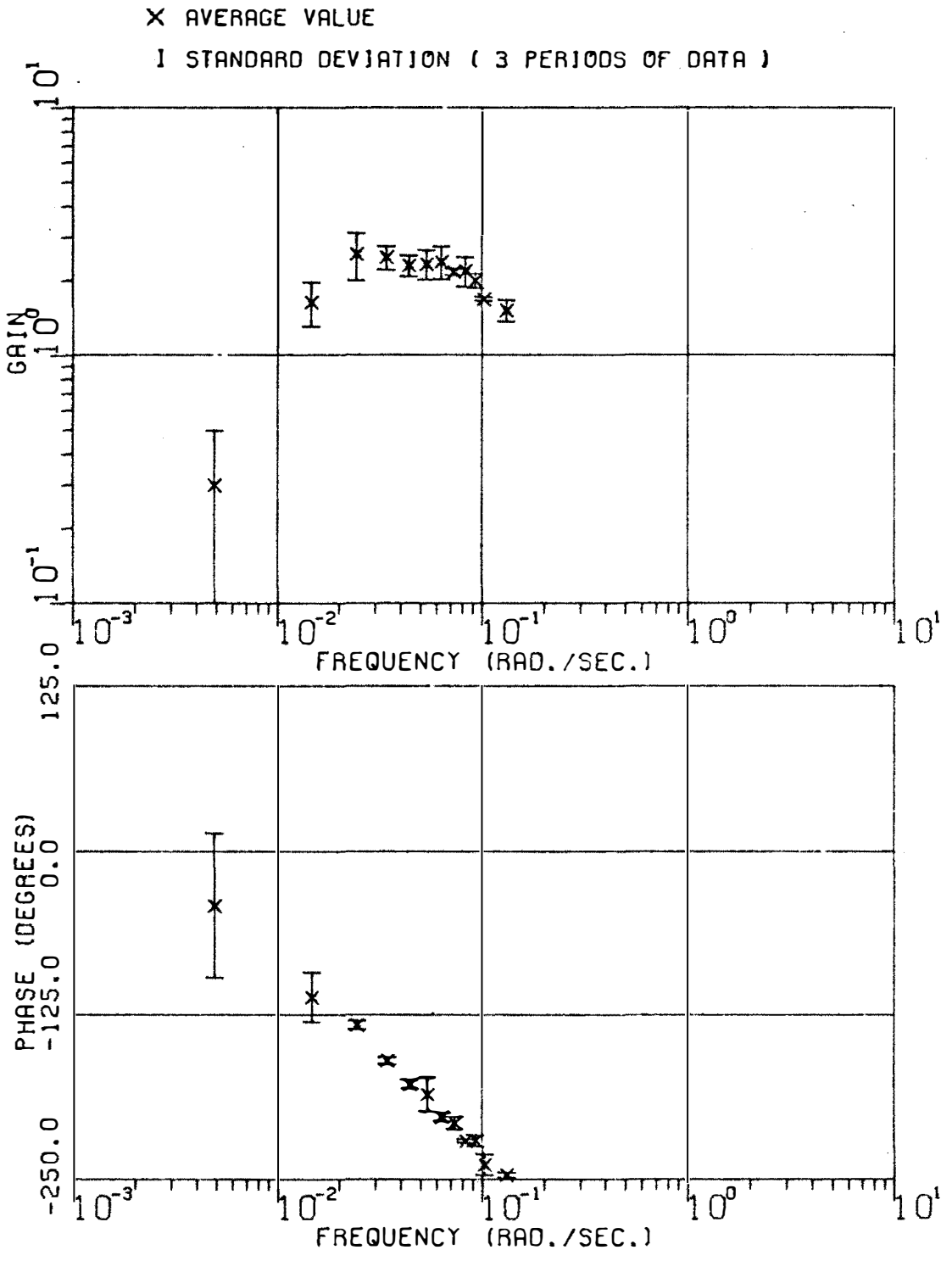

FIGURE IV-32. STANDARD DEVIATIONS OF PRESSURIZER PRESS. TO TURBINE (1-ST STAGE) PRESSURE TRANSFER FUNCTION RESULTS

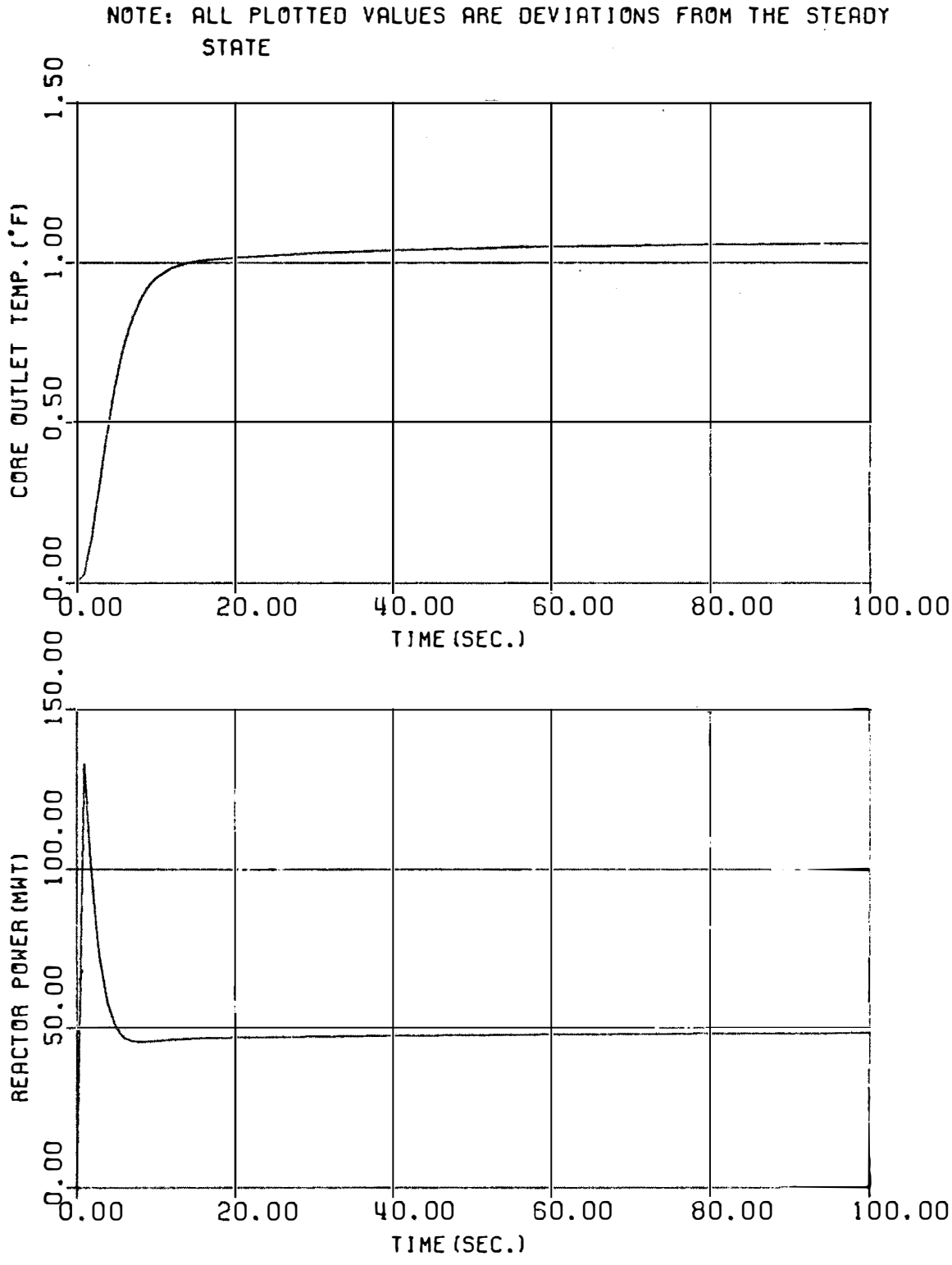

FIGURE A-1. TRANSIENT RESPONSE OF THE ISOLATED REACTOR FOR 0.071$ STEP CHANGE IN REACTIVITY

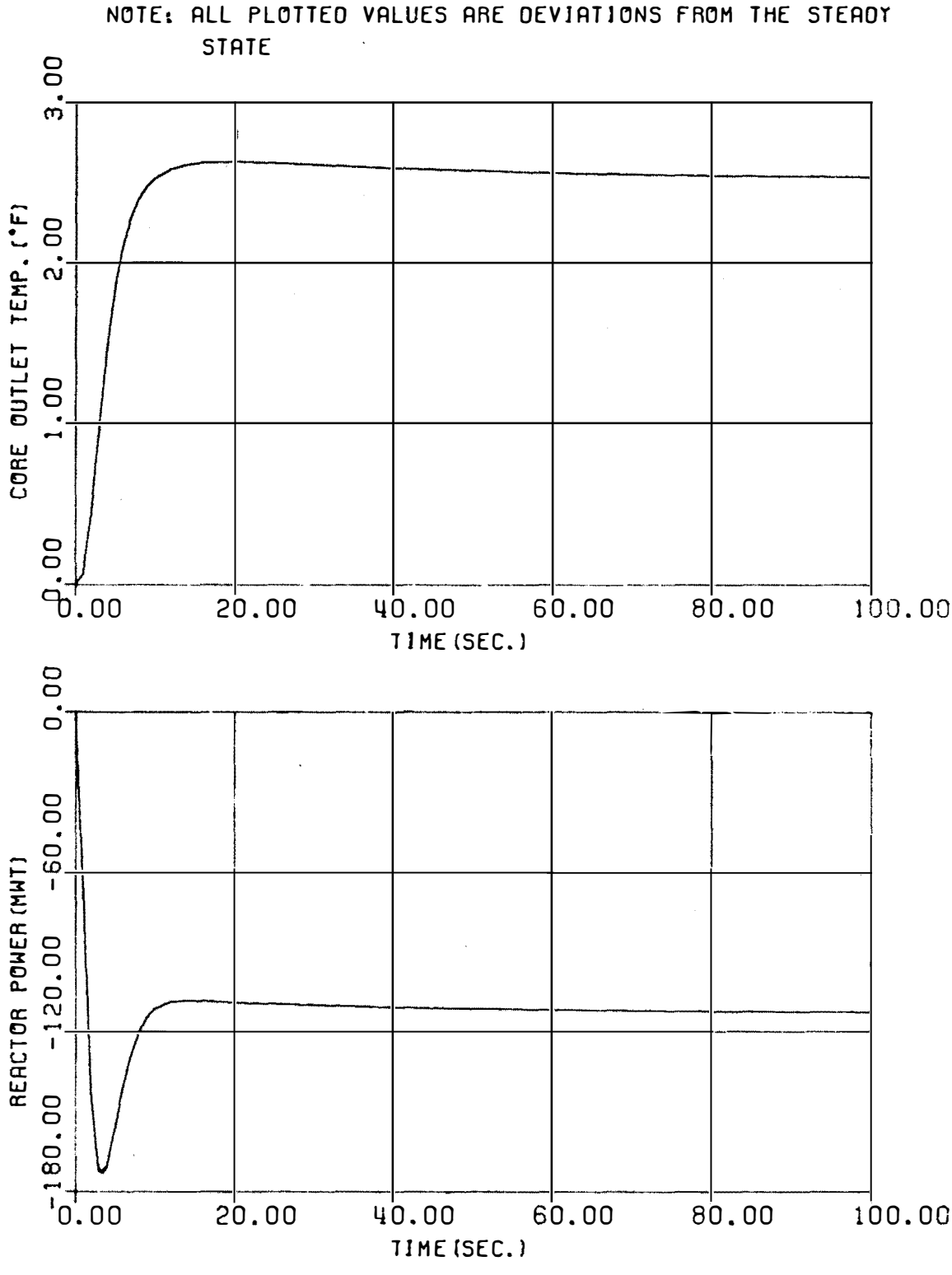

FIGURE A-2. TRANSIENT RESPONSE OF THE ISOLATED REACTOR FOR 5 °F STEP CHANGE IN RC INLET TEMPERATURE

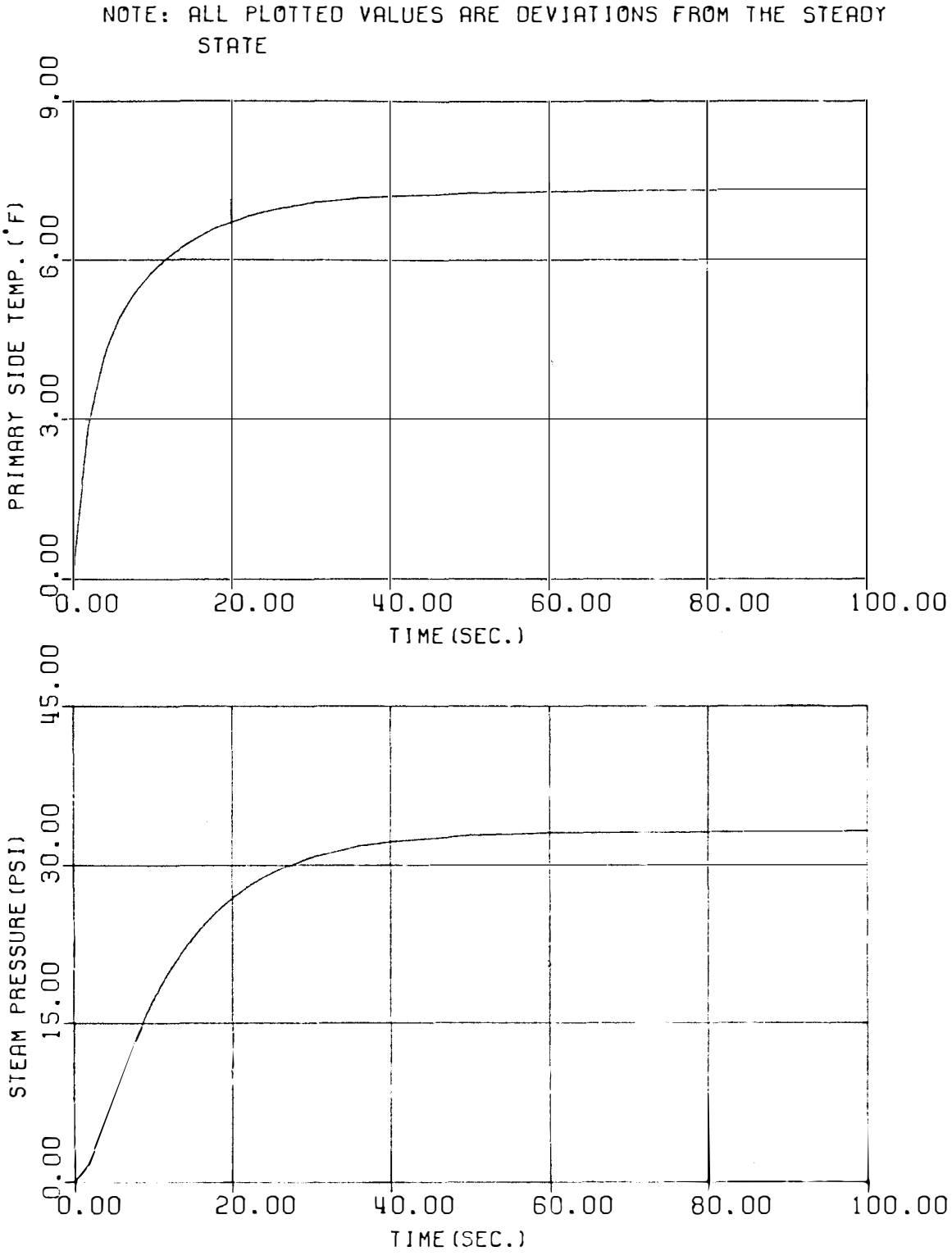

FIGURE B-1. TRANSIENT RESPONSE OF THE ISOLATED STEAM GENERATOR FOR 10°F STEP CHANGE IN THE PRIMARY SIDE INLET TEMP.

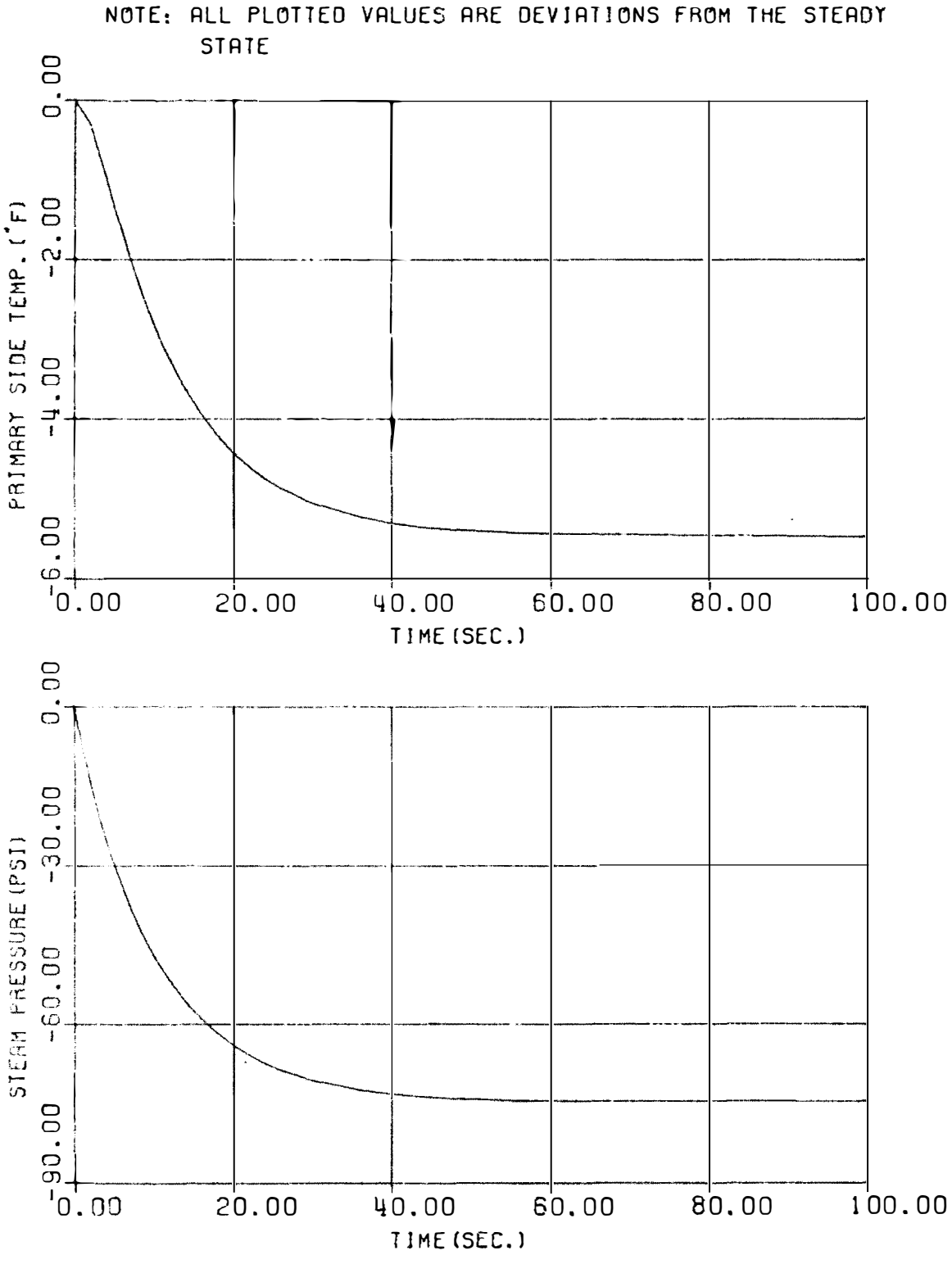

FIGURE B-2. TRANSIENT RESPONSE OF THE ISOLATED STEAM GENERATOR FOR 50 PSI STEP CHANGE IN THE TURBINE(1-ST STAGE) PRESSURE

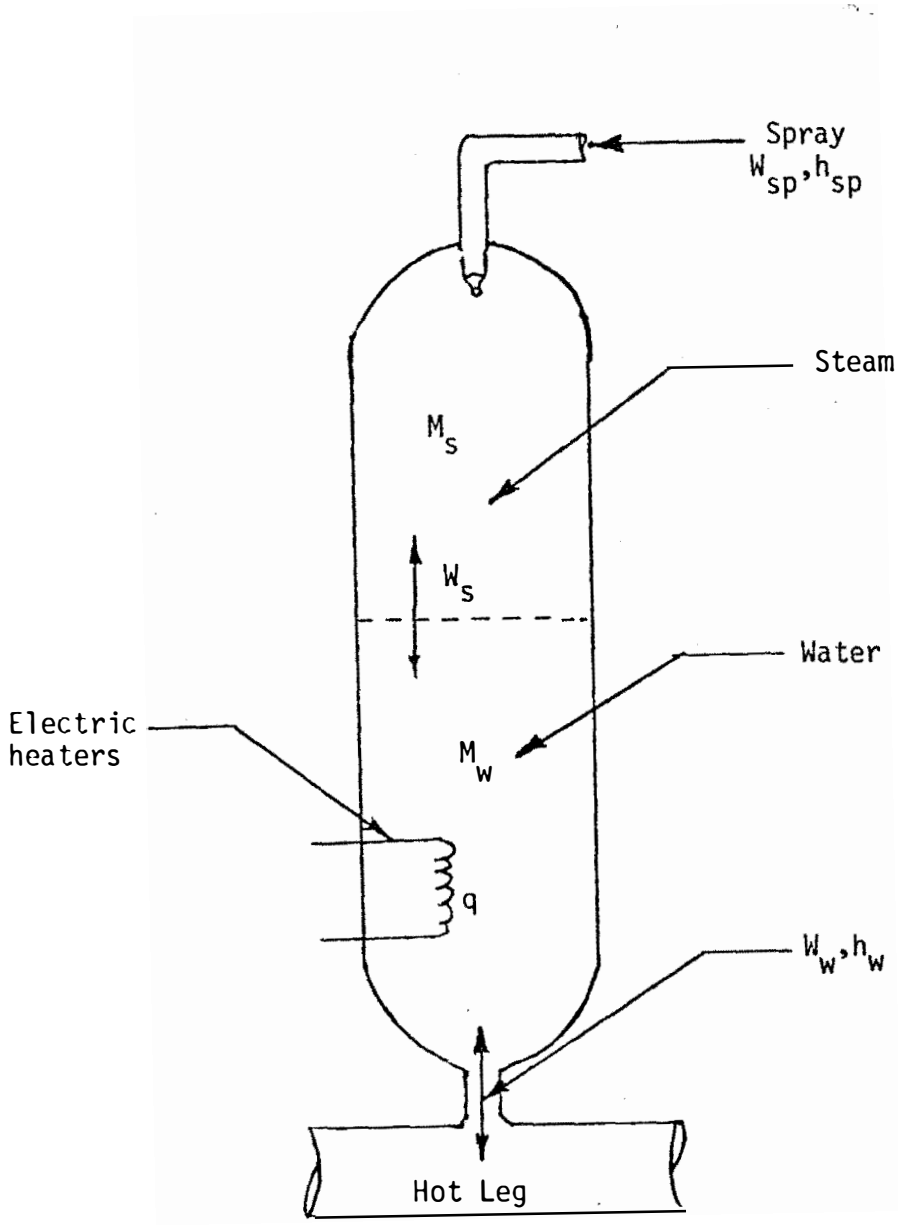

FIGURE C-1. Schematic Drawing of Pressurizer.

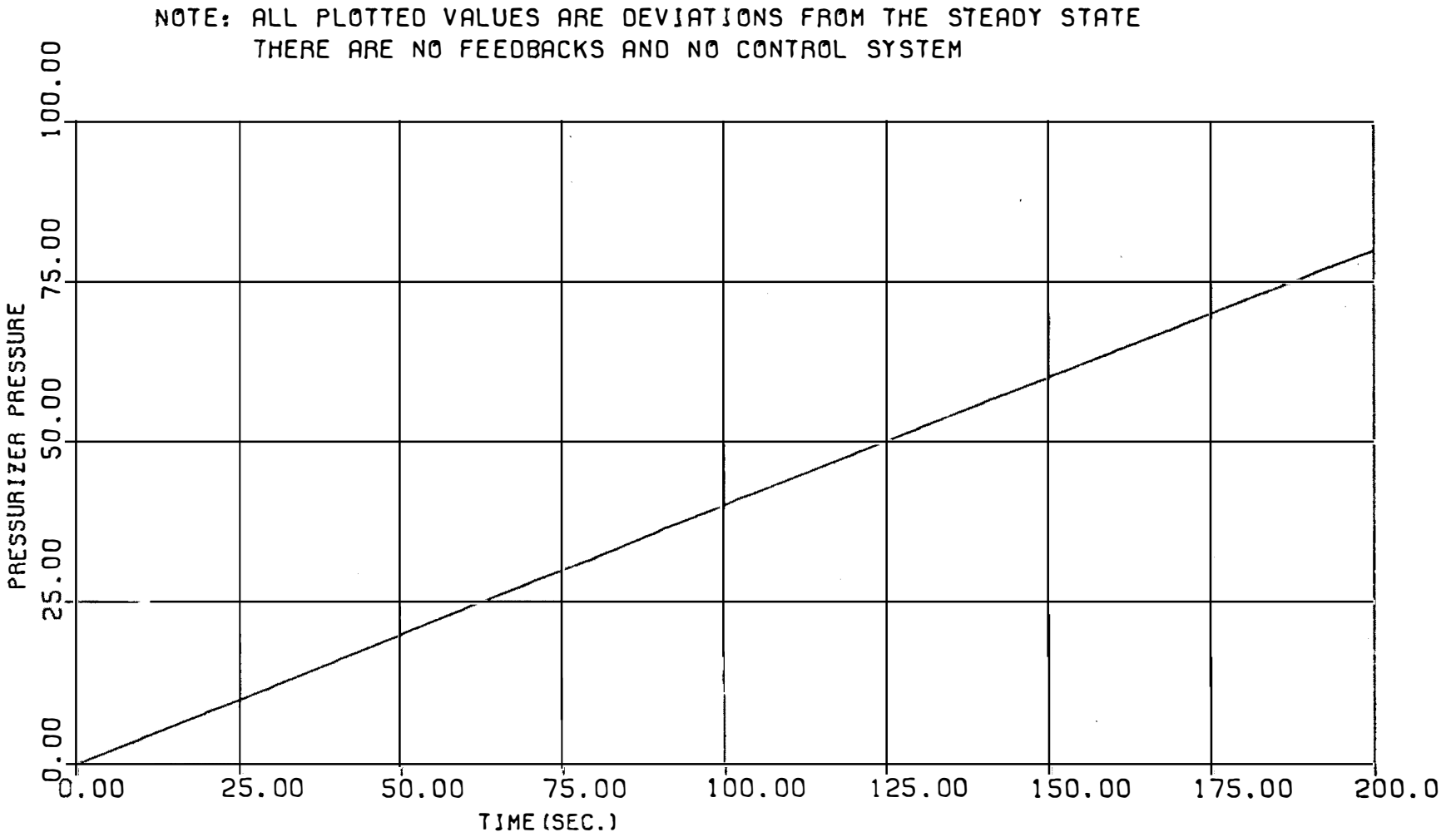

FIGURE C-2. TRANSIENT RESPONSE OF THE ISOLATED PRESSURIZER FOR 50.0 (LB/SEC.) STEP CHANGE IN INSURGE RATE

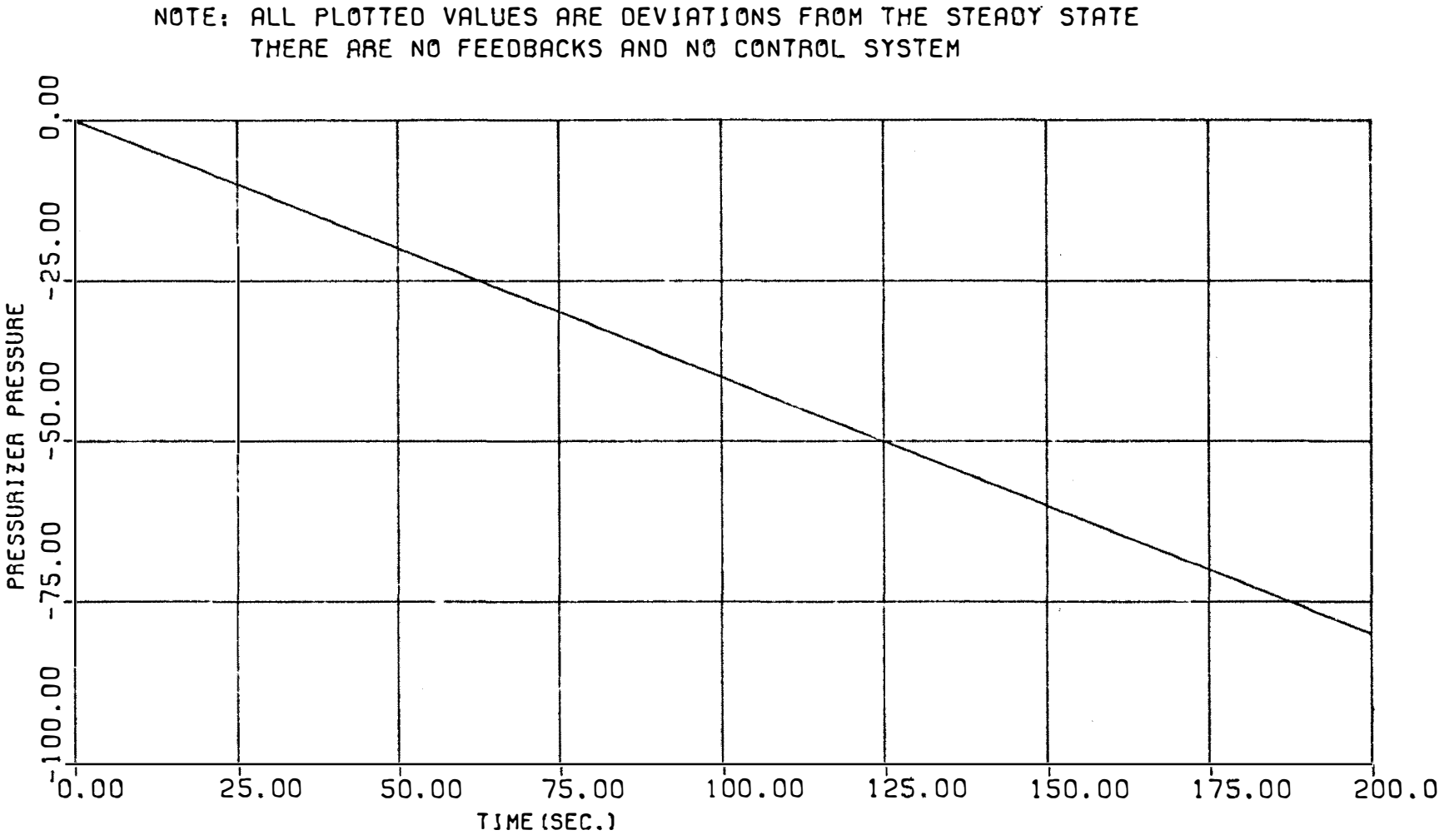

FIGURE C-3. TRANSIENT RESPONSE OF THE ISOLATED PRESSURIZER FOR 50.0 (LB/SEC.) STEP CHANGE IN THE SPRAY RATE

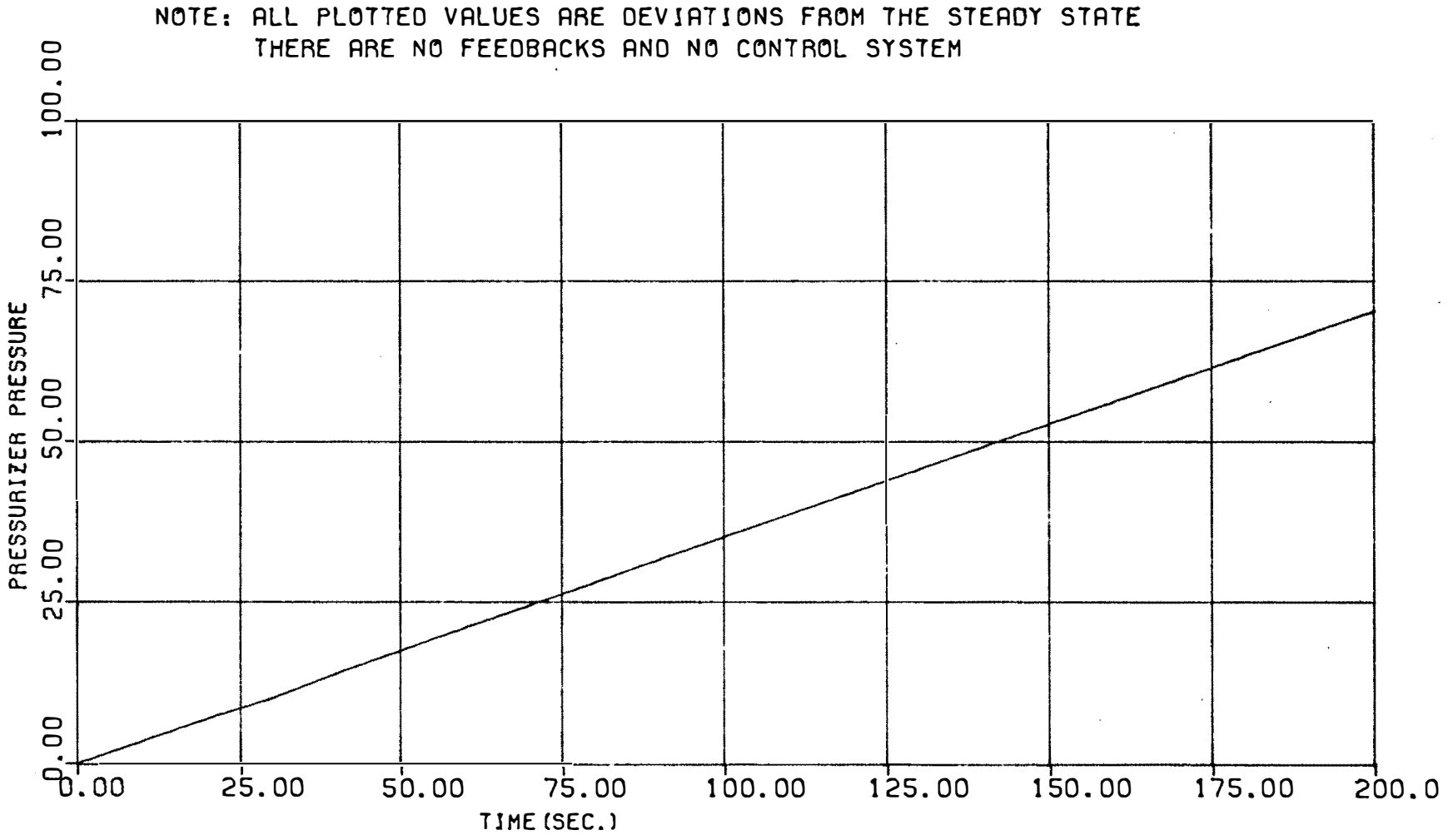

FIGURE C-4. TRANSIENT RESPONSE OF THE ISOLATED PRESSURIZER FOR 100 (KW.) STEP CHANGE IN THE ELECTRIC HEAT INPUT

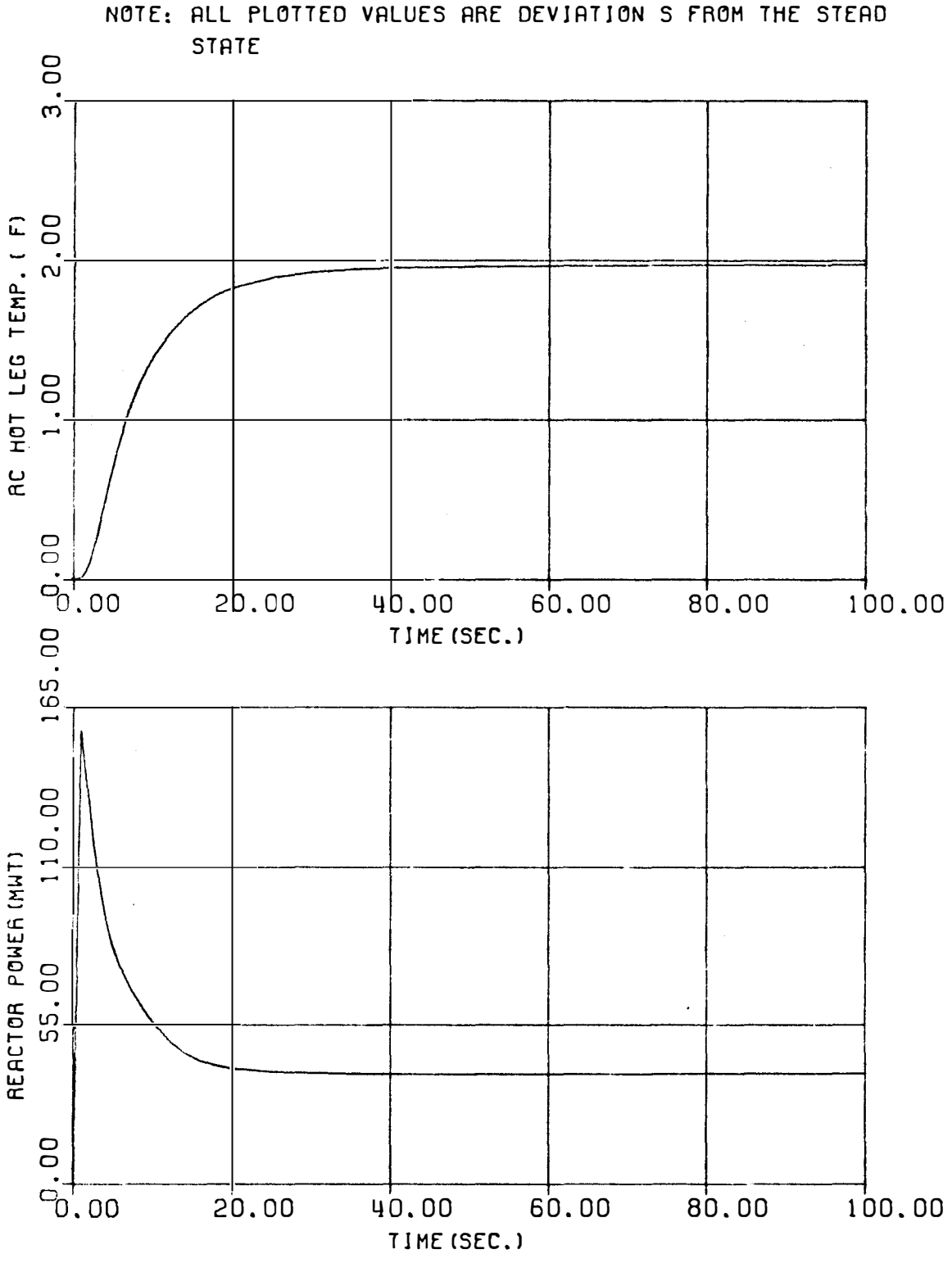

FIGURE D-1. TRANSIENT RESPONSE OF THE SYSTEM FOR 0.071$ STEP CHANGE IN REACTIVITY

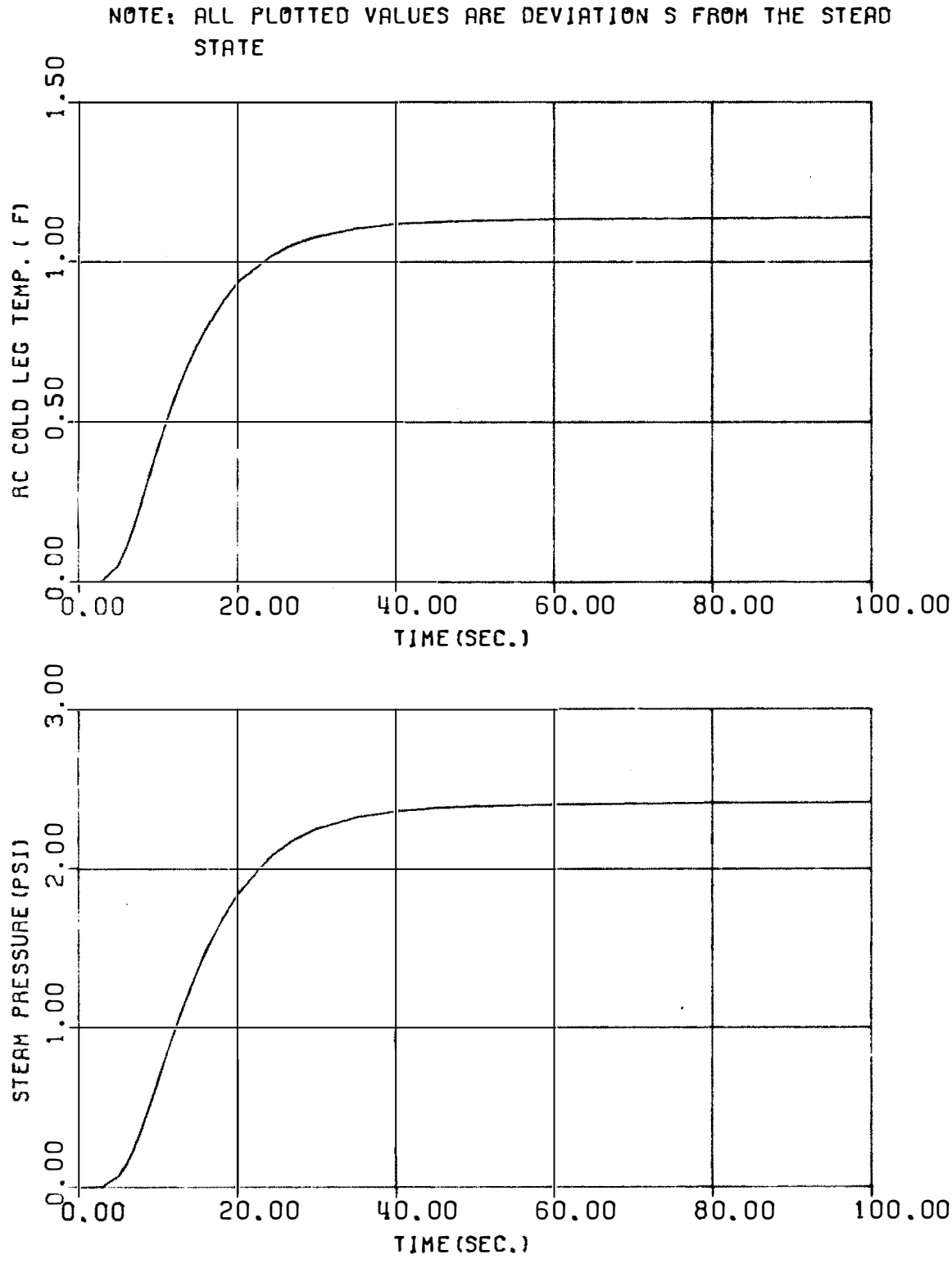

FIGURE D-2. Time Response of the System for 0.071$ Step Change in Reactivity.

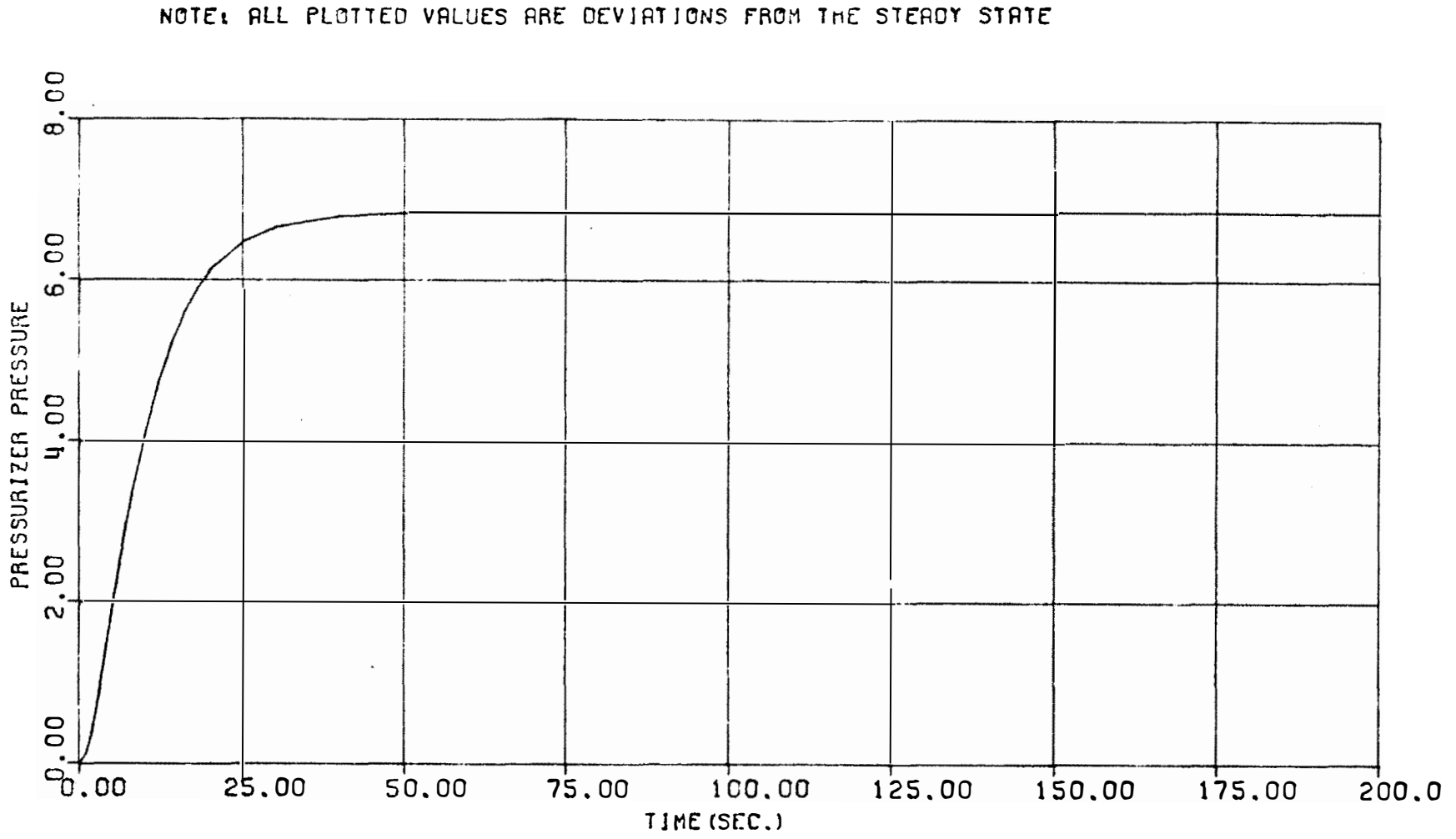

FIGURE D-3. Pressurizer Pressure Response for 0.017¢ Step Change in Reactivity.

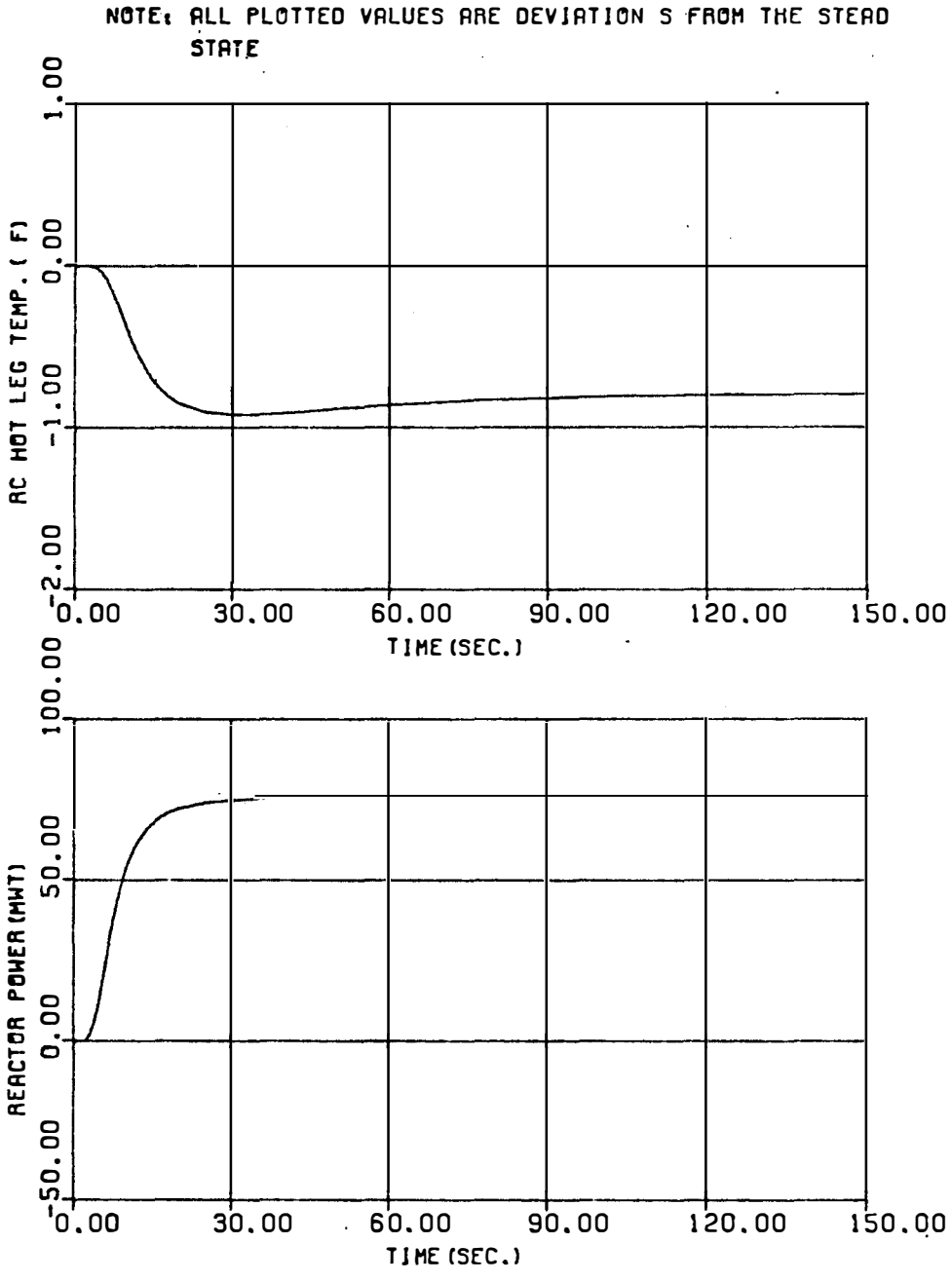

FIGURE D-4. TRANSIENT RESPONSE OF THE SYSTEM FOR 50 PSI STEP CHANGE IN THE TURBINE (1-ST STAGE) PRESSURE

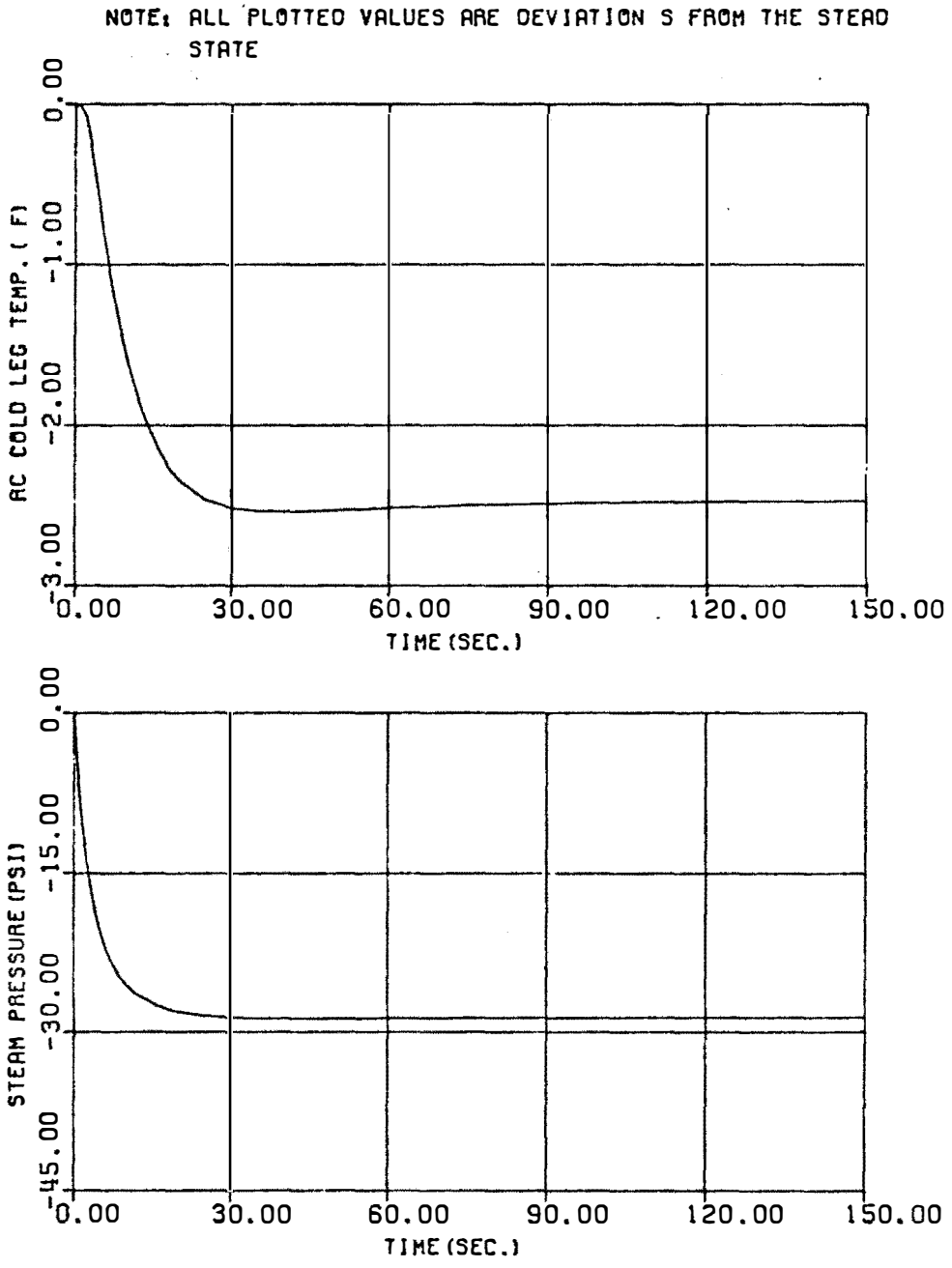

FIGURE D-5. Time Response of the System for 50 PSI Step Change in the Turbine (1-st Stage) Pressure.

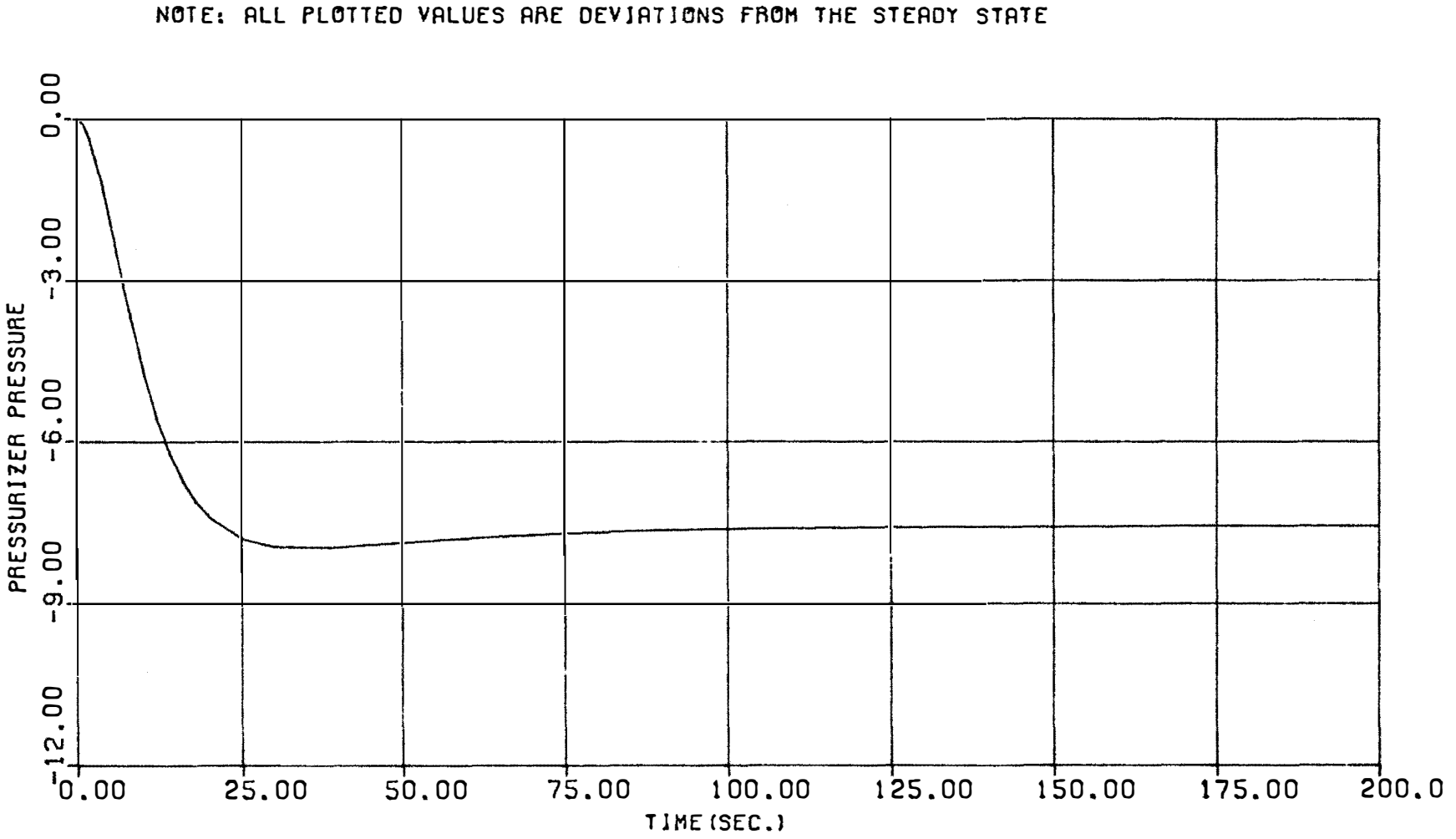

FIGURE D-6. Pressurizer Pressure Response for 50 PSI Step Change in the Turbine 1-st Stage Pressure.

VITA

Jivanlal Gandalal Thakkar was born in Kinkhlod, India on May 9, 1949. His parents are Gandalal Thakkar and former Bhanumatee Karia. Most of his "growing-up" years were spent in Kinkhlod, India where he attended primary and secondary school. He graduated from G. J. Sharda Mandir in June 1966 and entered St. Xavier's College. In 1968, he entered the nuclear engineering curriculum at The University of Tennessee and obtained a B.S. degree in Nuclear Engineering in 1971.